Heavy Flavor Production and Propagation in Heavy Ion Collision

By

Santosh Kumar Das

Variable Energy Cyclotron Centre, Kolkata

A thesis submitted to

The Board of Studies in Physical Sciences

For the Degree of

DOCTOR OF PHILOSOPHY

of

HOMI BHABHA NATIONAL INSTITUTE

March, 2012

Homi Bhabha National Institute

Recommendation of the Viva Voce Board

As members of the Viva Voce Board, we certify that we have read the dissertation prepared by **Mr Santosh Kumar Das** entitled **Heavy flavor production and propagation in heavy ion collision** and recommend that it may be accepted as fulfilling the dissertation requirement for the degree of Doctor of Philosophy.

.....**Date:**

Chairman- Prof. D K Srivastava

.....**Date:**

Convener- Dr. J. Alam

.....**Date:**

Member 1- Dr. S. Sarkar

.....**Date:**

Member 2- Prof. S. Ghosh

Finally approval and acceptance of this dissertation is contingent upon the candidate's submission of the final copies of the dissertation to HBNI.
I hereby certify that I have read this dissertation prepared under my direction and recommend that it may be accepted as fulfilling the dissertation requirement.

Date:

Place:

STATEMENT BY AUTHOR

This dissertation has been submitted in partial fulfillment of requirements for an advanced degree at Homi Bhabha National Institute (HBNI) and is deposited in the Library to be made available to borrowers under rules of the HBNI.

Brief quotation from this dissertation are allowable without special permission, provided that accurate acknowledgement of source is made. Requests for permission for extended quotation from or reproduction of this manuscript in whole or in part may be granted by the Competent Authority of HBNI when in his or her judgement the proposed use of the material is in the interests of scholarship. In all other instances, however, permission must be obtained from the author.

Santosh Kumar Das

DECLARATION

I, hereby declare that the investigation presented in the thesis has been carried out by me. The work is original and has not been submitted earlier as a whole or in part for a degree/diploma at this or any other Institution/University.

Santosh Kumar Das

Acknowledgments

First and foremost, I am thankful and owe my deepest gratitude to my supervisor, Prof. Jan-e Alam, whose encouragement, guidance and invaluable academic support from the initial to final level enabled me to develop an understanding of the subject. I am very fortunate to have him as my supervisor. This thesis would not have been possible without his patience and guidance.

It is my great pleasure to thank Prof. Sourav Sarkar for his encouragement and support. I have really enjoyed by working with him. I would like to convey my sincere thanks to Dr. R. K. Bhandari, Director VECC for his support and encouragement in all respect. I would like to convey my sincere thanks to Dr. D. K. Srivastava, Head Physics Group, VECC, for his support, advice and encouragement. I am very grateful to Prof. B. Sinha, Prof. S. Pal, Prof. A. Dhara, Prof D. N. Basu, Prof. P. Barat, Prof. T. Mukhopadhyay, Prof. T. Nayak, Prof. S.Chattopadhayay, Prof. V.S.Pandit, Prof. S. bandyopadhyay, Prof. P. R. Sahrma, Prof. S. Bhattacharya, Prof. C. Bhattacharya and many others of VECC group for their advice, support and words of encouragement. I would like to express my sincere thanks to Dr. B. Mohanty for useful discussions, co-operation and help at every stage. I am thankful to Dr. A. K. Dubey, Dr. Sarmista Banik, Dr. G. Mukhopadhyay, Dr. P. Das, Dr. M. Bhattacharya, Dr. T. Ghosh for their suggestions, advice and constant encouragement. I would like to convey my sincere thanks to J. K. Nayak. I feel fortunate to have worked with him, to learn and understand the varied aspects of heavy ion physics, while being a research scholar in theory division at VECC. I express my deep sense of gratitude to Prof. Qun Wang, Dr. Hui Dong and Prof. Ralf Rapp for useful discussions.

It is a pleasure to thank Payal Mohanty, Sabyasachi Ghosh, Victor Roy, Haridas Pai, Pratap Roy, Prithis Tribedi and Amlan Roy with whom I shared such great moments of friendship. I wish to deeply acknowledge for the many thrilling moments of discussion I had with them. I sincerely look forward to their association in future years. I would like to express my sincere thanks to Prasunu da, Jamili di, Jhilam da, Rupa didi, Pravash da, Partha da, Arnomitra di, Tapasi di, Sridharth da, Mriganka da, Saikat da, Sinjini, Sanjib and pradip for their encouragement and support. It is a pleasure to thank Nihar, Sudipan, Trambak, Surasree and Sukanya for their encouragement and useful discussions. I have really enjoyed by working with them. I also take this opportunity to thank Somnath, Younus, Manish, Arnab, Abhisek, Nasin, Subas, amal, Rehan, Sumit, Bisal subikash, arindam, Balaram, Maitri and many others for their support and words of encouragement.

I express my humble regards to all of family members, relatives and friends for their support, love and continuous encouragement during my research period.

This work is supported by DAE-BRNS project Sanction No. 2005/21/5-BRNS/2455.

Santosh Kumar Das

List of Publication

1. **Probing Quark Gluon Plasma Properties by Heavy Hlavors.**
   Santosh K Das, Jane Alam and Payal Mohanty
   Phys. Rev C 80, 054916(2009)
   arXiv:0910.4856

2. **Nuclear Suppression at Low Energy in Relativistic Heavy Ion Collision**.
   Santosh K Das, Jane Alam, Payal Mohanty and Bikash Sinha
   Phys. Rev C 81, 044912(2010)
   arXiv:0910.4853

3. **Dragging Heavy Quarks in Quark Gluon Plasma at the Large Hadron Collider.**
   Santosh K Das, Jane Alam and Payal Mohanty
   Phys. Rev C 82, 014908(2010)
   arXiv:1003.5508

4. **Soft Gluon Multiplicity Distribution Revisited.**
   Santosh K Das and Jane Alam
   Phys Rev D 82 (Rapid), 051502(R) (2010)
   arXiv:1007.4405

5. **Transport Coefficients of Gluonic Fluid.**
   Santosh K Das and Jane Alam
   Phys Rev D 83, 114011(2011)
   arXiv: 1011.4181

6. **Dragging D Mesons by Hot Hadrons.**
   Sabyasachi Ghosh, **Santosh K Das**, Sourav Sarkar and Jane Alam
   Phys Rev D 84 (Rapid), 011503(R) (2011)
   arXiv: 1104.0163

7. **Momentum Dependence of Drag Coefficients and Heavy Flavour Duppression in Quark Gluon Plasma.**
   Surasree Majumdar,Trambak Bhattacharyya, Jane Alam and **Santosh K Das**
   Phys Rev C 84, 044901(2011)
   arXiv:1106.2615

8. **Energy Loss of Fast Gluons in a Gluonic Fluid.**
   Trambak Bhattacharyya, Surasree Majumdar, **Santosh K Das** and Jane Alam
   Phys Rev D 85, 034033(2012)
   arXiv:1106.0609

9. **Radial Flow From Electromagnetic Probes and Signals of Quark Gluon Plasma.**
   Payal Mohanty, Jajati K Nayak, Jane Alam and **Santosh K Das**
   Phys Rev C 82, 034901(2010)
   arXiv:0910.4856

10. **Elliptic Flow of Thermal Dileptons as a Probe of QCD Matter.**
    Payal Mohanty, Victor Roy, Sabyasachi Ghosh, **Santosh K Das**,
    Bedangadas Mohanty, Sourav Sarkar, Jane Alam and Asis K Chaudhuri
    Accepted for publication in Phy. Rev. C (Rapid)
    arXiv:1111.2159

Conference Proceeding in Journal

1. **Heavy Flavour Suppression and Flow.**
   Santosh K Das and Jane Alam
   Nucl. Phys. A, 862-863 (2011) 289-292
   arXiv:1101.3385

2. **Probing Quark Gluon Plasma by Heavy Flavors.**
   Santosh K Das and Jane Alam
   To be published in POS, WPCF,2012
   arXiv:1202.1428

3. **Equilibration in Quark Gluon Plasma.**
   Santosh K Das, Jane Alam, and Payal Mohanty
   Indian J.Phys.85:1149-1153,2011
   arXiv:0912.4089

Arxiv Submission

1. **Elliptic Flow of Heavy Flavors.**
   Santosh K Das and Jane Alam
   arXiv:1008.2643

2. **Transport Coefficients of B Mesons in Hot Hadronic Matter.**
   Santosh K Das, Sabyasachi Ghosh, Sourav Sarkar and Jane Alam
   arXiv:1109.3359

Conference Proceeding

1. **Heavy Flavour Production and Propagation in Heavy Ion Collisions.**
   Santosh K Das
   Proc. of DAE Symp. on Nucl. Phys. (India) 56 (2011) 1178

2. **Transport Coefficients of B Mesons in Hot Hadronic Matter.**
   Santosh K Das, Sabyasachi Ghosh, Sourav Sarkar, Jan-e Alam
   Proc. of DAE Symp. on Nucl. Phys. (India) 56 (2011) 944

3. **Dragging D by Hot Hadrons.**
   Sabyasachi Ghosh, **Santosh K Das**, Sourav Sarkar, Jan-e Alam
   Proc. of DAE Symp. on Nucl. Phys. (India) 56 (2011) 974

4. **Shear Viscosity of a Pion Gas.**
   Sukanya Mitra, **Santosh K Das**, Sourav Sarkar, Jan-e Alam
   Proc. of DAE Symp. on Nucl. Phys. (India) 56 (2011) 978

5. **On the Soft Gluon Radiation in Partonic Plasma.**
   Trambak Bhattacharyya, Surasree Mazumder, **Santosh K Das**, Jan-e Alam
   Proc. of DAE Symp. on Nucl. Phys. (India) 56 (2011) 904

6. **Charged Hadron Hroduction in Proton-Proton Collisions at LHC Energy.**
   Santosh K Das, Nihar R Sahoo, Sudipan De and Tapan Nayak
   Proc. of DAE Symp. on Nucl. Phys. (India) 56 (2011) 988

7. **Probing Elliptic Flow of QCD Matter by Lepton Pairs.**
   Payal Mohanty, Victor Roy, Sabyasachi Ghosh, **Santosh K Das**,
   Bedangadas Mohanty, Sourav Sarkar, Jan-e Alam, Asis K Chaudhuri
   Proc. of DAE Symp. on Nucl. Phys. (India) 56 (2011) 910

8. **Heavy Flavours as a Probe of Quark Gluon Plasma.**
   Santosh K Das and Jane Alam

Proc. of DAE Symp. on Nucl. Phys. (India) 55 (2010) 584.

9. **Flow From Electromagnetic Radiation.**
   P. Mohanty, J. K. Nayak, Jan-e Alam and **Santosh K Das**
   Proc. of DAE Symp. on Nucl. Phys. (India) 55 (2010) 628

10. **Radiative Energy Loss in Gluon Gas.**
    Santosh K Das and Jan-e Alam
    Proc. of DAE Symp. on Nucl. Phys. (India) 55 (2010) 626.

11. **Freeze Out Time in Ultra-Relativistic Heavy Ion Collisions.**
    Santosh K Das, Payal Mohanty, Jajati K Nayak and Jan-e Alam
    Proc. of DAE Symp. on Nucl. Phys. (India) 52 (2007) 521

Synopsis

The theory of strong interaction - Quantum Chromodynamics(QCD) has a unique feature - it possess the properties of asymptotic freedom which implies that at very high temperatures and/or densities nuclear matter will exist in a deconfined state of quarks and gluons - called Quark Gluon Plasma(QGP). Recent lattice QCD based calculations confirm that the typical value of temperature for the quark-hadron transition is $O(150-180)$ MeV. It is expected that QGP can be created in the laboratory by colliding nuclei at relativistic energies. The Relativistic Heavy Ion Collider (RHIC) and the Large Hadron Collider (LHC) are two experimental facilities where matter in the state of QGP can be created. In QGP some of the symmetries of the physical vacuum may either be restored or broken - albeit transiently. The study of the quark-hadron phase transition is important because according to the Big Bang model the universe has under gone such transition after a few microsecond of the big bang. The issue is very crucial for astrophysics too, because the core of the compact astrophysical objects like neutron stars may contain deconfined quark matter at high baryon density and low temperature.

In these contexts, the study of QGP becomes a field of high contemporary interest and the heavy flavors namely, charm and bottom quarks play a crucial role in such studies, because they are produced in the early stage of the collisions and they do not dictate the bulk properties of the matter. The thermalization time of heavy quark is expected to be larger than light quarks and gluons. Therefore, the propagation of heavy quarks through QGP may be treated as the interactions between equilibrium and non-equilibrium degrees of freedom. Fokker-Planck (FP) equation provides an appropriate framework for such studies.

The drag and diffusion coefficients of charm and bottom quarks have been evaluated for both collisional and radiative processes using pQCD techniques. For the collisional processes, we evaluate the value of the drag and diffusion coefficients for the reaction: $g + Q \to g + Q$, $q + Q \to q + Q$ and $\bar{q} + Q \to \bar{q} + Q$. The matrix element for the radiative process (*e.g.* $Q + q \to Q + q + g$ and $Q + g \to Q + g + g$) can be factorized into an elastic process ($Q + g \to Q + g$) and a gluon emission ($Q \to Q + g$). The dead

cone and Landau-Pomeronchuk-Migdal (LPM) effects on the radiative loss of heavy quarks have been considered. Both radiative and collisional processes of energy loss are included in the effective drag and diffusion coefficients. For the initial distribution, we have employed the c-quark and b-quark spectra produced from p-p collisions through the flavour-creation mechanisms, $g + g \rightarrow Q + \bar{Q}$ and $q + \bar{q} \rightarrow Q + \bar{Q}$ along with the pair plus an extra parton, $g + g \rightarrow Q + \bar{Q} + g$, $q + \bar{q} \rightarrow Q + \bar{Q} + g$, $g + q \rightarrow Q + \bar{Q} + q$, $g + \bar{q} \rightarrow Q + \bar{Q} + \bar{q}$ upto the orders $O(\alpha_s^2)$ and $O(\alpha_s^3)$ in pQCD. With the effective transport coefficients and the initial distribution, the FP equation has been solved for the heavy quarks executing Brownian motion in the QGP. The solutions of the FP equation have been convoluted with the relevant fragmentation functions to obtain the D and B meson spectra. The p_T distribution of electrons have been calculated from the decays of D and B mesons.

The solution of the FP equation has been used to evaluate the nuclear suppression factor, R_{AA} and the elliptic flow, v_2 for the non-photonic single electron spectra resulting from the semi-leptonic decays of hadrons containing charm and bottom quarks. It is observed that the experimental data from RHIC on R_{AA} and v_2 of nonphotonic electrons can be reproduced simultaneously within the pQCD framework for the same set of inputs, when both the collisional and radiative processes are included and a non-ideal equation of state of the flowing QGP is used.

The effects of non-zero baryonic chemical potential on the drag and diffusion coefficients of heavy quarks propagating through a baryon rich quark gluon plasma have been studied. The nuclear suppression factor, R_{AA} for non-photonic single electron have been evaluated for low energy nuclear collisions. The role of non-zero baryonic chemical potential on R_{AA} has been studied. The effects of mass of the charm and bottom quarks as well as the role of the fragmentation on R_{AA} have also been highlighted.

Whether QGP is produced or not the formation of hadronic system is inevitable in high energy heavy ion collision. Therefore, dissipation of heavy flavored meson in hadronic medium assumes importance. In this context the drag and diffusion coefficients of the hadronic matter have been evaluated and its implication to heavy ion collision have been discussed in this dissertation.

Contents

List of Figures

List of Tables

Notations

$p + p$: Proton Proton collision

$A + A$: Nucleus Nucleus collision with mass number A

T_c: Transition temperature

T_i: Initial thermalization time

T_f: Freeze-out temperature

τ_i: Initial thermalization time

τ_f: Freeze-out time

μ_B: Baryonic chemical potential

μ: Quark chemical potential

m_D: Debye screening mass

Chapter 1

Introduction

Since the ancient time, the mankind has puzzled over and sought an understanding of the composition of matter. Scattering experiments have played a decisive role in unravelling the structure of matter. We are familiar with Ernest Rutherfords work, back scattering of α particle in the thin gold foil, introduced the idea of atomic nucleus. After the discovery of the neutron in 1932 it become clear that the main constituents of nuclei were protons and neutrons. It was the Deep Inelastic Scattering (DIS) where proton is the target and the electron is the scatterer, gives the first experimental evidence regarding the composite nature of proton and which led to the existence of quark. Quarks and gluons, along with the electrons, form almost all of the matter in our visible universe. The interaction between quarks is governed by a non-abelian gauge theory called Quantum Chromodynamics (QCD) where gluon plays the role of gauge boson. QCD has an unusual property called asymptotic freedom [1, 2, 3] that the interaction between quarks, which is weak as the quarks get closer to one another was introduce by David Gross, Franck Willczek and David Politzer. Along with the asymptotic freedom QCD also enjoy the peculiar property of confinement, which means that the force between quarks does not diminish as they are separated. The confinement is the key reason why free quark does not exist in nature, but only in colour singlet hadronic bound states. In the early days of QCD it was also referred to as infrared slavery. QCD has a characteristic energy scale on which the strength of the interaction depend, the intrinsic energy scale for the strong interactions is Λ_{QCD}, where the value of strong coupling becomes of the order of unity $O(\alpha_s)$. At energies much larger than

this, the coupling is small and one can usually use the familiar methods of perturbation theory to calculate various quantities in QCD. The perturbative approach is based on the asymptotic freedom, indeed works very well for reaction at large momentum transfer. The variation of the running coupling constant with momentum transfer, Q is given in Fig 1.1.

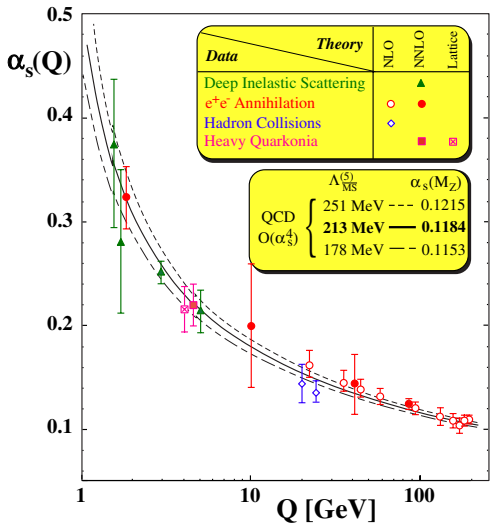

Figure 1.1: The running coupling constant $\alpha_s(Q^2)$ as a function of momentum transfer Q^2 determined from a variety of processes, taken from Ref. [4]

1.1 Basics of Quantum Chromodynamics (QCD)

The property that distinguished quarks from leptons is the color charge, so it is natural to attempt to construct a theory of the strong interactions among quarks and gluons based upon a local color gauge symmetry and the resulting theory is known as Quantum Chromodynamics(QCD). The basic quantity which, in principle, completely determine the theory of the strong interaction , is the Lagrangian of QCD. To constact a gauge Lagrangian for the QCD, let start with the free Lagrangian [5, 6, 7],

$$\mathcal{L}_0 = \bar{\Psi}_i^a(i\gamma^\mu\partial_\mu - m_i)\Psi_i^a \tag{1.1}$$

where Ψ_i^a and $\bar{\Psi}_i^a$ denote the elementary matter fields, quarks and antiquarks in the fundamental representation of the SU(3). These fields carry flavor (i) and color (a)

indices. To introduce interaction into the theory, let assume the Lagrangian is invariant under the local gauge transformation, then

$$\Psi(x) \to \Psi'(x) = G(x)\Psi(x) \tag{1.2}$$

where,

$$G(x) = \exp(\frac{i}{2}\lambda.\alpha(x)) \tag{1.3}$$

where λ is the Gell-Mann matrices, the generators of the SU(3) group and α is a function of x. Then the gradient transforms as (the color and flavor indices are suppressed)

$$\partial_\mu\Psi \to G(\partial_\mu\Psi) + (\partial_\mu G)\Psi \tag{1.4}$$

To ensure the local gauge invariance of the theory we first introduce a covariant derivative for the SU(3) gauge theory as:

$$D_\mu = \partial_\mu + igB_\mu \tag{1.5}$$

where B_μ denotes the gluon field and gauge coupling g quantifies the interaction strength. The object B_μ defined by

$$B_\mu = \frac{1}{2}\lambda.b_\mu = \frac{1}{2}\lambda^a b^a_\mu \tag{1.6}$$

The point of introducing the gauge fields and the covariant derivative is to obtain a generalization of the gradient that transforms as follow,

$$D_\mu\Psi' \to D'_\mu\Psi' = G(D_\mu\Psi) \tag{1.7}$$

Requiring this, we have to show how B_μ must behave under gauge transformations.

$$\begin{aligned} D'_\mu\Psi' &= (\partial_\mu + igB'_\mu)\Psi' \\ &= G(\partial_\mu\Psi) + (\partial_\mu G)\Psi + igB'_\mu(G\Psi) \\ &= G(\partial_\mu + igB_\mu)\Psi \end{aligned} \tag{1.8}$$

under the condition

$$igB'_\mu(G\Psi) = igG(B_\mu\Psi) - (\partial_\mu G)\Psi \tag{1.9}$$

Regarding the transformation law as an operator equation and multiplying on the right by G^{-1}, we obtain

$$\begin{aligned} B'_\mu &= GB_\mu G^{-1} + \frac{i}{g}(\partial_\mu G)G^{-1} \\ &= G[B_\mu + \frac{i}{g}G^{-1}(\partial_\mu G)]G^{-1} \end{aligned} \tag{1.10}$$

To see this explicitly, consider an infinitesimal gauge transformation, represented by

$$G = 1 + \frac{i}{2}\lambda.\alpha \tag{1.11}$$

From the transformation law Eq. 1.10, we have

$$\begin{aligned} B'_\mu &= (1 + \frac{i}{2}\lambda.\alpha)B_\mu(1 + \frac{i}{2}\lambda.\alpha)^{-1} + \frac{i}{g}(\partial_\mu(1 + \frac{i}{2}\lambda.\alpha))(1 + \frac{i}{2}\lambda.\alpha)^{-1} \\ &= B_\mu + \frac{i}{2}\lambda.\alpha B_\mu - \frac{i}{2}B_\mu\lambda.\alpha - \frac{1}{2g}\partial_\mu(\lambda.\alpha) + O(\alpha^2) \end{aligned} \tag{1.12}$$

which, in view of the definition of Eq. 1.6, is equivalent to

$$\lambda.b'_\mu = \lambda.b_\mu + \frac{i}{2}(\lambda.\alpha\lambda.b_\mu - \lambda.b_\mu\lambda.\alpha) - \frac{1}{g}\partial_\mu(\lambda.\alpha) \tag{1.13}$$

The middle term of RHS of Eq. 1.13 appear due to the non-abelian nature of the field and can be written in component form as

$$M = \frac{i}{2}\alpha^a b^b_\mu(\lambda^a\lambda^b - \lambda^b\lambda^a) = \frac{i}{2}\alpha^a b^b_\mu[\lambda^a, \lambda^b] \tag{1.14}$$

For the SU(3) group, the commutator is given by

$$[\lambda^a, \lambda^b] = 2if_{abc}\lambda^c \tag{1.15}$$

so that

$$M = -f_{abc}\alpha^a b^b_\mu\lambda^c = -\alpha \times b_\mu.\lambda \tag{1.16}$$

and

$$\lambda.b'_\mu = \lambda.b_\mu - \alpha \times b_\mu.\lambda - \frac{1}{g}\partial_\mu(\lambda.\alpha) \tag{1.17}$$

Since the eight components of the gauge field are linearly independent, we have as the transformation law for infinitesimal gauge transformations

$$b'_\mu = b_\mu - f_{abc}\alpha^a b^b - \frac{1}{g}\partial_\mu\alpha \tag{1.18}$$

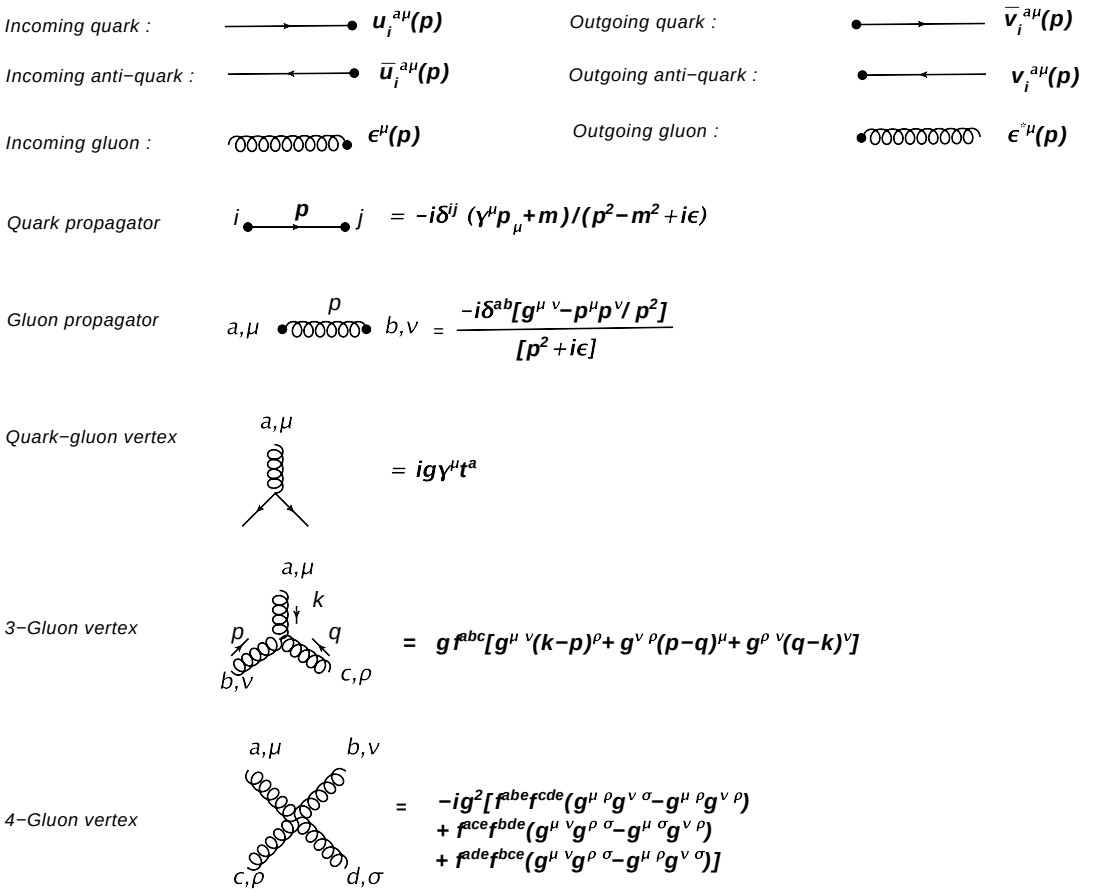

Figure 1.2: Feynman rules for QCD

So the gauge invariance Lagrangian given by

$$\mathcal{L} = \bar{\Psi}(i\gamma^{\mu}D_{\mu} - m_q)\Psi = \mathcal{L}_0 - g\bar{\Psi}\gamma^{\mu}B_{\mu}\Psi \tag{1.19}$$

mainly a free Dirac Lagrangian plus an interaction term. Including the kinetic term for the gauge field, the full QCD Lagrangian read

$$\mathcal{L}_{\mathcal{QCD}} = \bar{\Psi}(i\gamma^{\mu}\partial_{\mu} - m_q)\Psi - g\bar{\Psi}\gamma^{\mu}B_{\mu}\Psi - \frac{1}{4}G^{\mu\nu}G_{\mu\nu} \tag{1.20}$$

The gluons are massless particles with spin 1 and carry color charge, which comes in 8 different color-anticolor combinations, giving rise to gluon self interaction encoded in the third term of Eq. 1.20 i.e.

$$G_{\mu\nu} = \frac{1}{ig}[D_{\nu}, D_{\mu}] = \partial_{\nu}B_{\mu} - \partial_{\mu}B_{\nu} + ig[B_{\nu}, B_{\mu}]. \tag{1.21}$$

The commutator term $[B_\nu, B_\mu]$ is a consequence of the 3x3 matrix structure in color-charge space and generates 3 and 4 gluon interaction vertices which transforms as

$$ig[B'_\nu, B'_\mu] = ig[(GB_\mu G^{-1} + \frac{i}{g}(\partial_\mu G)G^{-1}), (GB_\mu G^{-1} + \frac{i}{g}(\partial_\mu G)G^{-1})] \qquad (1.22)$$

A set of Feynman rules for QCD could be constructed from the Lagrangian given in Eq. 1.20 to calculate the transition amplitude and other relevant quantities (see Fig 1.2).

1.2 Quark Gluon Plasma

Just after the discovery of asymptotic freedom, Collins and Perry [8] suggested that at very high densities the degrees of freedom of the strongly interacting matters are not hadrons but quarks and gluons. That means, when nuclear matter attain very high temperatures and densities the strong interactions would become so weak that individual quarks and gluons would no longer be confined within the hadrons but melt into a deconfined state of quarks and gluons, such a new phase of matters is called Quark Gluon Plasma(QGP).

Lattice QCD based calculation predicts that the typical value of the temperature for the quark-hadron transition is 170 MeV [9]. Because according to the cosmological big bang model the universe has undergone several phase transitions (GUT, Electroweak, quark to hadron etc) at different stages of its evolution and the quark-hadron transition occurred in the universe when it was few microsecond old - is the only transition which can be accessed in the laboratory currently. The study of quark-hadron transition assumes special importance in understanding the evolution of the early universe. The issue is very crucial for astrophysics too, as the core of the compact astrophysical objects like neutron stars may contain quark matter at high baryon density and low temperature. The deconfined state of quarks and gluons gives an opportunity to study condensed matter physics of elementary particles - in a new domain of non-abelian gauge theory. The study of QGP also puts QCD, the theory of strong interaction which is extremely successful in vacuum under test in a thermal medium.

The magnitude of temperature or energy density required to produce QGP in the laboratory can be achieved by colliding heavy ion at relativistic energies, under con-

trolled laboratory environment. The first relativistic heavy ion collisions that were done to investigate the quark-gluon plasma were performed at the Alternating Gradient Synchrotron (AGS) at Brookhaven and the Super Proton Synchrotron (SPS) at CERN having center of mass energy 4.83 GeV.and 17.3 GeV respectively. Experiments conducted with AGS and SPS facilities are fix target. The first facility specifically designed for colliding heavy ions at relativistic energies is the Relativistic Heavy Ion Collider (RHIC) at Brookhaven National Laboratory. The maximum centre of mass energy ($\sqrt{(}s_{\rm NN})$) at which heavy ion (like Au+Au) can be collided at RHIC is 200 GeV. Then the Large Hadron Collider (LHC) at CERN having maximum center of mass energy 5.4 TeV for Pb+Pb system (see Table 1.1).

Table 1.1: Experimental facilities to study the Heavy Ion Collision in Laboratory

Heavy Ion Experiment	$\sqrt{(}s_{\rm NN})$(GeV)	Place	Year of Commissioning
AGS	4.86	BNL	1960
SPS	17.3	CERN	1976
RHIC	200	BNL	2000
LHC	5400	CERN	2009

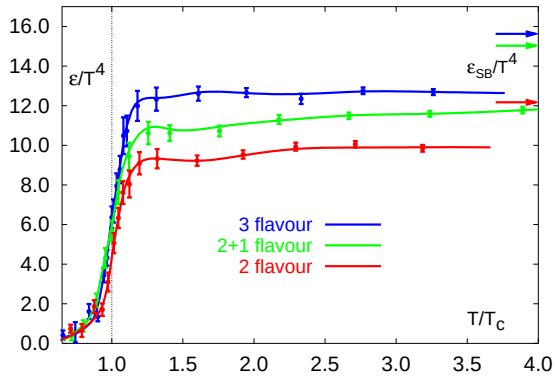

Figure 1.3: Energy density as a function of temperature scaled by the critical temperature T_c, taken from [11].

First Edward Shuryak [10] in 1980 have examined the high-temperature phase in detail and proposed a quark gluon plasma (QGP) phase to describe the deconfined state. Lattice QCD predicts as shown in Fig 1.3, ϵ/T^4 changes quite abruptly at the above

critical temperature T_c [11], increase from a low hadronic value to a system of massless quarks and gluons. This can be interpreted as an increase in the number of degrees of freedom, corresponding to a deconfinement transition from hadron to quark and gluons. The arrows (in Fig. 1.3) on right top indicate the values at the Stefan-Boltzmann limits. The exact order of the phase transition is still an unsettled issue [12].

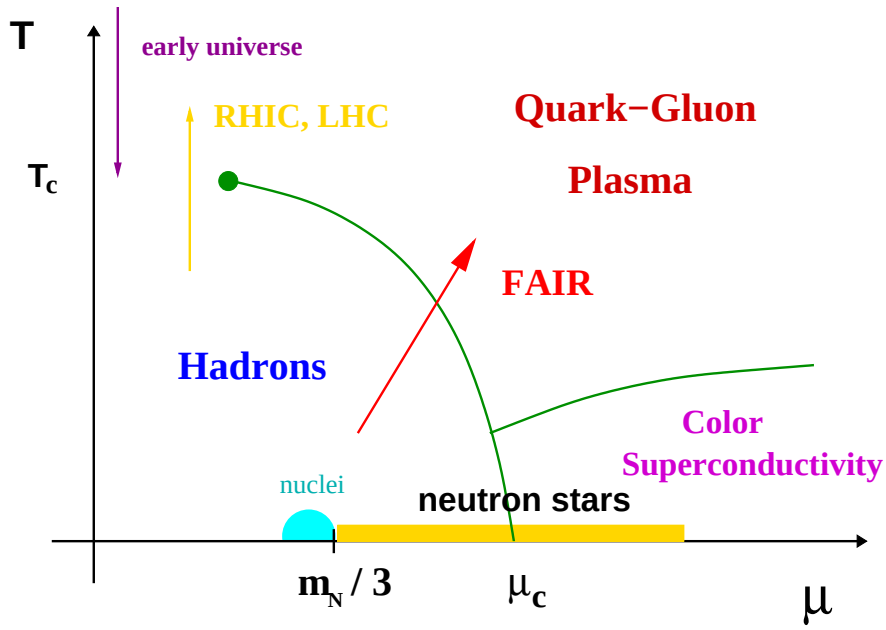

Figure 1.4: QCD phase diagram in temperatures-baryonic chemical potential plane.

The QCD phase diagram as shown in Fig 1.4 suggests a possible occurrence of deconfined phases of QCD matter at two extreme conditions [13]. The transition occurs at very high temperature (170 MeV [9]) and small chemical potential is similar to the early universe type, where matter and anti-matter was present with equal proportion. The transition occurs at low temperature and very high chemical potential is similar to the matter that exist at the core of the neutron star. At very high chemical potential, quarks may form Cooper pairs and a new state of colour superconducting phase may be realized. An important objective of modern nuclear physics is to explore the phase diagram of QCD matter in various temperatures and chemical potential to ensure the existence of the QGP.

The first variable considered in finite-temperature lattice QCD as a measure of

deconfinement is the Polyakov loop [14, 15, 16]

$$L(T) \sim \lim_{r\to\infty} \exp(-V(r)/T), \tag{1.23}$$

where V(r) is the potential between a pair of static quark-antiquark separated by a distance r. In pure gauge theory without light quark,

$$V(r) \sim \sigma r, \tag{1.24}$$

where σ is the string tension. So $V(\infty) = \infty$, hence $L = 0$. But in a deconfined medium, colour screening among the gluon leads to a melting of the string, which makes V(r) finite at large r and leads to a finite value of L. So it becomes an order parameter for the confinement to deconfinement transition, for the temperature range $0 \leq T \leq T_c$, L=0 and hence confinement, while for $T_c < T$, $L > 0$ is the deconfined phase.

In the Early Universe, it was believed that the degrees of freedom associated with all the fundamental forces were unified to one with a vanishing mass. However, as the very hot and dense Universe expanded and cooled, the degrees of freedom for each of the fundamental forces acquired a nonzero mass, and the previous symmetry among the degrees of freedom was said to be spontaneously broken. In the case of Quantum Chromodynamics (QCD), the relevant symmetry that is spontaneously broken is chiral symmetry [17] and the associated order parameter is the the vacuum expectation value (VEV) of quark-antiquark condensate, i.e. $\langle\bar{q}q\rangle$.

One can expect at very high temperature or densities the VEV of the antiquark-quark condensate, $\langle\bar{q}q\rangle$, may melts away resulting in a system, where chiral symmetry is not spontaneously broken anymore. However, as the temperature of the system cool down below the T_c, chiral symmetry is spontaneously broken, and the VEV of the $\langle\bar{q}q\rangle$ attains a nonzero value. The study of the change of the $\langle\bar{q}q\rangle$ with temperature is one of the vital goal of the ongoing heavy ion program.

1.3 Organisation of the Thesis

The thesis is organized as follows. In chapter 2 various signals of QGP like electromagnetic probes, strangeness enhancement, J/ψ suppression, jet quenching and elliptic flow

are discussed. Chapter 3 is devoted to the description of the Fokker-Planck equation, evaluation of the drag and diffusion coefficients of quark gluon plasma including both the collisional and radiative processes. The space-time evolution, initial conditions, the non-photonic single electron spectra and the heavy quark nuclear suppression factor are discussed in chapter 4. The elliptic flow of heavy quarks have been addressed in chapter 5. The drag and diffusion coefficients of the heavy flavoured mesons have been evaluated in the hadronic matter consisting of pions, kaons and eta mesons and its implication on nuclear suppression has been highlighted in chapter 6. Chapter 7 contains the thesis summary and outlook. The derivation of the invariant amplitude for the process: $gg \to ggg$ has been outlined in the Appendix.

Chapter 2

Signals of Quark Gluon Plasma

2.1 Introduction

Nucleus-nucleus collisions create a phase of hot and dense matter [18, 19, 20] that subsequently goes through various stages of evolution, as shown in Fig 2.1. Two Lorentz contracted nuclei moving in the opposite direction with very high energy collide at $z = 0$ and deposit a substantial part of their kinetic energy into a small region of space. In the very early stages after the nuclei interact, particle production is dominated by initial hard scatterings which can be described by perturbative QCD techniques. At a somewhat later time, many more softer particles materialize from collisions and rescatterings of these partons lead to locally thermalized QGP. When the expansion of the system make the temperature too low for the deconfinement of the partons, the hadronization occurs. The resulting hadronic matter expands and cools as long as the system can sustain interactions. Once the mean free path of the hadrons becomes comparable to the dimensions of the system they decouple and free stream towards the detector. The temperature when free stream occurs is the freeze-out temperature, T_f.

Therefore, irrespective of whether a QCD phase transition took place or not during the evolution of the collision process, only photons, leptons, and hadrons escape from the collision region and reach the detectors. The challenge in relativistic heavy-ion collision experiments is to reconstruct the hot and dense phase, which survives for a time interval $\sim 10^{-23}s$ and has spatial size $\sim 10^{-15}m$. Various signals have been proposed for the detection of their transient state of matter, expected to be produced

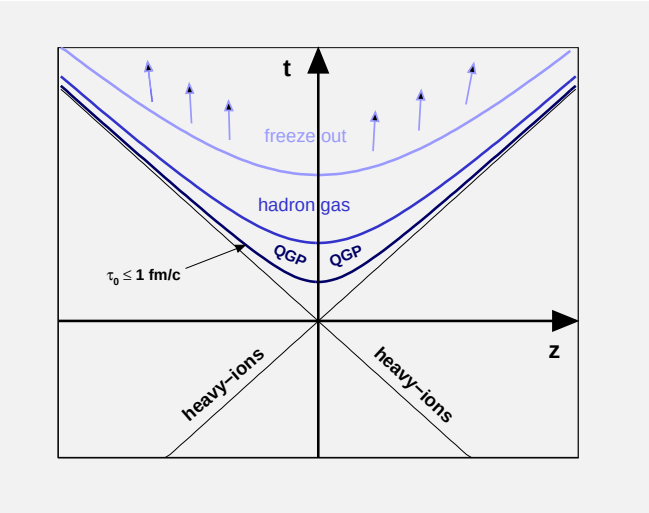

Figure 2.1: A schematic representation of the dynamical evolution of the heavy-ion collision along the collisional axis, taken from Ref. [21]

in heavy ion collision (HIC) at relativistic energies. Some of these signals are discussed below.

2.2 Electromagnetic Probes

Photons and dileptons [22, 23, 24] are produced from each stage of the collisions. Being weakly interacting in nature, their mean free path is larger than the typical size of the system. As a consequence, once produced they do not suffer further interaction and carry the undistorted information of the source environment. Therefore, photons and dileptons may considered as effective probe for the detection of QGP.

2.2.1 Photons

In nuclear collision at relativistic energies charged particles are produced either in QGP or in hadronic phase and therefore, emission of photon are inevitable from such system. There are several sources of photons from relativistic heavy ion collision. These sources may be categorized as: (i) photons produced from the hard collision of the partons from the nucleons of the colliding nuclei, these are called prompt photons which can be estimated by using techniques of pQCD [25]. Experimental data from

pp interaction may be used to validate the pQCD calculation [26]. Prompt photons from A+A collision ($dN^{A+A}/d^2p_T dy$) can be estimated from the pQCD calculation as $dN^{A+A}/d^2p_T dy = (dN^{p+p}/d^2p_T dy) \times N_{\rm coll}$, where $N_{\rm coll}$ stands for the number of nucleon-nucleon interactions in nucleus-nucleus collision. (ii) Photons from the decays of hadrons (e.g. $\pi^0 \rightarrow \gamma + \gamma$ and $\eta \rightarrow \gamma + \gamma$ etc), which can be estimated from the invariant mass analysis [27].

Once we have the estimation of prompt photons and photons from decays then the remaining (if any) photons will be from thermal sources. In heavy ion collision in a scenario when QGP is formed will have two types of thermal sources. These are (i) from QGP and (ii) thermal hadrons. Theoretically one has to estimate photons from these thermal sources and look for a window in p_T domain where photons from QGP dominates over its hadronic counter part. The relevant reactions for the production of photons from QGP and hot hadrons are given below.

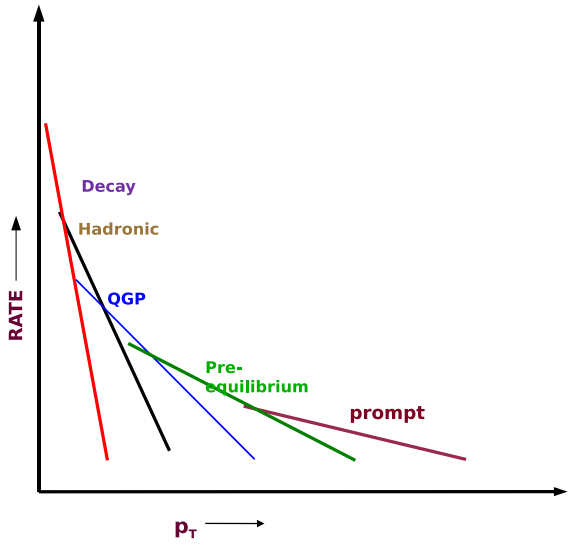

Figure 2.2: Schematic representation of the p_T dependence of the photons spectra from different sources

Thermal photons from the QGP phase arise mainly due to the QCD Compton

$(q(\bar{q}) + g \rightarrow q(\bar{q}) + \gamma)$ and annihilation $(q + \bar{q} \rightarrow g + \gamma)$ processes [28, 29, 30]. It is shown that photons from the processes [31] $q + g \rightarrow q + g + \gamma$, $q + q \rightarrow q + q + \gamma$, $q + q + \bar{q} \rightarrow q + \gamma$ and $g + q + \bar{q} \rightarrow g + \gamma$ contribute in the same order $O(\alpha\alpha_s)$ as Compton and annihilation processes. Therefore, in estimating photon spectra from QGP all these processes should be considered.

In the hadronic phase the relevant reactions and decays for photon productions are mainly: $\pi + \rho \rightarrow \pi + \gamma$, $\pi + \pi \rightarrow \rho + \gamma$, $\pi + \pi \rightarrow \eta + \gamma$, $\pi + \eta \rightarrow \pi + \gamma$, $\rho \rightarrow \pi + \pi + \gamma$, $\omega \rightarrow \pi + \gamma$, $\rho + K \rightarrow K + \gamma$ and $\pi + K \rightarrow K + \gamma$ [32, 33, 34, 35, 36, 37] . Fig 2.2 displays the photon spectra from various soures, indicating a window in p_T spectra where photons from QGP dominates over other sources. One observes that the higher the transverse momentum of the photon the earlier they are produced in the collision process.

2.2.2 Dileptons

Similar to photons, dileptons are also produced from: (i) the hard collision of the partons in the nucleons of the colliding heavy ions (Drell-Yan [38]) (ii) decays of hadrons (Dalitz decay, $\pi^0 \rightarrow e^+ + e^- + \gamma$, $\omega \rightarrow \pi^0 + e^+ + e^-$, $\eta \rightarrow \gamma + e^+ + e^-$ etc) (iii) decay of heavy flavors [39, 40] (iv) thermal hadrons and (v) QGP. The contributions from hard process can be estimated by using pQCD techniques. The yield from Dalitz decays can be estimated from the hadronic spectra measured in heavy ion collision.

Production of thermal dileptons [20] from hadronic matter and QGP have been extensively discussed in the literature [22, 23, 41] (see [42, 43, 44] for review). The dominant thermal process of dileptons from the partonic phase [45, 46, 47] are $q + \bar{q} \rightarrow l^+ + l^-$, $q + \bar{q} \rightarrow g + l^+ + l^-$ and $q(\bar{q}) + g \rightarrow q(\bar{q}) + l^+ + l^-$. In the low invariant mass domain thermal lepton pairs from the decays of the vector mesons [37, 48] e.g. $\rho \rightarrow l^+ + l^-$, $\omega \rightarrow l^+ + l^-$, $\phi \rightarrow l^+ + l^-$ dominates. The dilepton spectra originating from various sources as discussed above is schematically shown in Fig. 2.3. For the detection of QGP one needs to find out a domain of invariant mass where dileptons from QGP dominates

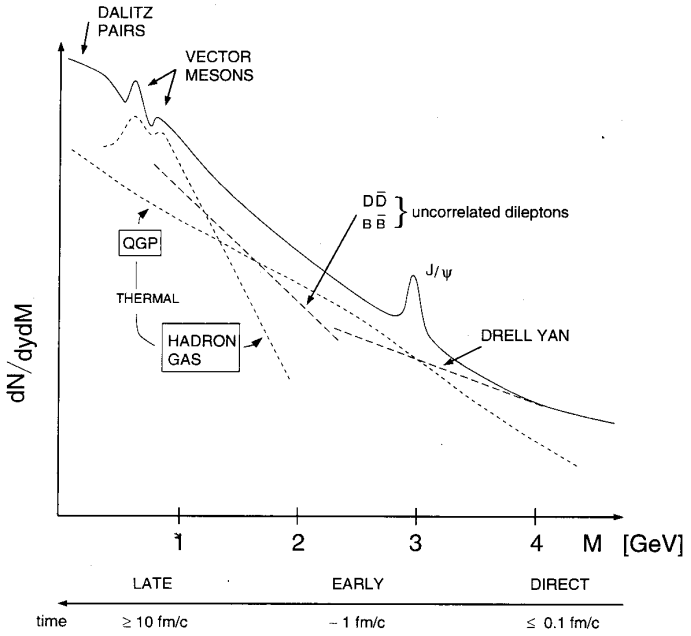

Figure 2.3: Schematic representation of the invariant mass distribution of dileptons taken from Ref [37].

2.3 Strangeness Enhancement

The abundance of strange flavored hadrons [49, 50] produced in high energy heavy ion collision is a direct consequence of the existence of a partonic phase. Let us consider a two flavour system at high baryonic chemical potential and low temperature with baryon density $\rho = 10\rho_0$, where ρ_0 is the normal nuclear matter density. If we assume the up and down quarks number density are equal, total number density can be written as

$$\rho = \frac{n_u + n_d}{3} = \frac{2n_u}{3} \tag{2.1}$$

where n_u and n_d are the number density of the up and down quarks respectively. From Eq. 2.1 with $\rho_0 = 0.16fm^{-3}$,

$$n_u = \frac{3\rho}{2} = 15 \times 0.16fm^{-3} = 2.4fm^{-3} \tag{2.2}$$

But the Fermi momentum of a massless particle can be expressed in terms of n_u as

$$p_F^3 = \frac{2\pi^2}{g} 3n_u \tag{2.3}$$

where g is the degeneracy and for a two flavour system $g = 2 \times 2 \times 3 = 12$. Substituting Eq. 2.2 in Eq. 2.3, we get $p_F = \mu_B = 450$ MeV, where μ_B is the chemical potential. As we know the mass of s quark is around 200 MeV, so $s\bar{s}$ production threshold is around 400 MeV. Therefore, the production of $s\bar{s}$ become less costly compared to $u\bar{u}$ and $d\bar{d}$ production. The $u\bar{u}$ and $d\bar{d}$ production is inhibited by Pauli exclusion principle

In contrast to the partonic phase, the hadronic channels responsible for the strange flavored hadron production are

$$N + N \rightarrow N + \Lambda + K \tag{2.4}$$

and

$$\pi + \pi \rightarrow K + \bar{K} \tag{2.5}$$

associated with Q-value around 670 MeV and 700 MeV respectively, which is much larger than $s\bar{s}$ production threshold. Hence the strangeness production is much easier in the partonic phase as compared to the hadronic phase. Therefore, the strange flavored hadrons production will be enhanced if a deconfined system of quark is formed. Therefor, enhanced production of strange hadrons may be treated as a possible signal of deconfinement.

On the other hand, let us consider the case at very high temperature and low baryonic chemical potential. At finite temperature, the density of strange quark is given by

$$\frac{N_s}{V} = \frac{N_{\bar{s}}}{V} = g \int \frac{d^3p}{(2\pi)^3} e^{-\frac{\sqrt{p^2+m_s^2}}{T}} = g\frac{Tm_s^2}{2\pi^2} K_2(m_s/T) \tag{2.6}$$

where g is the degeneracy and $K_2(m_s/T)$ is the modified Bessel's function.

Similarly the light antiquark density is given by

$$\frac{N_{\bar{q}}}{V} = g \int \frac{d^3p}{(2\pi)^3} e^{\frac{-(p+\mu)}{T}} = \frac{g}{\pi^2} T^3 e^{\frac{-\mu}{T}} \tag{2.7}$$

where μ ($\mu_B/3, \mu_B$ is the baryonic chemical potential) is the quark chemical potential. Finlay we arrive with the fraction of strange anti quark to the light anti quark as [51]

$$\frac{N_{\bar{s}}}{N_{\bar{q}}} = \frac{1}{2}\left(\frac{m_s}{T}\right)^2 K_2(m_s/T) e^{\frac{-\mu_B}{3T}} \tag{2.8}$$

For example, with $x = m_s/T$ =1.5 and 2 the value of $\frac{N_{\bar{s}}}{N_{\bar{q}}}$ varies between 1.3 and 1.

Hence, from Eq. 2.8, we always have more $\bar{s}$ than $\bar{q}$ [51]. As a consequence at low colliding energy, it is always easy for a $\bar{s}$ to find a u (say) to become a $K^+(u\bar{s})$ rather than a $K^-(s\bar{q})$. Some of the s may find two light quark to make a $\Lambda(uds)$. As a result the $K^+(u\bar{s})$ and $\Lambda(uds)$ [52, 53] production will enhanced. Therefore, enhanced production of $K^+(u\bar{s})$ and $\Lambda(uds)$ may be treated as a possible signal of deconfinement.

2.4 J/Ψ Suppression

J/Ψ is a bound state of charm quark (c) and anti charm quark ($\bar{c}$). In free space the potential between c and $\bar{c}$ pair can be represented phenomenologically as [54, 55]:

$$V(r) = \frac{q}{4\pi r} + \kappa r \tag{2.9}$$

where the first term represent the long-range Coulomb like potential and the second term represent the confining linear potential with κ is the string tension.

In QGP , the interaction between the charm and the anticharm quark get weaken mainly due to two effects. The first one is due to the screening of the charm quark color charge, in analogy to the familiar Debye screening of electric charge in QED. The screening length is a temperature dependent quantity. Second, the quantity, κ appear the linear term of V(r) is called string tension, is a temperature dependent quantity which vanishes at high temperature.

Therefore, at high temperature the only interaction remain between the c and $\bar{c}$ is the Coulomb like interaction, which also get modified because of Debye screening. Screening effectively reduces the range of interaction and the coulomb like potential reduces to Yukawa like interaction,

$$V(r) = \frac{qe^{-r/\lambda_D}}{4\pi r} \tag{2.10}$$

where λ_D is the Debye screening length and varies inversely with temperature. This inverse dependence arises because the greater the temperature, the greater the plasma density around the charm quark, will further weaken the interaction between the c and $\bar{c}$. When λ_D becomes less than the Bohr radius (r_b), the c $\bar{c}$ system will no more be a bound state.

If QGP is formed then the screening effect will make the J/Ψ unbound, indicating less J/Ψ as compared to case when QGP is not produced (In p-p collision). Therefore, J/Ψ suppression [56, 57] can be a signal of QGP formation.

2.5 Jet Quenching

In QCD, when an incoming parton from one hadron scatters off an incoming parton from the other hadron to produce two high transverse momentum partons are called jets. If the jets propagate through a medium formed after the nuclear collision due to multiple scattering, they suffer further interaction with the medium and loss their energy. This parton energy loss is referred to as jet quenching [58] and provides fundamental information on the thermodynamical and transport properties of the traversed medium. It was Bjorken [59] who first suggested that partons traversing bulk partonic matter might undergo significant energy loss, with observable consequences on the parton subsequent fragmentation into hadrons. Results from nucleus-nucleus collisions at the RHIC [60, 61] have shown evidence for the quenching effect through the suppression of inclusive high p_T hadron production.

The quenching can occurs through both collisional as well as radiative processes and can be directly mapped through the nuclear suppression factor (R_{AA}), defined as

$$R_{AA}(p_T) = \frac{\frac{dN}{d^2p_T dy}^{\mathrm{Au+Au}}}{N_{\mathrm{coll}} \times \frac{dN}{d^2p_T dy}^{\mathrm{p+p}}} \tag{2.11}$$

a ratio that summarizes the deviation from what would be obtained if the nucleus-nucleus collision is an incoherent superposition of nucleon-nucleon collisions. In Eq. 2.11 N_{coll} stands for the number of nucleon-nucleon interactions in a nucleus-nucleus collision.

If nucleus-nucleus collision is a incoherent superposition of nucleon-nucleon collisions, then nuclear suppression factor will be unity, indicatings the absence of any medium. If nuclear suppression factor is less than unity, that will signify the interaction of the high energy jets with the thermal medium formed in the nuclear collisions. The amount of energy loss and hence the suppression will display the properties of the medium.

2.6 Elliptic Flow

The azimuthal momentum anisotropy [62, 63] of particle emission from non-central heavy-ion collisions can be quantified as the coefficients of the Fourier expansion

$$E\frac{d^3N}{d^3p} = \frac{1}{2\pi}\frac{d^2N}{dp_T dy}\left[1 + \sum_{n=1}^{\infty} 2v_n cos(n\phi)\right] \tag{2.12}$$

where ϕ is the azimuthal angle and v_n's are the Fourier coefficients. The second coefficient of the expansion, v_2, is usually referred to as elliptic flow. This is because, if we draw a polar plot of $1 + v_2 cos(2\phi)$, we will have a ellipse of major and minor axis $1 + v_2$ and $1 - v_2$ respectively.

If nucleus-nucleus collisions were simple superpositions of nucleon-nucleon collisions, the produced particles would have isotropic distributions, irrespective of the shape of the collision zone in the transverse plane. However, if produced particles rescatter, the particles moving in the direction of the longer axis of the reaction zone are more likely to change their direction than the particles moving in the direction of the shorter axis. Therefore, the observed emission pattern of particles will be azimuthally anisotropic, and the more frequent the rescattering, the more anisotropic the particle distribution. In this way, the anisotropy of the final particle distribution is a measurement of the frequency of rescatterings during the dense phase of the collision.

In a hydrodynamic picture [64], the momentum anisotropies could be understood in terms of pressure gradients. The average pressure gradient between the center of the system and the surrounding vacuum is larger in the direction where the collision system is thinner. Therefore, the collective flow is stronger in that direction and more particles are emitted there than in the direction, where the collision system is longer.

The elliptic flow (v_2) of the produced particles have been shown to be sensitive to the initial condition and the equation of state (EoS) of the evolving matter formed in heavy ion collision [21, 65, 66]. The large elliptic flow (v_2) [67, 68], in Au + Au collisions at RHIC energy indicate the possibility of fast equilibration [69, 70] of a partonic phase.

Chapter 3

Non-Equilibrium Processes

3.1 Introduction

The system produced in high energy heavy ion collision consists of mainly light quarks and gluons. The heavy flavours namely, charm and bottom quarks may play a crucial role in understanding the properties of such medium because they do not constitute the bulk part of the system and their thermalization time scale is larger than the light quarks and gluons and hence can retain the interaction history very effectively. The perturbative QCD (pQCD) calculations indicate that the heavy quark (HQ) thermalization time, τ_i^Q is larger [71, 72, 73] than the light quarks and gluons thermalization scale τ_i. Gluons may thermalized even before up and down quarks [74, 75]. In the present work we assume that the Quark Gluon Plasma (QGP) is formed at time τ_i. Therefore, the interaction of the non-equilibrated heavy quarks with the equilibrated QGP for the time interval $\tau_i < \tau < \tau_i^{HQ}$ can be treated within the ambit of the Fokker-Planck (FP) equation [76, 77], *i.e.*, the heavy quark can be thought of executing Brownian motion [71, 74, 78, 79, 80, 81, 82, 83, 84] in the heat bath of QGP during the said interval of time. Just like evolution of pollen grain on the background of water molecule, where water molecule are in equilibrium and the pollen grains execute Brownian motion in the water.

The special role of heavy quarks as a probe of the medium created in heavy-ion collision resides on the fact that their mass is significantly larger than the typically attained temperatures and other nonperturbative scales, $M \gg T_c, \Lambda_{QCD}$(intrinsic energy

scale for the strong interaction), i.e. the production of heavy quarks is essentially constrained to the early, primordial stage of a heavy-ion collision and they do not dictate the bulk properties of the matter. Therefore, the heavy flavours are the witness to the entire space-time evolution of the system and can act as an effective probe to extract information of the system.

3.2 Fokker-Planck Equation

As the relaxation time for heavy quarks of mass M at a temperature T are larger than the corresponding quantities for light partons by a factor of $M/T(> 1)$ [71] *i.e.* the light quarks and the gluons get thermalized faster than the heavy quarks, the propagation of heavy quarks through QGP (mainly contains light quarks and gluons) therefore, may be treated as the interactions between equilibrium and non-equilibrium degrees of freedom. The FP equation provides an appropriate framework for such processes. To arrive with the FP equation, let us stats from the Boltzmann transport equation.

The Boltzmann transport equation describing a non-equilibrium statistical system reads:

$$\left[\frac{\partial}{\partial t} + \frac{\mathbf{p}}{E}.\nabla_{\mathbf{x}} + \mathbf{F}.\nabla_{\mathbf{p}}\right] f(x,p,t) = \left[\frac{\partial f}{\partial t}\right]_{col} \tag{3.1}$$

where p and E denote momentum and energy, $\nabla_{\mathbf{x}}$ ($\nabla_{\mathbf{p}}$) are spatial (momentum space) gradient and $f(x,p,t)$ is the phase space distribution (in the present case f stands for heavy quark distribution). The assumption of uniformity in the plasma and absence of any external force leads to

$$\frac{\partial f}{\partial t} = \left[\frac{\partial f}{\partial t}\right]_{\text{col}} \tag{3.2}$$

If we define $\omega(p,k)$, the rate of collisions which change the momentum of the charmed quark from p to $p-k$, then we have [79]

$$\left[\frac{\partial f}{\partial t}\right]_{col} = \int d^3k \left[\omega(p+k,k)f(p+k) - \omega(p,k)f(p)\right] \tag{3.3}$$

The first term in the integrand represents gain of probability through collisions which knock the charmed quark into the volume element of momentum space at p, and the second term represents loss out of that element. ω is the sum of contributions from

gluon,light-quark and antiquark scattering. If we expand $\omega(p+k,k)f(p+k)$ around k,

$$\omega(p+k,k)f(p+k) \approx \omega(p,k)f(p) + k\frac{\partial}{\partial p}(\omega p) + \frac{1}{2}k_i k_j \frac{\partial^2}{\partial p_i \partial_j}(\omega p) \tag{3.4}$$

and substitute in Eq. 3.3, we get:

$$\left[\frac{\partial f}{\partial t}\right]_{col} = \frac{\partial}{\partial p_i}\left[A_i(p)f + \frac{\partial}{\partial p_i}[B_{ij}(p)f]\right] \tag{3.5}$$

where we have defined the kernels

$$\begin{aligned} A_i &= \int d^3k\omega(p,k)k_i \\ B_{ij} &= \int d^3k\omega(p,k)k_i k_j. \end{aligned} \tag{3.6}$$

for $\mid \mathbf{p} \mid \rightarrow \mathbf{0}$, $A_i \rightarrow \gamma p_i$ and $B_{ij} \rightarrow D\delta_{ij}$ where γ and D stand for drag and diffusion coefficients respectively. The function $\omega(p,k)$ is given by

$$\omega(p,k) = g\int \frac{d^3q}{(2\pi)^3} f'(q) v \sigma_{p,q\rightarrow p-k,q+k} \tag{3.7}$$

where f' is the phase space distribution, in the present case it stands for light quarks/anti-quarks and gluons, v is the relative velocity between the two collision partners, σ denotes the cross section and g is the statistical degeneracy. The coefficients in the first two terms of the expansion in Eq. 3.5 are comparable in magnitude because the averaging of k_i involves greater cancellation than the averaging of the quadratic term $k_i k_j$. The higher power of k_i's are assumed to be smaller [76].

With these approximations the Boltzmann equation reduces to a non-linear integro-differential equation known as Landau kinetic equation:

$$\frac{\partial f}{\partial t} = \frac{\partial}{\partial p_i}\left[A_i(p)f + \frac{\partial}{\partial p_i}[B_{ij}(p)f]\right] \tag{3.8}$$

The nonlinearity is caused due to the appearance of f' in A_i and B_{ij} through $w(p,k)$. It arises from the simple fact that we are studying collision process which involves two particles - it should, therefore, depend on the states of the two participating particles and hence on the product of the two distribution functions. Considerable simplicity may be achieved by replacing the distribution functions of one of the collision partners by their equilibrium distribution either Fermi-Dirac or Bose-Einstein (depending on the

particle type) in the expressions of A_i and B_{ij}. Then Eq. 3.8 reduces to a linear partial differential equation - usually referred to as the Fokker-Planck equation[77] describing the interaction of a particle which is out of thermal equilibrium with the particles in a thermal bath. The quantities A_i and B_{ij} are related to the usual drag and diffusion coefficients and we denote them by γ and D_{ij} respectively (*i.e.* these quantities can be obtained from the expressions for A_i and B_{ij} by replacing the distribution functions by their thermal counterparts):

Following Bjorken we assume the invariance of central rapidity region under Lorentz boost along the longitudinal direction. Because of this invariance the distribution function at a point z at time t is same as that at $z = 0$ and $\tau = \sqrt{(}t^2 - z^2)$ [85, 86].

The evolution of the heavy quark distribution (f) is governed by the FP equation [79]

$$\frac{\partial f}{\partial \tau} = \frac{\partial}{\partial p_i}\left[p_i \gamma_i(p) f + \frac{\partial}{\partial p_i}[D_{ij}(p) f]\right] \tag{3.9}$$

where γ and D_{ij} are the drag and diffusion coefficients.

3.3 Solution of Fokker-Planck Equation

We investigate the time evolution of the FP equation for a heavy quark propagating through an expanding QGP. To have an analytic solution of the FP equation we assume momentum independent drag and diffusion coefficients. We will see later that in view of the weak momentum dependent of these transport coefficients this is a reasonable assumption. The time dependence of the drag and diffusion coefficients enters through their dependence on temperature for an expanding bath.

For the initial HQ (c and b) momentum distribution we take

$$f(t = 0, p) = f_0(p), \tag{3.10}$$

where $f(t = 0, p)$ is obtained from the c-quark and b-quark spectra originated from p-p collisions through the flavour-creation mechanisms [87, 88], $g + g \to Q + \bar{Q}$ and $q + \bar{q} \to Q + \bar{Q}$ along with the pair plus an extra parton,$g + g \to Q + \bar{Q} + g$, $q + \bar{q} \to Q + \bar{Q} + g$, $g + q \to Q + \bar{Q} + q$, $g + \bar{q} \to Q + \bar{Q} + \bar{q}$ upto the orders $O(\alpha_s^2)$ and $O(\alpha_s^3)$ in pQCD.

The initial-value problem can be conveniently solved employing Greens function techniques [81]. Let $G(t, p, p_0)$ be the solution (Greens function) of Eq. 3.9 with the

initial condition,

$$G(t=0,p,p_0)=\delta^3(p-p_0), \tag{3.11}$$

then the full solution of Eq. 3.9 with initial condition, Eq. 3.10 is:

$$f(t,p)=\int d^3p_0 G(t,p,p_0)f_0(p_0) \tag{3.12}$$

To determine the Green function for the Eq. 3.9, we define its Fourier transform,

$$G(t,p,p_0)=\int d^3q \exp(-iq.p)g(t,q,p_0) \tag{3.13}$$

where q is the position coordinate. Using 3.13 in 3.9, leading to the first-order differential equation

$$\frac{\partial g}{\partial t}+\gamma q\frac{\partial g}{\partial q}=-Dq^2 g \tag{3.14}$$

With the initial condition for g determined by Eq. 3.11

$$g(0,q,p_0)=\frac{1}{(2\pi)^3}\exp(-ip_0.q), \tag{3.15}$$

the solution reads,

$$g(t,q,p_0)=\frac{1}{(2\pi)^3}\exp\{-ip_0.q\exp[-\Gamma(t)]\}\exp[-\triangle(t)q^2] \tag{3.16}$$

where

$$\Gamma(t)=\int_0^t d\tau\gamma(\tau) \tag{3.17}$$

and

$$\triangle(t)=\exp\left[-2\Gamma(t)\right]\int_0^t d\tau D(\tau)\exp\left[2\Gamma(\tau)\right] \tag{3.18}$$

The Fourier transformation Eq. 3.13 yields the result for the Greens function

$$G(t,p,p_0)=\left[\frac{1}{4\pi\triangle(t)}\right]^{\frac{3}{2}}\exp\left[-\frac{(p-p_0\exp[-\Gamma(t)])^2}{4\triangle(t)}\right] \tag{3.19}$$

Then the solution of the FP equation is given by

$$f(t,p)=\int d^3p_0\left[\frac{1}{4\pi\triangle(t)}\right]^{\frac{3}{2}}\exp\left[-\frac{(p-p_0\exp[-\Gamma(t)])^2}{4\triangle(t)}\right]f_0(p_0) \tag{3.20}$$

$$=\int d^2p_{t0}\left[\frac{1}{4\pi\triangle(t)}\right]^{\frac{3}{2}}\exp\left[-\frac{(p_t-p_{t0}\exp[-\Gamma(t)])^2}{4\triangle(t)}\right]f_0(p_0) \tag{3.21}$$

$$\exp\left[-\frac{(p_z-p_{z0}\exp[-\Gamma(t)])^2}{4\triangle(t)}\right]dp_z \tag{3.22}$$

Performing the p_z integration

$$\int \exp\left[-\frac{(p_z - p_{z0}\exp[-\Gamma(t)])^2}{4\triangle(t)}\right] dp_z = \sqrt{4\pi\triangle(t)}\exp[\Gamma(t)] \tag{3.23}$$

We arrive at

$$f(t,p_t) = \int d^2p_{t0}\left[\frac{\exp[\Gamma(t)]}{4\pi\triangle(t)}\right]\exp\left[-\frac{(p_t - p_{t0}\exp[-\Gamma(t)])^2}{4\triangle(t)}\right] f_0(p_0) \tag{3.24}$$

3.4 Heavy Quark Transport in the Quark-Gluon Plasma

To solve the Fokker-Planck equation along with the initial distribution, one needs the drag and diffusion coefficient as inputs. The drag may be defined as the thermal average of the momentum transfer weighted by the square of the invariant transition amplitude

,

$$\begin{aligned} A_i = \frac{1}{2E_p}\int\frac{d^3q}{(2\pi)^3E_q}\int\frac{d^3p'}{(2\pi)^3E'_p}\int\frac{d^3q'}{(2\pi)^3E'_q} \\ \frac{1}{\gamma_c}\sum|M|^2(2\pi)^4\delta^4(p+q-p'-q') \\ \hat{f}(q)[(p-p')] \equiv \langle\langle(p-p')\rangle\rangle \end{aligned} \tag{3.25}$$

where γ_c is the spin and color degeneracy of the charm/bottom quarks. The temperature dependence of the drag coefficient enter through the phase space distribution. As the temperature of the thermal bath increases the light quarks (q) and the gluons move faster and gain the ability to transfer larger momentum during their interaction with the heavy quarks may result the increase of the drag coefficients of the heavy quarks propagating through the partonic medium. It may be mentioned here that the drag increases with T when the system behave like a gas. In case of liquid the drag may decrease with temperature (except very few cases) - because a substantial part of the thermal energy goes in making the attraction between the interacting particles weaker - allowing them to move more freely and hence making the drag force lesser. The drag coefficient of the partonic system with non-perturbative effects may decrease with temperature as shown in Ref. [89] - because in this case the system interacts strongly more like a liquid.

The nuclear collisions at low energy RHIC run [90, 91] and GSI-FAIR [92] is expected to create a thermal medium with large baryonic chemical potential (μ_B) and moderate temperature (T). So the effect of baryonic chemical potential (μ_B) should also been taken into account. Both the T and quark chemical potential, μ ($\mu_B/3$) dependence of drag enter through the thermal distribution.

A_i depends only on p, thus we may write [79]

$$A_i = p_i A(p^2) \tag{3.26}$$

with the scalar functions

$$A = \frac{p_i A_i}{p^2} = \langle\langle 1 \rangle\rangle - \frac{\langle\langle p.p\prime \rangle\rangle}{p^2} \tag{3.27}$$

Similarly the diffusion coefficients is a measure of the thermal average of the square momentum transfer, weighted by the interaction through the square of the invariant amplitude, $\overline{\mid M \mid^2}$,

$$B_{ij} = \langle\langle (p-p')_i (p-p')_j \rangle\rangle \tag{3.28}$$

with the scalar function

$$B_{ij} = \frac{1}{4}\left[\langle\langle p\prime^2 \rangle\rangle - \frac{\langle\langle (p.p\prime)^2 \rangle\rangle}{p^2}\right] \tag{3.29}$$

Like the drag coefficient, the diffusion coefficient may increase with temperature, as it involves the square of the momentum transfer.

With an appropriate choice of $T(p\prime)$ both the drag and diffusion coefficients can be evaluated from the following expression:

$$\begin{aligned} << T(p) >> = & \frac{1}{512\pi^4}\frac{1}{E_p}\int_0^\infty q dq d(cos\chi)\hat{f}(q) \\ & \frac{(s-m^2)}{s}\int_1^{-1} d(cos\theta_{c.m.}) \\ & \frac{1}{\gamma_c}\sum |M|^2 \int_0^{2\pi} d\phi_{c.m.} T(p\prime) \end{aligned} \tag{3.30}$$

with an appropriate replacement of $T(p\prime)$ as defined above through Eq. 3.27 and Eq. 3.29.

3.4.1 General Discussion

To have a clear understanding about the physical meanings of the drag and diffusion coefficients, let us use the approximation of constant coefficients, $\gamma(p)$= A(p)=constant and D_{ij}=$B_{ij}(p)$=constant, in which case the Fokker-Planck equation further simplifies to

$$\frac{\partial f}{\partial t} = \gamma \frac{\partial}{\partial p}(pf) + D\frac{\partial^2}{\partial p^2} f \tag{3.31}$$

for the initial condition, $f(p, t = 0) = \delta^3(p - p_0)$, the solution of the above equation takes the form of a Gaussian distribution,

$$f(t,p) = \left[\frac{\gamma}{2\pi D[1-\exp(-2\gamma t)]}\right]^{\frac{3}{2}} \exp\left[\frac{\gamma}{2D}\frac{[p - p_0\exp(-\gamma t)]^2}{1-\exp(-2\gamma t)}\right] \tag{3.32}$$

From the above Eq. 3.32, the mean momentum

$$< p >= p_0 \exp(-\gamma t), \tag{3.33}$$

one sees that γ determines the relaxation rate of the average momentum to its equilibrium value, i.e., it is a drag or friction coefficients. With the momentum fluctuation given by

$$< p^2 > - < p >^2 = \frac{3D}{\gamma}\left[1 - \exp(-2\gamma t)\right] \tag{3.34}$$

where D is the momentum-diffusion constant.

Therefore, the role of the drag coefficients on momentum distribution is to shift the average momentum towards the lower p, *i.e.* the average momentum of the given distribution will decrease due to energy dissipation, as a results the high p particle will shift towards the low p, shown in Fig. 3.1. On the other hand diffusion coefficients change the width of the momentum distribution keeping the quark momentum constant as shown in Fig. 3.2. Effect of both the drag and diffusion coefficients on the given distribution as shown in Fig. 3.3 will change the width as well as shift its peak towards the lower p, where as the area under the curve will remain same in all the three cases.

For $t \to \infty$, Eq. 3.32 approaches a Maxwell-Boltzmann distribution,

$$f(p,t) = \left(\frac{2\pi D}{\gamma}\right)^{\frac{3}{2}} \exp\left(-\frac{\gamma p^2}{2D}\right) \tag{3.35}$$

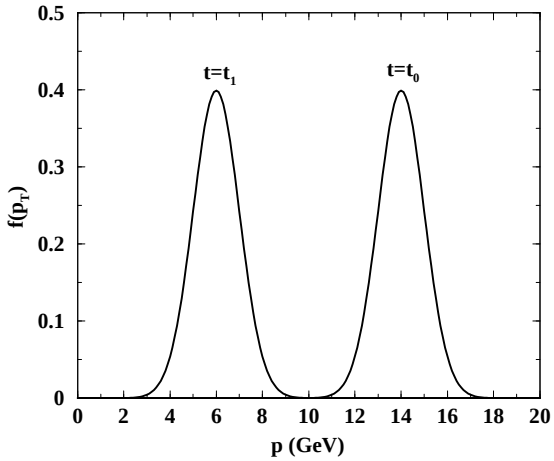

Figure 3.1: Effect of the drag coefficients on the momentum distribution.

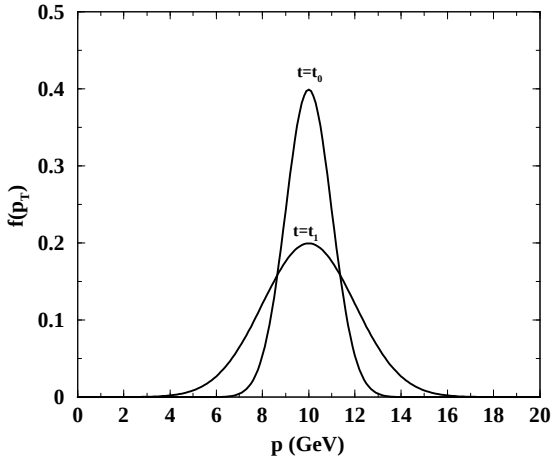

Figure 3.2: Effect of the diffusion coefficients on the momentum distribution.

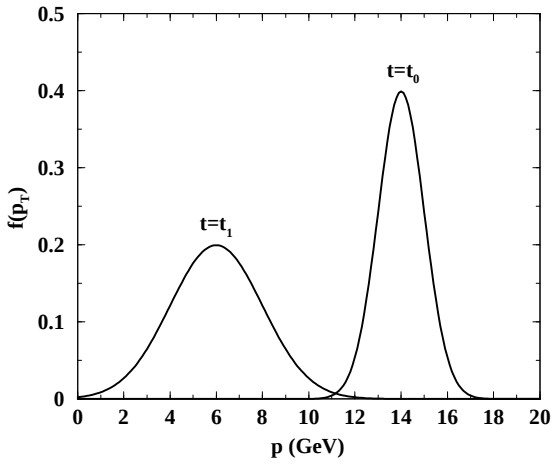

Figure 3.3: Effect of both drag and diffusion coefficients on the momentum distribution.

and thermal equilibrium implies the dissipation-fluctuation theorem,

$$D = M_Q \gamma T \tag{3.36}$$

reducing the problem to a single transport coefficient. This demonstrates that the FP equation is a consistent approximation to the Boltzmann equation in the sense that it achieve the proper equilibrium limit.

3.5 Heavy Quark Energy Loss

Energy dissipation of heavy quarks in QCD matter is considered as one of the most promising probe for the quark gluon plasma (QGP) diagnostics. The energy loss of energetic heavy quarks (HQ) while propagating through the QGP medium is manifested in the suppression of heavy flavoured hadrons at high transverse momentum (p_T). The depletion of high p_T hadrons (D and B mesons) produced in Nucleus + Nucleus collisions with respect to those produced in proton + proton (pp) collisions has been measured experimentally [93, 94, 95, 96] through their semi-leptonic decays. The two main processes which cause this depletion are (i) elastic collisions and (ii) the bremsstrahlung or radiative loss due to the interaction of the heavy quarks with the quarks, anti-quarks and gluons in the thermal bath.

3.5.1 Collisional Loss

The importance of collisional energy loss in QGP diagnostics was discussed first by Bjorken [59]. The calculations of elastic loss were performed with improved techniques [97, 98] and its importance were highlighted subsequently [99, 100] in heavy ion collisions. The collisional energy loss of heavy quarks [101] has gained importance recently in view of the measured nuclear suppression in the p_T spectra of non-photonic single electrons. Several ingredients like inclusion of non-perturbative contributions from the quasi-hadronic bound state [89], 3-body scattering effects [102], the dissociation of heavy mesons due to its interaction with the partons in the thermal medium [103] and employment of running coupling constants and realistic Debye mass [104] have been proposed to improve the description of the experimental data.

Here we have treated the problem within the pQCD framework. The interaction of charm and bottom quarks in a QGP is dominated by its interactions with the the light quarks, anti-quarks and gluons. The quantity, we need to calculate is the matrix element for the elastic $2 \to 2$ processes like, $g + Q \to g + Q$, $q + Q \to q + Q$ and $\bar{q} + Q \to \bar{q} + Q$, which can be further utilized to evaluate the drag and diffusion coefficients appeared in the FP equation.

The corresponding scattering matrix elements for the Feynman diagrams in Fig. 3.4 is given by [105]

$$\sum |M_a|^2 = 3072\pi^2\alpha_s^2 \frac{(m^2-s)(m^2-u)}{(t-\mu^2)^2} \tag{3.37}$$

$$\sum |M_b|^2 = \frac{2048}{3}\pi^2\alpha_s^2 \frac{(m^2-s)(m^2-u) - 2m^2(m^2+s)}{(m^2-s)^2} \tag{3.38}$$

$$\sum |M_b|^2 = \frac{2048}{3}\pi^2\alpha_s^2 \frac{(m^2-s)(m^2-u) - 2m^2(m^2+u)}{(m^2-u)^2} \tag{3.39}$$

$$\sum M_a M_b^* = \sum M_a^* M_b = 768\pi^2\alpha_s^2 \frac{(m^2-s)(m^2-u) + m^2(u-s)}{(t-\mu^2)(m^2-s)} \tag{3.40}$$

$$\sum M_a M_b^* = \sum M_a^* M_b = 768\pi^2\alpha_s^2 \frac{(m^2-s)(m^2-u) + m^2(u-s)}{(t-\mu^2)(m^2-s)} \tag{3.41}$$

$$\sum M_a M_c^* = \sum M_c^* M_a = 768\pi^2\alpha_s^2 \frac{(m^2-s)(m^2-u) + m^2(s-u)}{(t-\mu^2)(m^2-u)} \tag{3.42}$$

$$\sum M_b M_c^* = \sum M_c^* M_b = \frac{256}{3}\pi^2\alpha_s^2 \frac{m^2(t-4m^2)}{(m^2-u)(m^2-s)} \tag{3.43}$$

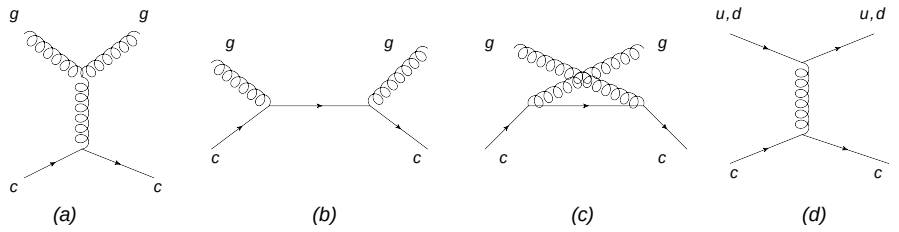

Figure 3.4: Feynman diagrams for scattering of charm quark by gluon (a-c) and light quark (d).

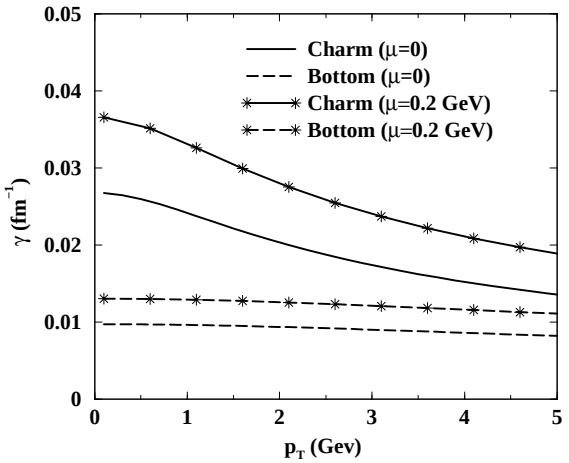

Figure 3.5: Variation of drag coefficient with p_T for $T = 200$ MeV

$$\sum |M_d|^2 = 256 N_f \pi^2 \alpha_s^2 \frac{(m^2 - s)^2 + (m^2 - u)^2 + 2m^t}{(t - \mu^2)^2} \tag{3.44}$$

The divergence associated with the t-channel diagram due to massless intermediate particle exchange can be shielded introducing a mass m_D into the internal gluon propagator to include the effects of Debye screening. To the lowest order in perturbation theory, the Debye mass of gluon is given by $m_D \sim gT$.

Now we can proceed to calculate the drag and diffusion coefficients using the heavy-light scattering matrix elements using Eq. 3.30.

In Fig. 3.5 we depict the variation of the drag coefficients as a function of the transverse momentum of the charm and bottom quarks at a temperature, $T = 200$ MeV. The momentum dependence is weak. For non-zero quark chemical potential the value of the drag increases, however, the nature of the variations remain same. This is

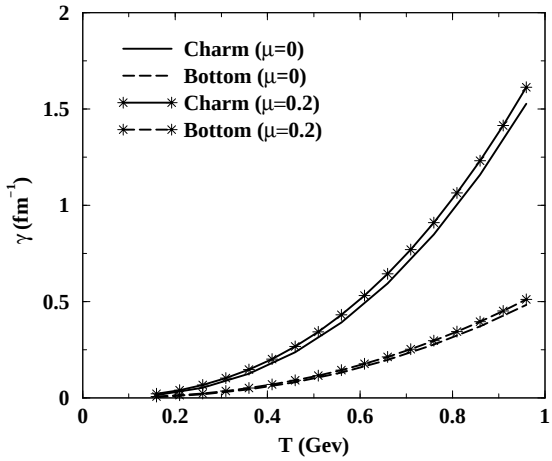

Figure 3.6: Variation of drag coefficient with temperature for $p_T = 100MeV$.

because for nonzero chemical potential the heavy quarks encounters more q than $\bar{q}$. In Fig. 3.6 the temperature variation of the drag co-efficient is plotted for both zero and non-zero quark chemical potential. Qualitatively, the inverse of the drag co-efficient gives the magnitude of the relaxation time. Therefore, the present results indicate that a system with fixed temperature achieves equilibrium faster for non-zero μ. In Fig. 3.7 the diffusion coefficients are plotted as a function of p_T for $T = 200$ MeV. The diffusion co-efficient for non-zero μ is larger as compared to the case of vanishing μ. The same quantity is displayed in Fig. 3.8 as a function of temperature. As the temperature of the thermal bath increases the light quarks (q) and the gluons move faster and gain the ability to transfer larger momentum during their interaction with the heavy quarks - resulting in the increase of the drag of the heavy quarks propagating through the partonic medium. Similarly the diffusion coefficients increase with T too, as it involve the square of the momentum transfer.

The inverse of the drag co-efficient gives an estimation of the thermalization time scale. Results obtained in the present work within the framework of pQCD indicate that the heavy quarks are unlikely to attain thermalization at RHIC and LHC energies.

The variation of the drag coefficients of charm quarks (due to its interactions with quarks and anti-quarks) with the baryonic chemical potential for different T are displayed in Fig. 3.9. The drag co-efficient for the process : $Qg \to Qg$ is $\sim 8.42 \times 10^{-3}$

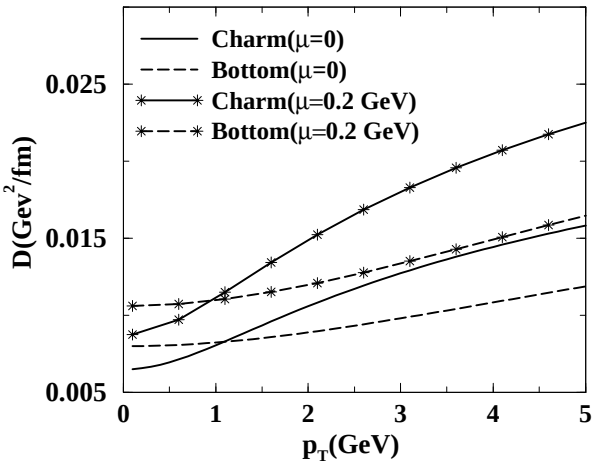

Figure 3.7: Variation of drag coefficient with p_T for $T = 200$ MeV

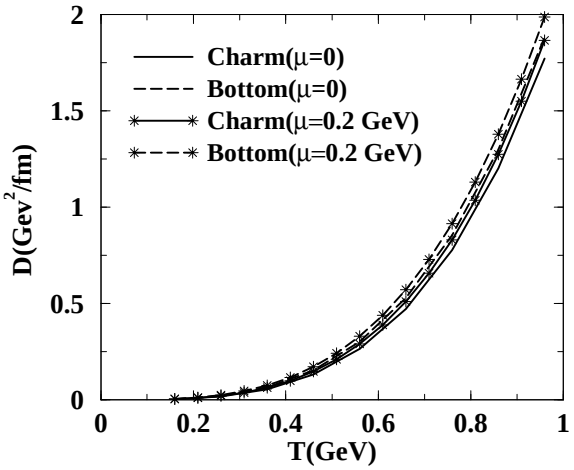

Figure 3.8: Variation of drag coefficient with temperaturefor $p_T = 100$ MeV.

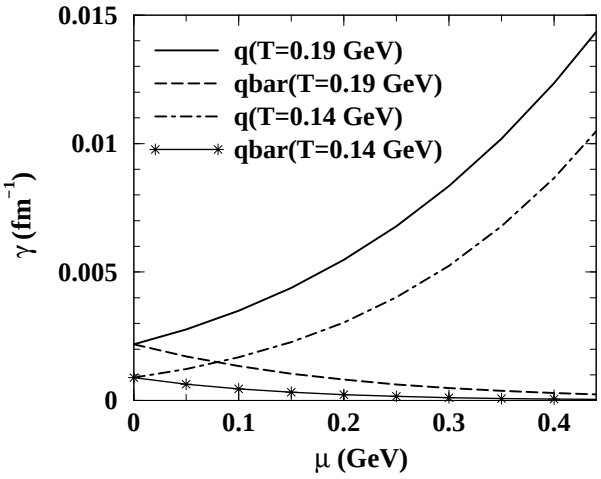

Figure 3.9: Variation of the drag coefficient of charm quark due to its interactions with light quarks and anti-quarks as a function of μ for different temperatures.

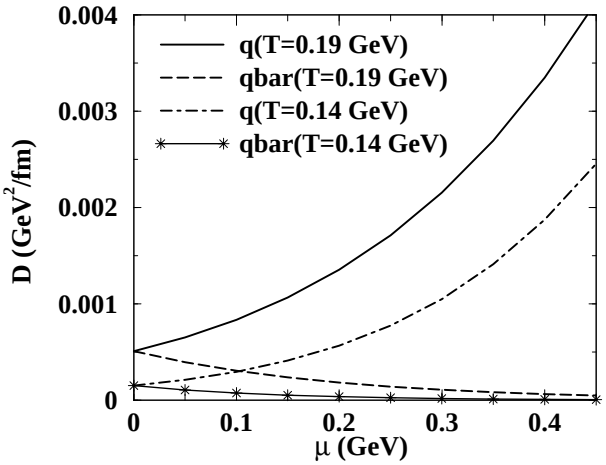

Figure 3.10: Variation of the diffusion coefficient of charm quark due to its interactions with light quarks and anti-quarks as a function of μ for different temperatures.

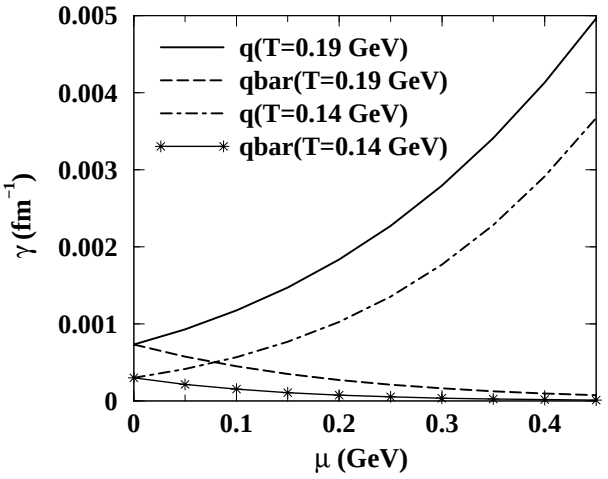

Figure 3.11: Same as Fig. 3.9 for bottom quark

fm^{-1} (1.86×10^{-2} fm^{-1}) for $T = 140$ MeV (190 MeV) (not displayed in Fig. 3.9). The T and μ dependence of the drag and diffusion co-efficients may be understood as follows. As discussed earlier, the drag may be defined as the thermal average of the momentum transfer weighted by the square of the invariant transition amplitude for the reactions $qQ \to qQ$, $Q\bar{q} \to Q\bar{q}$ and $gQ \to gQ$.

The average momentum of the thermal bath quarks increases with both T and μ, which will enable the thermal quarks to transfer larger momentum , which will in turns enhance the drag coefficient. This trend is clearly observed in the results displayed in Fig. 3.9 for charm quark. The drag due to the process $Qq \to Qq$ is larger than the $Q\bar{q} \to Q\bar{q}$ interaction because for non-zero chemical potential, the Q propagating through the medium encounters more q than $\bar{q}$ at a given μ. For vanishing chemical potential the contributions from quarks and anti-quarks are same.

In the same way it may be argued that the diffusion coefficient involves the square of the momentum transfer - which should also increase with T and μ as observed in Fig. 3.10. The diffusion co-efficient for charm quarks due to its interaction with gluons is given by $\sim 1.42\times10^{-3}$ GeV^2/fm (4.31×10^{-3} GeV^2/fm) for $T = 140$ MeV (190 MeV). The drag and diffusion coefficients for bottom quarks are displayed in Figs. 3.11 and 3.12 respectively, showing qualitatively similar behaviour as charm quarks. The drag co-

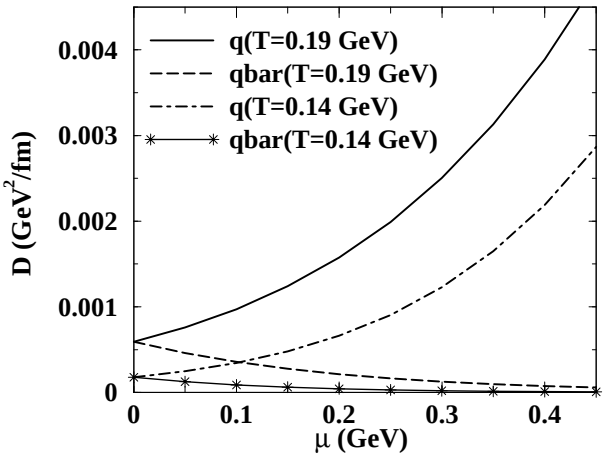

Figure 3.12: Same as Fig. 3.10 for bottom quark.

efficients for bottom quarks due to the process $Qg \to Qg$ is given by $\sim 3.15 \times 10^{-3}$ fm^{-1} and 6.93×10^{-3} fm^{-1} at $T = 140$ MeV and 190 MeV respectively. The corresponding diffusion coefficients are $\sim 1.79 \times 10^{-3}$ GeV^2/fm and 5.38×10^{-3} GeV^2/fm at T=140 MeV and 190 MeV respectively. The μ dependent drag and diffusion coefficients will be used later to evaluate the nuclear suppression of the heavy flavors for low energy RHIC experiments.

3.5.2 Radiative Loss

The energy loss of energetic partons by radiation is a field of high current interest [106, 107, 108, 109, 110, 111]. For mass dependence of energy loss due to radiative processes Dokshitzer and Kharzeev [112] argue that heavy quarks will lose less energy than light quarks due to dead cone effects [113]. However, Aurenche and Zakharov claim that the radiative process has an anomalous mass dependence [114] due to the finite size of the QGP which leads to small difference in energy loss between a heavy and a light quarks. The mass dependence of the transverse momentum spectrum of the radiated gluons from the heavy quarks is studied in [115]. They found that the medium induced gluon radiation fills up the dead cone with a reduced magnitude at large gluon energies compared to the radiation from a light quarks. For high energy heavy quarks the effects of the dead cone, however, reduces because the magnitude

of the angle forbidden for gluon emission behave as $\sim$ heavy quark mass/energy [116]. From the study of the mass dependence of the radiative loss it is shown in [117] that the very energetic charm (not the bottom) quarks behave like massless partons. Although the authors in [118] concluded that the suppression of radiative loss for heavy quarks is due to dead cone effects but it will be fair to state that the issue of similar suppression pattern of HQ and light quark is not settled yet.

The other mechanism which can affect the radiative loss is the LPM effect [119] which depends on the relative magnitude of two time scales of the system [120]: the formation time (τ_F) and the mean scattering time scale (τ_c) of the emitted gluons. If $\tau_F > \tau_c$ then LPM suppression will be effective. The LPM effect is built-in in the expression for radiative energy loss of heavy quarks derived in [115, 116, 117, 121]. In contrast to those, in the present work we will separately introduce the LPM effects in the energy loss formula. Before discusing radiative loss of HQ the radiative loss of gluons is discussed in the next section.

3.6 Radiative Energy Loss of Gluon

Generically the radiative energy loss can be written as $2 \to 2 + g$ process, here we first consider the process $gg \to gg + g$, and the results for other process can be obtained from it in a straight forward way. The typical Feynman diagram for $gg \to gg + g$ is shown in Fig. 3.13. The momentum k_5 of the radiative gluon (Fig. 3.13) is taken to be

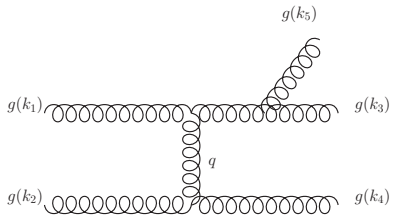

Figure 3.13: A typical Feynman diagram for the process: $gg \to ggg$

a soft radiation around zero rapidity in the centre of momentum frame. The invariant amplitude for this process in medium is given by [122] (see the appendix):

$$|M_{gg\to ggg}|^2 = \left(\frac{4g^4N_c^2}{N_c^2-1}\frac{s^2}{(q_\perp^2+m_D^2)^2}\right)\left(\frac{4g^2N_cq_\perp^2}{k_\perp^2[(k_\perp-q_\perp)^2+m_D^2]}\right) + \frac{16g^6N_c^3}{N_c^2-1}\frac{q_\perp^2}{k_\perp^2[(k_\perp-q_\perp)^2+m_D^2]} \tag{3.45}$$

where $k_\perp$ and $q_\perp$ are the perpendicular component of k_5 and that of the momentum transfer in the centre of momentum frame respectively, m_D is the Debye mass, N_c is the number of colour degrees of freedom. The first parenthesis in the first term in Eq. 3.45 stands for the square of the invariant amplitude for the process: $gg \to gg$

$$|M_{gg\to gg}|^2 = \left(\frac{4g^4N_c^2}{N_c^2-1}\frac{s^2}{(q_\perp^2+m_D^2)^2}\right) \tag{3.46}$$

and the second parenthesis in the first term represents the soft gluon emission spectrum [123]. The second term of Eq. 3.45 is the correction to the squared modulus of the matrix elements. The first term of Eq. 3.45 is reported in Ref. [123]. In the limit $m_D \to 0$ the first term also reproduces the results obtained in Ref. [124] (see also [125, 126, 127]).

The soft gluon multiplicity distribution at fixed $q_\perp$ is given by [123, 124]:

$$\frac{dn_g}{d\eta dk_\perp^2} = \frac{C_A\alpha_s}{\pi^2}\left(\frac{q_\perp^2}{k_\perp^2[(k_\perp-q_\perp)^2+m_D^2]}\right) + \frac{C_A\alpha_s}{\pi^2}\left(\frac{q_\perp^2(q_\perp^2+m_D^2)^2}{s^2k_\perp^2[(k_\perp-q_\perp)^2+m_D^2]}\right) \tag{3.47}$$

where $k = (k_0, k_\perp, k_{3z})$ and $q = (q_0, q_\perp, q_{3z})$ are the four momenta of the emitted and exchanged gluon respectively, $\eta = 1/2\, ln(k_0+k_{3z})/(k_0-k_{3z})$ is the rapidity and $C_A = 3$ is the Casimir invariant of the adjoint representation of SU(3) and $\alpha_s = g^2/4\pi$ is the strong coupling constant.

In Eq. 3.47 the second term is the correction to the soft gluon multiplicity distribution and the first term is know as Gunion-Bertsch (GB) [124] soft gluon multiplicity distribution. Eq. 3.47 can be written as:

$$\frac{dn_g}{d\eta dk_\perp^2} = \left[\frac{dn_g}{d\eta dk_\perp^2}\right]_{GB}\left(1+\frac{(q_\perp^2+m_D^2)^2}{s^2}\right) \tag{3.48}$$

where

$$\left[\frac{dn_g}{d\eta dk_\perp^2}\right]_{GB} = \frac{C_A\alpha_s}{\pi^2}\frac{q_\perp^2}{k_\perp^2[(k_\perp-q_\perp)^2+m_D^2]} \tag{3.49}$$

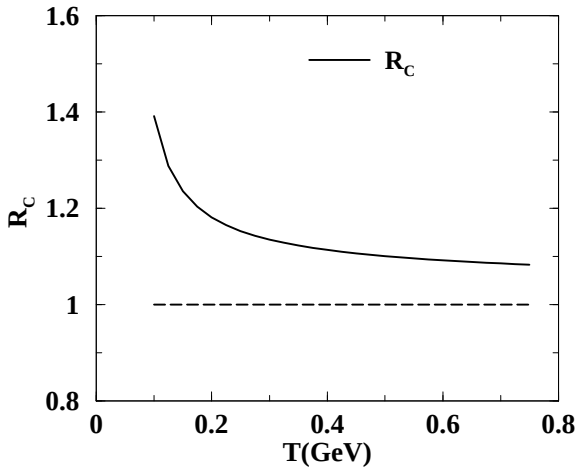

Figure 3.14: The variation of R_c (see Eq. 3.50) with temperature.

To estimate the contributions from the correction term we consider the ratio, R_c given by

$$R_c = \frac{\frac{dn_g}{d\eta dk_\perp^2}}{\left[\frac{dn_g}{d\eta dk_\perp^2}\right]_{GB}} = 1 + \frac{(q_\perp^2 + m_D^2)^2}{s^2} \tag{3.50}$$

We evaluate R_c by substituting $s =< s >= 18T^2$, $m_D = \sqrt{4\pi\alpha_s(T)}\,T$ and $q_\perp^2 =< q_\perp^2 >$ which is calculated by using the following relation:

$$< q_\perp^2 >= \frac{\int dt\, t\, (d\sigma/dt)}{\int dt\, (d\sigma/dt)} \tag{3.51}$$

The lower and upper limits of the above integration are, $= m_D^2$ and $s/4$ respectively. The variation of R_c with T is depicted in Fig. 3.14. The temperature dependence of the strong coupling α_s is taken from [128]. It is observed that the correction to the gluon spectrum is appreciable for low temperature domain. The similar correction in the soft gluon multiplicity distribution can be obtained for the processes $qg \to qgg$ and $qq \to qqg$.

With the soft gluon multiplicity distribution given in Eq. 3.47, the dE/dx is evaluated (details are given in the next section). In Fig. 3.15 the variation of radiative energy loss with T has been depicted for the process $gg \to ggg$. The solid line (dotted line) represents the energy loss when Eq. 3.47(GB) gluon multiplicity distributions are used.

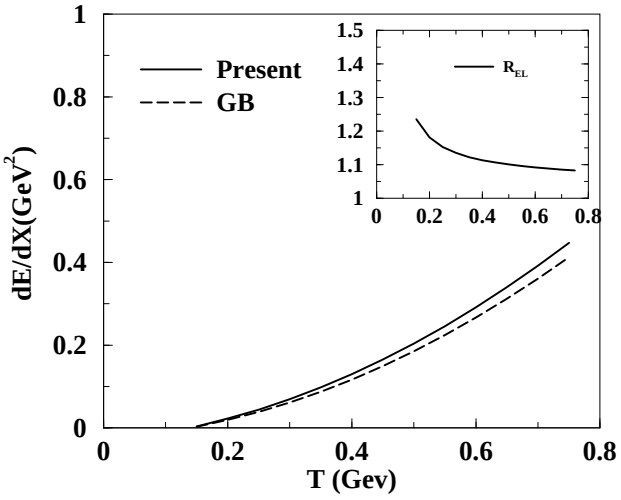

Figure 3.15: The variation of energy loss with temperature for the process: $gg \to ggg$. Here the present in the legend indicates that dE/dx is calculated using gluon spectrum of Eq. 3.47. Inset: The Variation of R_{EL} (Eq. 3.52) with temperature.

To emphasize the importance of the corrections to GB formula we display the ratio,

$$R_{EL} = \frac{Eq.\ 3.47_{EL}}{\mathrm{GB_{EL}}} \tag{3.52}$$

in the inset of Fig. 3.15. It is observed that the correction to the gluon spectrum, which leads to the energy loss is appreciable for lower temperature domain [129]. This may affect the suppression of high p_T partons in QGP and the elliptic flow of the matter formed at RHIC [130] and LHC [131] energies. So it is expected that the values of η/s and ζ/s will also be affected by the correction term in the lower temperature (higher coupling) domain and has been studied in Ref. [129] .

3.7 Radiative Energy Loss of Heavy Quark

The result discussed above can be used for radiative energy loss of heavy quarks due to gluon emission. The matrix element for the radiative process (*e.g.* $Q + q \to Q + q + g$ and $Q + g \to Q + g + g$) can be factorized into an elastic process ($Q + q \to Q + q$ and $Q + g \to Q + g$) and a gluon emission ($Q \to Q + g$). The effects of quark mass can be taken into account by multiplying the emitted gluon distribution from massless quarks

by a factor, F^2 which takes into account the dead cone effects [112, 113]:

$$F = \frac{k_\perp^2}{\omega^2\theta_0^2 + k_\perp^2} \tag{3.53}$$

where $\theta_0 = M/E$, M is the mass and E is the energy of the heavy quarks. This implies in the projectile direction gluon emission off heavy quarks is strongly reduced at radiation angle $\theta < \theta_0 = M/E$. This cone is know as dead cone. Since dead cone effect depends on $\theta = M/E$, for high energy heavy quarks, the effects of the dead cone reduced. For $M = 0$, the factor F^2 will reduced to unity.. The results for the gluon spectrum emitted by a heavy quark of mass M can be obtained by multiplying the Eq. 3.47 by F^2.

Although the correction to GB formula is significant at low temperature domain for the light flavor, however the the correction to the gluon spectrum is not appreciable for the heavy flavor. This is because in case of heavy flavor

$$s =< s >= 2M^2 + 18T^2 \tag{3.54}$$

This indicates that the correction term in Eq. 3.50 will be small for heavy quarks.

As the energy loss of heavy quark by radiative process is equal to the energy which is taken away by the radiated gluon, we can estimate the energy loss of heavy quark by multiplying the interaction rate, Λ and the average energy loss per collision ϵ, which is equal to the average of the probability of radiating a gluon times the energy of the gluon.

The minimum value of the momentum of the exchanged gluon in the process: $gg \to ggg$ sets time (length) scale for the formation time (length) of the emitted gluon. This formation length is the distance over which the amplitude from several interactions can add up coherently to the total cross section. The interaction cross section can change depending on the environment in which the interaction occurs. Multiple scattering [120] can suppress the gluon radiation. If the formation time is comparable to or larger than the mean free time (path) then the scattering of the gluons from the successive scatterers in the medium can not be treated as independent and the scattering amplitudes between two adjacent interaction may interfere destructively leading to the suppression of the emission process - called LPM suppression [119]. The LPM suppression has been taken

into account by including a formation time restriction on the phase space of the emitted gluon in which the formation time, τ_F must be smaller than the interaction time, $\tau = \Gamma^{-1}$, Γ^{-1} being the interaction rate. The radiative energy loss of heavy quark can be written as [148]

$$-\frac{dE}{dx} \mid_{\rm rad} = \Lambda\epsilon = \tau^{-1}.\epsilon \tag{3.55}$$

where ϵ, the average energy loss per collision is [132, 133]

$$\epsilon = <n_g k_0> = \int d\eta d^2k_\perp \frac{dn_g}{d\eta d^2k_\perp} k_0 \Theta(\tau - \tau_F) F^2 \tag{3.56}$$

where $\tau_F = \cosh\eta/k_\perp$. As mentioned before for the infrared cut-off $k_\perp^{min}$ we choose the Debye screening mass of gluon.

$$k_\perp^{min} = m_D = \sqrt{4\pi\alpha_s}T \tag{3.57}$$

The maximum transverse momentum of the emitted gluon is given by [132]:

$$\begin{aligned}(k_\perp^{max})^2 = <\frac{(s-M^2)^2}{4s}> = \frac{3ET}{2} - \frac{M^2}{4} \\ + \frac{M^4}{48pT} ln[\frac{M^2 + 6ET + 6pT}{M^2 + 6ET - 6pT}]\end{aligned} \tag{3.58}$$

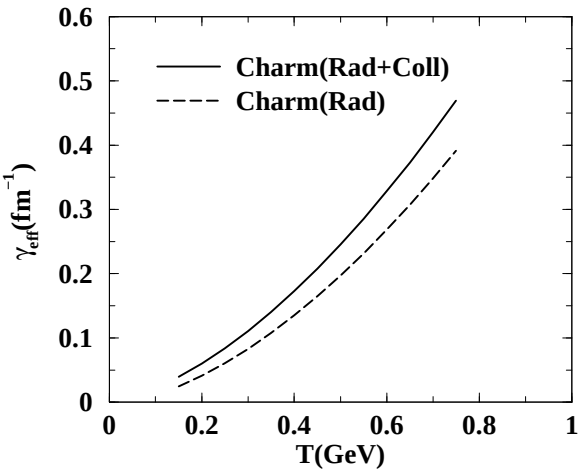

Figure 3.16: Variation of effective drag coefficient with temperature for charm quarks

The radiative energy loss as obtained above is used to obtain the drag coefficient. The action of drag on the heavy quark can be defined through the relation:

$$-\frac{dE}{dx} \mid_{\rm rad} = \gamma_{\rm rad}\, p \tag{3.59}$$

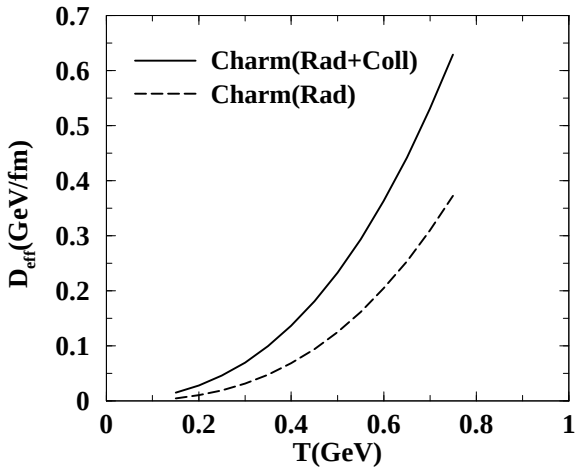

Figure 3.17: Variation of effective diffusion coefficient with temperature for charm quarks

where $\gamma_{\rm rad}$ denotes the drag-coefficient and p is the momentum of the heavy quark. Knowing γ_{rad}, we evaluate the diffusion coefficients for radiative process from the Einstein relation $D_{rad} = \gamma_{rad} MT$.

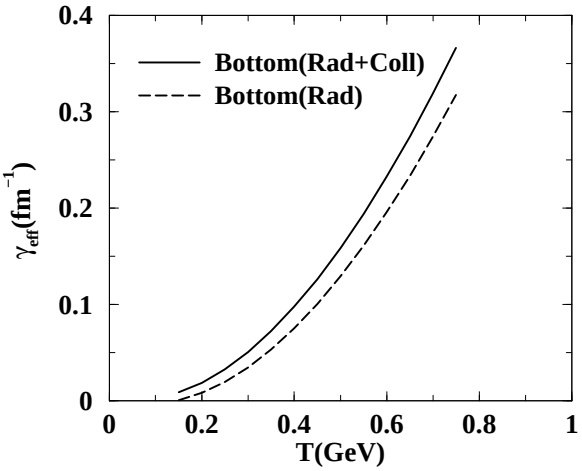

Figure 3.18: Same as Fig. 3.16 for bottom quarks

Following the procedure given in subsection 3.5.1, we evaluate the γ and D for the elastic processes and redefined them as $\gamma_{\rm coll}$ and $D_{\rm coll}$ respectively. It should be mentioned here that the collisional and the radiative processes are not entirely independent,

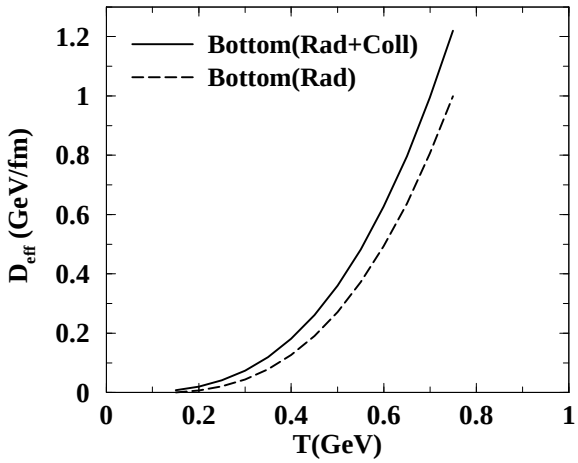

Figure 3.19: Same as Fig. 3.17 for bottom quarks

i.e. the collisional process may influence the radiative one, therefore strictly speaking dE/dx and hence the transport coefficients for radiative and collisional process may not be added to obtain the net energy loss or net value of the drag coefficient. However, in the absence any rigorous way, we add them up to obtain the effective drag and diffusion coefficients as, $\gamma_{\rm eff} = \gamma_{\rm rad} + \gamma_{coll}$ and $D_{\rm eff} = D_{\rm rad} + D_{\rm coll}$ respectively. This is a good approximation for the present work because the radiative loss is large compared to the collisional loss at Relativistic Heavy Ion Collider (RHIC) and Large Hadron Collider (LHC) energies.

With these effective transport coefficients the FP equation reads:

$$\frac{\partial f}{\partial t} = \frac{\partial}{\partial p_i}\left[\gamma_{\rm eff}(p) f + \frac{\partial}{\partial p_i}[D_{\rm eff}(p) f]\right] \tag{3.60}$$

where $\gamma_{\rm eff}$ and $D_{\rm eff}$ contain contributions from both the mechanisms (collisional and radiative). In evaluating the drag coefficient we have used temperature dependent strong coupling, α_s from [128]. The Debye mass, $\sim g(T)T$ is also a temperature dependent quantity used as cut-off to shield the infrared divergences arising due to the exchange of massless gluons.

In Figs. 3.16 and 3.17 the variation of effective drag and diffusion coefficients with T have been depicted for charm quarks. We observe that the contribution of the radiative loss is large compared to the collisional or elastic one. The difference between the colli-

sional and radiative loss increases with temperature - indicating very small contribution from the former at large T. Similar difference is reflected in the diffusion coefficients as we have used Einstein's relation to obtain it from the drag coefficients. We observe that at low T and p_T the contributions from collisional processes is more than or comparable to that from radiative processes. For the bottom quark we find that the gap between the drag coefficients with radiative and elastic processes is smaller (compared to charm) at lower temperature domain. Quantitatively the value of drag is smaller for bottom than charm quarks because of their larger relaxation time. However, the qualitative behaviour is similar to charm quarks as shown in Fig. 3.18. The diffusion coefficient of the bottom quark is large (Fig.3.19) compared to the charm quark because of the large mass of the former introduced through the Einstein's relation.

Chapter 4

Nuclear Suppression Factor

4.1 Introduction

The main aim of this chapter is to study the heavy flavor transport in an expanding system of QGP produced in relativistic heavy-ion collisions. One of the most interesting observable investigated at RHIC is the depletion of high p_T hadrons (D and B mesons) produced in Nucleus + Nucleus collisions with respect to those produced in proton + proton (pp) collisions expressed through the nuclear modification factor $R_{\rm AA}$ [93, 94, 95]. The $R_{\rm AA}$ involves measurement of the non-photonic single electron spectra originating from the semi-leptonic decays of the D and B mesons. To compare our results with the experiment, we need to have a realistic evolution of the expanding QGP as well as hadronization of the charm and bottom quarks into D and B mesons spectra and their subsequent decay to the non-photonic single electrons.

4.2 Space-Time Evolution

The system formed in nuclear collisions at relativistic energies evolves dynamically from the initial state (T_i) to the final state (T_c). The time evolution of such systems may be studied by using the relativistic hydrodynamic equations:

$$\partial_\mu T^{\mu\nu} = 0 \tag{4.1}$$

where $T^{\mu\nu} = (\epsilon + P)u^\mu u^\nu - g^{\mu\nu}P$, is the energy momentum tensor for ideal fluid, ϵ is the energy density, P is the pressure and u^μ is the hydrodynamic four velocity, and $g^{\mu\nu}$

is the metric tensor. We will solve this equation for longitudinal expansion with boost invariance along the z direction [85]. It is expected that the central rapidity region of the system formed after nuclear collisions at RHIC and LHC energy is almost net baryon free. Therefore, the equation governing the conservation of net baryon number need not be considered here. Under this circumstance Eq. 4.1 reduces to:

$$\frac{\partial \epsilon}{\partial \tau} + \frac{\epsilon + P}{\tau} = 0 \tag{4.2}$$

To solve Eq. 4.2, we use the relation $P = c_s^2 \epsilon$, where c_s is the velocity of sound. With this we arrive with the relation

$$\epsilon \tau^{1+c_s^2} = C \tag{4.3}$$

where C is a constant. For the ideal equation of state, $c_s^2 = \frac{1}{\sqrt{3}}$, the above Eq. reads $\epsilon \tau^{\frac{4}{3}} = C$. In terms of temperature this relation can be written as $\tau T^3 = C$.

The total amount of energy dissipated by a heavy quark in the expanding QGP depends on the path length it traverses. Each parton traverse different path length which depends on the geometry of the system and on the point where its is created. The probability that a parton is produced at a point (r, ϕ) in the plasma depends on the number of binary collisions at that point which can be taken as [134]:

$$P(r, \phi) = \frac{2}{\pi R^2}(1 - \frac{r^2}{R^2})\theta(R - r) \tag{4.4}$$

where R is the nuclear radius. It should be mentioned here that the expression in Eq. (4.4) is an approximation for the collisions with zero impact parameter. A parton created at (r, ϕ) in the transverse plane propagate a distance $L = \sqrt{R^2 - r^2 sin^2\phi} - rcos\phi$ in the medium. In the present work we use the following equation for the geometric average of the integral involving drag coefficient [$\int d\tau \gamma(\tau)$, e.g. the factor in Eq. 3.17]:

$$\Gamma = \frac{\int r dr d\phi P(r, \phi) \int^{L/v} d\tau \gamma(\tau)}{\int r dr d\phi P(r, \phi)} \tag{4.5}$$

where v is the velocity of the propagating partons. Similar averaging has been performed for the diffusion coefficient. For a static system the temperature dependence of the drag and diffusion coefficients of the heavy quarks enter via the thermal distributions of light quarks and gluons through which it is propagating. However, in the present scenario

the variation of temperature with time is governed by the equation of state or velocity of sound of the thermalized system undergoing hydrodynamic expansion. In such a scenario the quantities like Γ (Eq. 4.5) and hence the HQ suppression becomes sensitive to c_s.

4.3 Initial Condition

As discussed earlier, the propagation of HQ through QGP can be treated as the interactions between equilibrium and non-equilibrium degrees of freedom, where the non-equilibrium heavy quark executing Brownian motion in the thermal bath of QGP. So we are solving two sets of differential equations, (i) relativistic hydrodynamic equations (given in Eq. 4.1) for the thermal bath and (ii) Fokker-Planck equation (given in Eq. 3.9) for the heavy quarks. Therefore, any change in the properties of the bath affect the heavy quarks Brownian motion through the drag and diffusion coefficients. Hence, the nuclear suppression for heavy quarks depend on the parameters like initial temperature (T_i), thermalization time (τ_i), equation of state (EOS) and the transition temperature (T_c).

We assume that the system reaches equilibration at a time τ_i after the collision at temperature T_i which are related to the produced hadronic (predominantly mesons) multiplicity through the following relation:

$$T_i^3 \tau_i \approx \frac{2\pi^4}{45\zeta(3)} \frac{1}{4a_{eff}} \frac{1}{\pi R_A^2} \frac{dN}{dy}. \tag{4.6}$$

where R_A is the radius of the system, $\zeta(3)$ is the Riemann zeta function and $a_{eff} = \pi^2 g_{eff}/90$, g_{eff} $(= 2 \times 8 + 7 \times 2 \times 2 \times 3 \times N_F/8)$ is the degeneracy for the QGP, N_F=number of flavours.

For the RHIC and the LHC energies we consider a net baryon-free QGP, therefore the baryonic chemical potential (μ_B) is zero. At the RHIC energy, the predicted hadron multiplicity $dN/dy = 1100$ [130] goes as input to Eq. 4.6. We have taken initial thermalization time $\tau_i = 0.2$ fm/c, which gives $T_i = 400$ MeV. Similarly at the LHC energy the predicted hadron multiplicity at mid-rapidity, $dN/dy = 2100$ [135]. The value of the initial thermalization time is assumed as 0.08 fm/c. The corresponding initial tem-

perature is T_i = 700 MeV. For both RHIC and LHC the transition temperature has been taken as $T_c = 170MeV$. The initial condition required to solve the FP equation is already discussed in section 3.3.

4.4 D and B-meson Spectra

To establish a connection with the experimental results, we need to implement the hadronization mechanisms once the temperature of the system produced in high energy heavy ion collision, reached the quark-hadron transition temperature (T_c). For the hadronization, we have employed the fragmentation function, $D_{h/x}$, which gives the probability distribution of a parton x of momentum p_x to hadronizes into a hadron, h, carrying a momentum fraction $z = p_h/p_x$ of the parent parton, where $0 < z < 1$.

We convolute the solution of the FP equation with the fragmentation functions of the heavy quarks to obtain the p_T distribution of the heavy mesons (D and B) ($dN^{D,B}/q_T dq_T$). For heavy quark fragmentation, the following three sets of fragmentation functions are used: 1. SET-I [136]

$$f(z) \propto \frac{1}{z^{1+r_Q bm_Q^2}}(1-z)^a exp(-\frac{bm_T^2}{z}) \tag{4.7}$$

where m_Q is the mass of the charm quark, r_Q =1, $a = 5, b = 1$ and $m_T^2 = m_Q^2 + p_T^2$. It has been explicitly checked that the R_{AA} is not very sensitive to the values of a and b.
2. SET-II [137]

$$f(z) \propto z^\alpha (1-z) \tag{4.8}$$

where $\alpha = -1$ for charm quark and it is 9 for bottom
3. SET-III [138]

$$f(z) \propto \frac{1}{[z[z - \frac{1}{z} - \frac{\epsilon_c}{1-z}]^2]} \tag{4.9}$$

for charm quark $\epsilon_c = 0.05$ and for bottom quark $\epsilon_b = (m_c/m_b)^2 \epsilon_c$. The role of different fragmentation function on the experimental observables will discuss in the next section.

Recently, the p_T spectra of D mesons has been measured by the STAR collaboration [139] in Au+Au collisions at $\sqrt{s_{NN}}$ = 200 GeV. The p_T spectrum of hadrons can

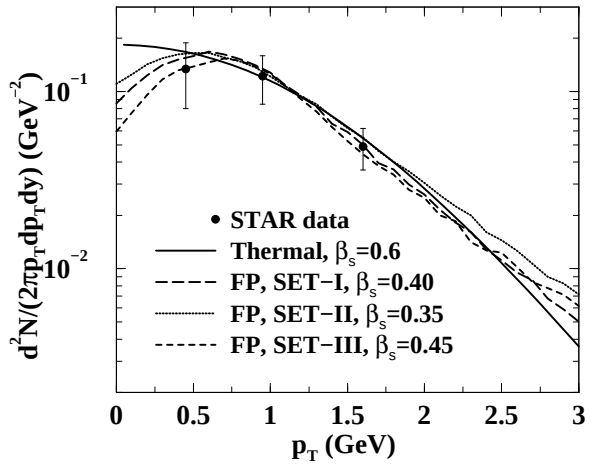

Figure 4.1: Invariant momentum distribution of the D-meson as a function of p_T.

be written as [140]

$$\frac{dN}{d^2p_T dy} = \frac{g}{(2\pi)^3}\int \tau r d\phi d\eta (m_T cosh(\eta - y) dr - p_T cos\phi d\tau) f(u^\mu p_\mu) \tag{4.10}$$

η is the space time rapidity, p^μ is the four momentum and $u^\mu = \gamma(1, \beta)$ is the hydrodynamic four velocity, $u^\mu p_\mu$ is the energy of the hadrons in the co-moving frame of the plasma and $f(u^\mu p_\mu)$ is the momentum space distribution. In the spirit of the blast wave method we can write Eq. 4.10 as [141]:

$$\frac{dN}{d^2p_T dy} = \frac{g}{(2\pi)^3}\int \tau r d\phi d\eta \; m_T cosh(\eta - y) f(u^\mu p_\mu) dr \tag{4.11}$$

Taking the surface velocity profile as:

$$\beta(r) = \beta_s \left(\frac{r}{R}\right)^n \tag{4.12}$$

and choosing n=1, the p_T spectra of D mesons is evaluated. Before comparing the data with non-equilibrium momentum distribution we analyze the data within the ambit of the blast wave method [141] assuming a equilibrium distribution for the D-meson. The values of the blast wave parameters *i.e.* the radial flow velocity at the surface, β_s and the freeze-out temperature, T_F are 0.6 and 0.170 GeV respectively. The data

is reproduced well (Fig.4.1). The value of T_F is close to T_c, which indicate that the D-mesons (even if the charm is in equilibrium in the partonic phase) can not maintain it in the hadronic phase. This is reasonable because of the low interaction cross sections of the D mesons with other hadrons. Next we replace the equilibrium distribution in Eq. 4.11 by the solution of FP equation appropriately boosted by the radial velocity. The results are displayed in Fig. 4.1. The data is reproduced well for all the three sets of fragmentation functions mentioned before. The value of the freeze-out temperature is 170 MeV and the flow velocity at the surface is 0.45, 0.35 and 0.4 for SET-I, SET-II and SET-III fragmentation functions respectively. The values of β_s is lower here than the equilibrium case for all the fragmentation function. It is interesting to note that at low $p_T(\leq 0.5$ GeV) domain the results for equilibrium distribution substantially differ from the non-equilibrium distribution for all the three sets of fragmentation functions. Therefore, measurements of the heavy meson spectra at low p_T domain will be very useful to distinguish between the equilibrium and the non-equilibrium scenarios. The two scenarios also give different kind of variation at large p_T. The p_T integrated quantity, *i.e.* the D meson multiplicity may also be useful to understand the difference between the equilibrium and non-equilibrium scenarios.

4.5 Semileptonic Decay of D an B-meson

The non-photonic single electron spectra originating from the decays of heavy flavoured mesons - *e.g.* $D \rightarrow Xe\nu$ or $B \rightarrow Xe\nu$ at mid-rapidity ($y = 0$) can be obtained as follows [142, 143]:

$$\frac{dN^e}{p_T dp_T} = \int dq_T \frac{dN^D}{q_T dq_T} F(p_T, q_T) \tag{4.13}$$

where

$$F(p_T, q_T) = \omega \int \frac{d(\mathbf{p_T}.\mathbf{q_T})}{2p_T \mathbf{p_T}.\mathbf{q_T}} g(\mathbf{p_T}.\mathbf{q_T}/\mathbf{M}) \tag{4.14}$$

where M is the mass of the heavy mesons (D or B), $\omega = 96(1 - 8m^2 + 8m^6 - m^8 - 12m^4 ln m^2)^{-1} M^{-6}$ ($m = M_X/M$) and $g(E_e)$ is given by

$$g(E_e) = \frac{E_e^2 (M^2 - M_X^2 - 2ME_e)^2}{(M - 2E_e)} \tag{4.15}$$

related to the rest frame spectrum for the decay $D \rightarrow Xe\nu$ through the following relation [142]

$$\frac{1}{\Gamma_H}\frac{d\Gamma_H}{dE_e} = \omega g(E_e). \tag{4.16}$$

We evaluate the electron spectra from the decays of heavy mesons originating from the fragmentation of the heavy quarks propagating through the QGP. Similarly the electron spectrum from the p-p collisions can be obtained from the charm and bottom quark distribution which goes as the initial conditions to the solution of FP equation. The ratio of these two quantities can be treated as the nuclear suppression factor, R_{AA} measured in experiments, will be unity in the absence of any medium. The experimental data [93, 94, 95] for single electron originated from both D and B-decays at RHIC energy ($\sqrt{s_{NN}}$=200 GeV) shows substantial suppression ($R_{AA} < 1$) for $p_T \geq 2$ GeV indicating substantial interaction of the plasma particles with charm and bottom quarks from which electrons are produced through the process: $c(b)$ (hadronization)$\longrightarrow D(B)$(decay)$\longrightarrow e + X$. The loss of energy of high momentum heavy quarks propagating through the medium created in Au+Au collisions causes a depletion of high p_T electrons.

4.6 Nuclear Suppression at RHIC

4.6.1 Collisional Loss

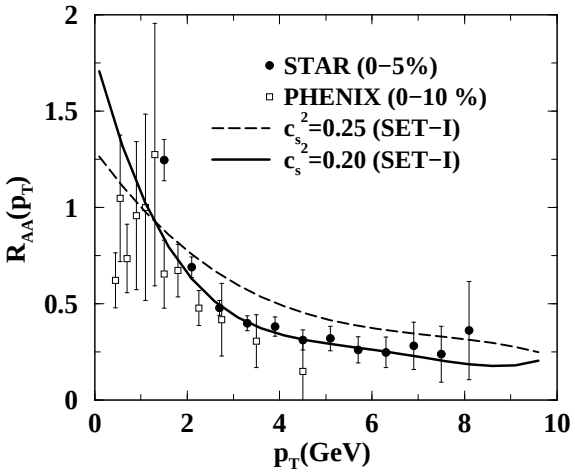

Figure 4.2: Nuclear suppression factor, $R_{\rm AA}$ as function of p_T.

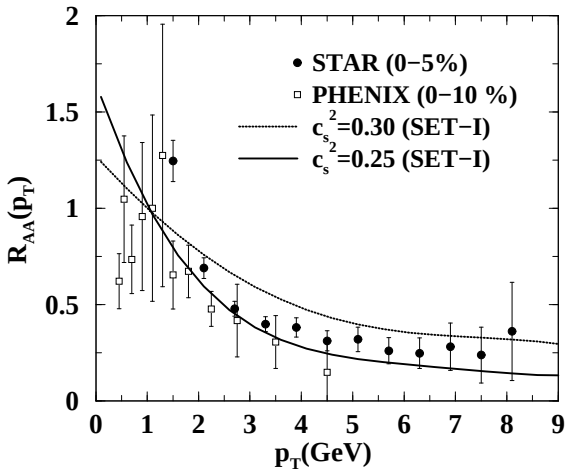

Figure 4.3: Same as Fig. 4.2 with enhancement of the cross section by a factor of 2.

In this section the focus is on the R_{AA} along with its sensitivity to EoS and fragmentation function within the framework of collisional loss [144] for the RHIC energy. The results for R_{AA} is displayed in Fig. 4.2. The theoretical results are obtained for fragmentation function of SET-I [136]. The velocity of sound for the QGP phase is taken as $c_s = 1/\sqrt{4}$ corresponds to the equation of state, $p = \epsilon/4$. The results failed to describe the data in this case. Next we generate R_{AA} by changing the value of c_s to $1/\sqrt{5}$ and keeping all the other parameters fixed. The resulting spectra describes the data reasonably well. Lower value of c_s makes the expansion of the plasma slower enabling the propagating heavy quarks to spend more time to interact in the medium and hence lose more energy before exiting from the plasma.

We enhance the cross section by a factor of 2 and find that the experimental results can also be explained by taking an EoS $P = \epsilon/4$ (Fig4.3) and keeping all other quantities unchanged. The ideal gas EoS $P = \epsilon/3$ can not reproduce the data even if the cross section is enhanced by a factor of 2. With $c_s = 1/\sqrt{4}$ and enhanced cross section (by a factor 2) the data can also be described with for fragmentation functions of set-II and set-III as shown in Fig. 4.4. Several mechanisms like inclusions of non-perturbative contributions from the quasi-hadronic bound state [89], 3-body scattering effects [102] and employment of running coupling constants and realistic Debye mass [104] have been proposed to improve the description of the experimental data. As the effect of different

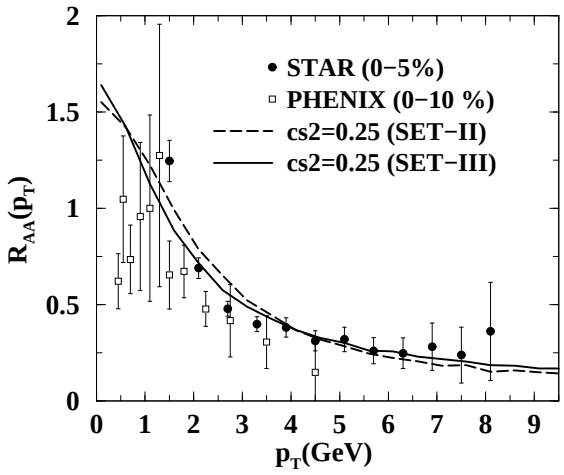

Figure 4.4: Same as Fig. 4.3 for fragmentation functions of SET-II and III.

fragmentation functions on the nuclear suppression is small, from the next section we will only consider set-III, commonly called Peterson fragmentetion function [138].

4.6.2 Radiative loss

For electromagnetic processes, it is well known that at large energies, radiative losses are much higher than the collisional loss. In QCD several authors [59, 97, 101, 132, 145, 146, 147, 148] have emphasized on the radiative energy loss mechanism. In [100, 149] it was shown that, radiative and collisional energy losses for heavy quarks were comparable to each other, and therefore, radiative energy loss can not be neglected in the computation of the nuclear suppression factor. In this section implementation of radiative loss [148] has been done as an improvement to our earlier calculation of collisional loss. This will also give an opportunity to study, whether the inclusion of radiative loss compensate the additional enhanced factor (by a factor 2), as required to reproduce the data. As a further improvement along with the inclusion of radiative loss, we have used temperature dependent strong coupling, α_s [128] for evaluating the drag and diffusion co-efficients. The Debye mass, $\sim g(T)T$ is also a temperature dependent quantity used as cut-off to shield the infrared divergences arising due to the exchange of massless gluons. It may be mentioned here that the implementation of running coupling and temperature dependent Debye mass change the drag and diffusion coefficients

significantly in compare to the fixed value of strong coupling [104].

The value of R_{AA} is plotted against the p_T of the non-photonic single electron resulting from D and B decays in Fig 4.5. The results show substantial depletion at large p_T indicating large interaction rate of the charm quarks with the thermal medium of partons.

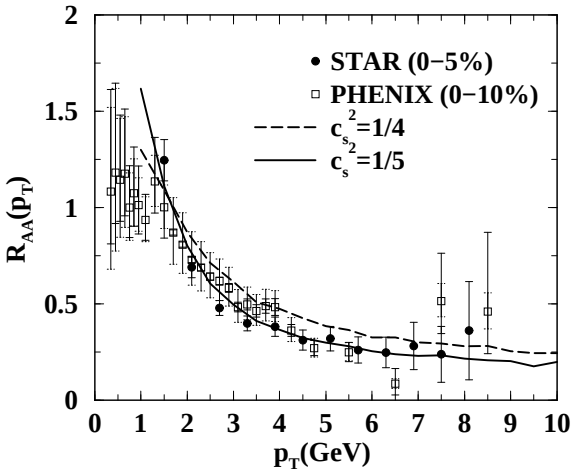

Figure 4.5: Comparison of $R_{\rm AA}$ obtained in the present work with the experimental data obtained by STAR and PHENIX collaboration for $\sqrt{s_{\rm NN}} = 200$ GeV. The experimental data of STAR and PHENIX collaborations are taken from [93] and [95] respectively.

In Fig. 4.5 we compare the experimental data obtained by the STAR [93] and PHENIX [95] collaborations for Au + Au collisions at $\sqrt{s_{\rm NN}} = 200$ GeV with theoretical results obtain in the present work. We observe that the data can reasonably be reproduced by taking velocity of sound $c_s = 1/\sqrt{4}$. It should be mentioned here that the inclusion of both radiative and elastic losses in the effective drag enables us to reduce the gap between the experiment and theory without any enhancement of the pQCD cross section as has been done in previously [144].

As data is well reproduced without any enhancement of the pQCD cross section for the RHIC energy, the same formalism has been applied to study the non-photonic single electron spectra at the LHC energy. The value of R_{AA} is plotted against the p_T of the non-photonic single electron resulting from D decays in Fig 4.6. The results show substantial depletion at large p_T indicating large interaction rate of the charm quarks

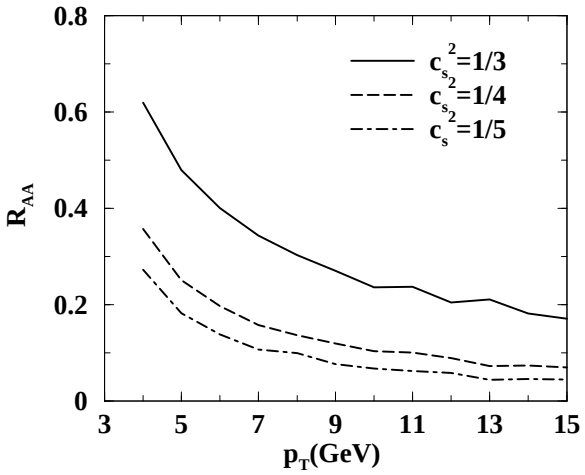

Figure 4.6: Nuclear suppression factor, $R_{\rm AA}$ as a function of p_T for various equation of state for non-photonic single electron resulting form D-mesons decay.

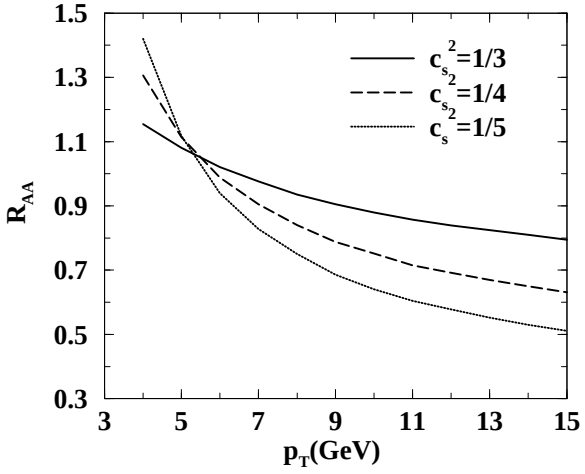

Figure 4.7: Same as Fig. 4.6 for B mesons.

with the thermal medium of partons. The sensitivity of the results on the equation of state is also demonstrated in Fig. 4.6. The value of c_s for the QGP produced at LHC may be larger than the value of c_s for QGP that produced at RHIC. Keeping this in mind we predict the nuclear suppression factors for three values of $c_s = 1/\sqrt{3}$ (maximum possible), $1/\sqrt{4}$ and $1/\sqrt{5}$ (Fig.4.6).

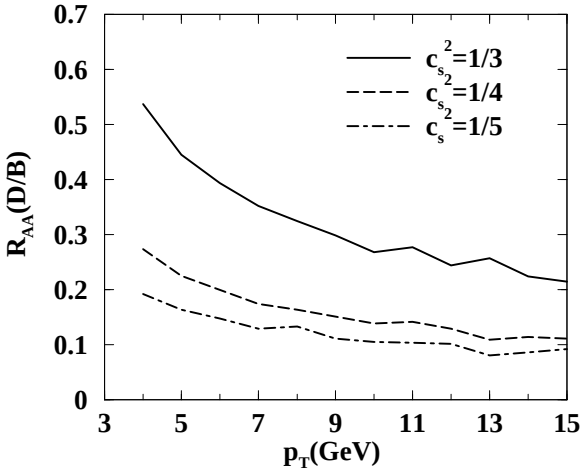

Figure 4.8: Variation of the ratio of nuclear suppression factor, $R_{\rm AA}$ for charm to bottom quarks as a function of p_T.

The nuclear suppression for the bottom quarks are displayed in Fig. 4.7. We observe quantitatively less suppression compare to charm quarks. The difference between the charm and bottom quarks suppression are affected chiefly by two factors: (i) for different values transport coefficients and (ii) for the different kind of initial p_T distributions. The bottom quark has less drag coefficients and has harder p_T distributions - both these factors are responsible for the smaller suppression of bottom quark. The present results on $R_{\rm AA}$ is similar to that obtained in [150] (see also [151]) in a different approach.

In Fig 4.8 we have plotted the ratio: $R^D_{\rm AA}/R^B_{\rm AA}$ as a function of p_T, from where the effect of the mass and the role of the initial p_T distributions (soft or hard) can be understood (see also [152]). Within the range of p_T considered here the suppression of D is always seems to be larger than B.

4.7 Nuclear Suppression in Baryon Rich QGP

For low energy collisions, the radiative energy loss of heavy quarks will be much smaller than the loss caused by elastic processes. Moreover, the thermal production of charm and bottom quarks can be ignored in the range of temperature and baryonic chemical potential under study. Therefore, we can apply the FP equation for the description of HQ evolution in the baryon rich QGP. Here we need to solve the FP equation for non-zero μ_B. The drag and diffusion coefficients are functions of both the thermodynamical variables: μ_B and T.

The energy dependence of the chemical potential can be obtained from the parametrization of the experimental data on hadronic ratios as [153] (see also [154]),

$$\mu_B(s_{\rm NN}) = a(1 + \sqrt{s_{\rm NN}}/b)^{-1} \tag{4.17}$$

where $a = 0.967 \pm 0.032$ GeV and $b = 6.138 \pm 0.399$ GeV. The parametrization in Eq. 4.17 gives the values of μ_B(chemical potential carried by the quarks $\mu(= \mu_B/3)$) at the freeze-out. At mid rapidity, the chemical potential of the system decrease with respect to the colliding energy as observed in Fig. 4.9. So the composition of matter produced at LHC and RHIC is different from the matter produced at low energy collision. At LHC and RHIC the matter produced at the mid rapidity is almost baryon free, where as the matter produced at the low colliding energy are dominated by baryons.

To take care of this extra baryons we need to solve the baryon-number conservation equation along with the energy-momentum conservation equation. i.e. we simultaneously solve

$$\partial_\mu T^{\mu\nu} = 0 \tag{4.18}$$

and

$$\partial_\mu n_B^\mu = 0 \tag{4.19}$$

for (1+1) dimension with boost invariance along the longitudinal direction [85]. In the above equation $n_B^\mu = n_B u^\mu$ is the baryonic flux and u^μ is the hydrodynamic four velocity. The initial baryonic chemical potential carried by the quarks $\mu(= \mu_B/3)$ are shown in Table 4.1 for various $\sqrt{s_{\rm NN}}$ under consideration.

Table 4.1: The values center of mass energy , dN/dy, initial temperature (T_i) and quark chemical potential - used in the present calculations.

$\sqrt{(s_{\rm NN})}$(GeV)	$\frac{dN}{dy}$	T_i(MeV)	μ(MeV)
39	617	240	62
27	592	199	70
17.3	574	198	100
7.7	561	197	165

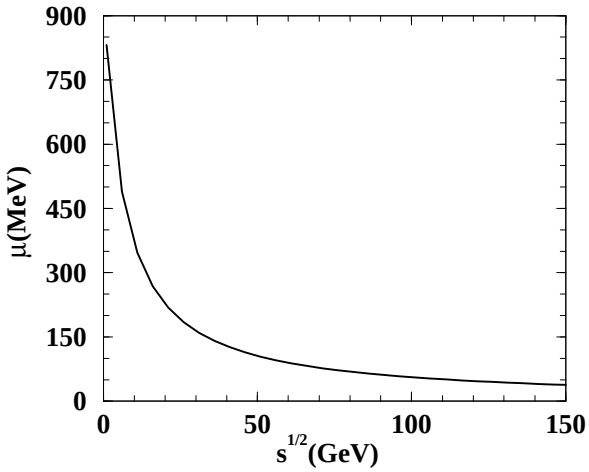

Figure 4.9: Variation of μ_B with respect to the $\sqrt{s_{\rm NN}}$.

The value of the multiplicities for various $\sqrt{s_{\rm NN}}$ have been calculated from the Eq. below [155];

$$\frac{dN}{dy} = \frac{dn_{pp}}{dy}\left[(1-x)\frac{< N_{part} >}{2} + x < N_{coll} >\right] \tag{4.20}$$

N_{coll} is the number of collisions and contribute x fraction to the multiplicity dn_{pp}/dy measured in pp collision. The number of participants, N_{part} contributes a fraction $(1-x)$ to dn_{pp}/dy, which is given by

$$\frac{dn_{pp}}{dy} = 2.5 - 0.25ln(s) + 0.023ln^2(s) \tag{4.21}$$

The values of N_{part} and N_{coll} are estimated for $(0-5\%)$ centrality's by using Glauber Model [156]. The value of x depends very weakly on $\sqrt{s_{\rm NN}}$ [157], in the present work we have taken $x = 0.1$ for all the energies.

We need the initial heavy quark momentum distributions for solving the FP equa-

tion. For low collision energy rigorous QCD based calculations for heavy flavour production is not available. In the present work the initial HQ distribution is obtained from pQCD calculation [105, 158] for the processes: $gg \to Q\bar{Q}$ and $q\bar{q} \to Q\bar{Q}$.

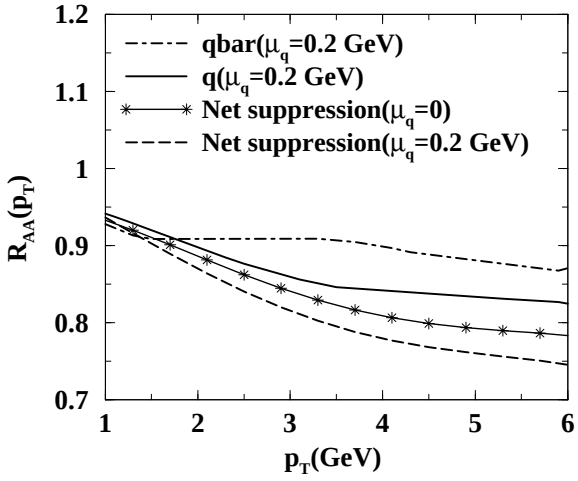

Figure 4.10: The nuclear suppression factor R_{AA} as a function of p_T due to the interaction of the charm quark (solid line) and anti-quark (dashed-dot line) for $\mu = 200$ MeV. The net suppressions including the interaction of quarks, anti-quarks and gluons for $\mu = 200$ MeV (dashed line) and $\mu = 0$ (with asterisk) are also shown.

To demonstrate the effect of non-zero baryonic chemical potential we evaluate $R_{\rm AA}$ for $\mu = 200$ MeV and $\mu = 0$ for a given $T_i = 200$ MeV. The results are displayed in Fig. 4.10 - representing the combined effects of temperature and baryon density on the drag and diffusion coefficients. The drag on the heavy quarks due to its interaction with quarks is larger than that of its interactions with the anti-quarks (Fig.3.9). Resulting in larger suppression in the former case than the later. The net suppression of the electron spectra from the Au+Au collisions compared to p+p collisions is effected by quarks, anti-quarks and gluons. The results for net suppressions are displayed for $\mu = 200$ MeV (dashed line) and $\mu = 0$ (with asterisk). The experimental detection of the non-zero baryonic effects will shed light on the net baryon density (and hence baryon stopping) in the central rapidity region. However, whether the effects of non-zero baryonic chemical potential is detectable or not will depend on the overall experimental performance.

The results for R_{AA} are shown in Fig. 4.11 for various $\sqrt{s_{NN}}$ with inputs from Ta-

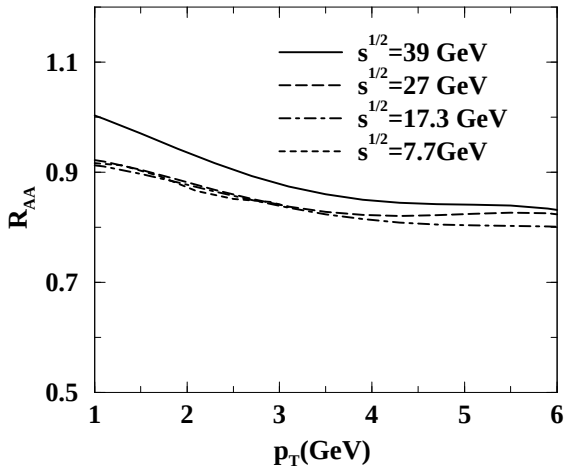

Figure 4.11: Nuclear suppression factor, $R_{\rm AA}$ as function of p_T for various $\sqrt{s_{NN}}$.

ble 4.1. We observe that at large p_T the suppression is similar for all energies under consideration. This is because the collisions at high $\sqrt{s_{NN}}$ are associated with large temperature but small baryon density at mid-rapidity- which is compensated by large baryon density and small temperature at low $\sqrt{s_{NN}}$ collisions. Low p_T particles predominantly originate from low temperature and low density part of the evolution where drag is less and so is the nuclear suppression.

It has been shown in [159] that a large enhancement of the pQCD cross section is required for the reproduction of experimental data on elliptic flow at RHIC energies. In our earlier work [144] we have evaluated the $R_{\rm AA}$ for non-photonic single electron spectra resulting from the semileptonic decays of hadrons containing heavy flavours and observed that the data from RHIC collisions at $\sqrt{s_{NN}} = 200$ GeV are well reproduced by enhancing the pQCD cross sections by a factor 2 and with an equation of state $P = \epsilon/4$ for collisional loss. In the same spirit we evaluate $R_{\rm AA}$ with twice enhanced pQCD cross section and keeping all other quantities unaltered (Fig. 4.12). The results in Fig. 4.12 show stronger suppression as compared to the results displayed in Fig. 4.11, but it is similar in all the energies under consideration. When we have enhanced the pQCD cross section for the interaction of the heavy quarks with the thermal system by a factor of two - the resulting suppressions in R_{AA} are between $20\% - 30\%$ for $\sqrt{s_{NN}} = 39 - 7.7$ GeV.

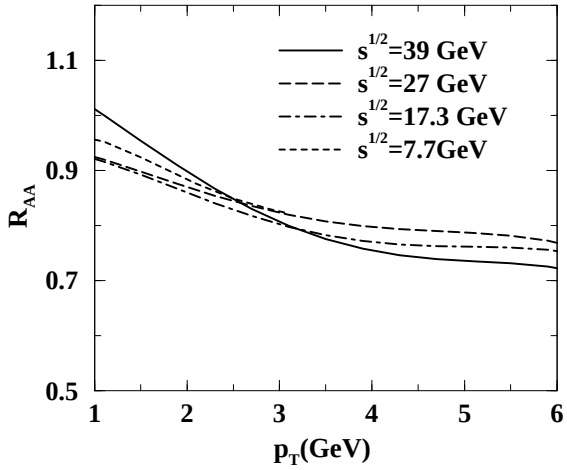

Figure 4.12: Same as Fig. 4.11 with enhancement of cross section by a factor of 2.

Chapter 5

Elliptic Flow

5.1 Introduction

The elliptic flow (v_2) of the produced particles have been considered as one of the most promising signals for the early thermalization of the matter formed in heavy ion collision. It is also sensitive to the initial condition and the equation of state (EoS) of the evolving matter formed in heavy ion collision [21, 65, 66]. Our aim is to calculate the elliptic flow of Heavy Flavor (v_2^{HF}) produced in nuclear collision at relativistic energies [95, 96] within the framework of FP equation.

If nucleus-nucleus collisions were simple superpositions of nucleon-nucleon collisions, the produced particles would have isotropic distributions, irrespective of the shape of the collision zone in the transverse plane. However, if the interactions among the produced particles are sufficiently strong to bring the system close to local equilibrium, then a collective motion emerges: strong pressure gradients are induced by the anisotropy of the initial interaction zone, leading to anisotropic momentum distributions. The elliptic flow has been observed at RHIC, and is a beautiful evidence of collective behavior and (at least partial) thermalization of the produced matter.

5.2 Formalism

The azimuthal momentum anisotropy of particle emission from non-central heavy-ion collisions can be quantified as the coefficients of the Fourier expansion of the invariant

momentum distribution of particles:

$$E\frac{d^3N}{d^3p} = \frac{1}{2\pi}\frac{d^2N}{dp_T dy}\left[1 + \sum_{n=1}^{\infty} 2v_n cos(n\phi)\right] \tag{5.1}$$

where ϕ is the azimuthal angle and v_n's are the Fourier coefficients. Why v_2 is called elliptic flow? This is because if we make a polar plot of $1 + v_2 cos(2\phi)$, we will have a ellipse of major and minor axes of magnitude proportional to $1 + v_2$ and $1 - v_2$ respectively. Therefore, the domain described with major and minor axes proportional to $1 + v_2$ and $1 - v_2$ will have an ellipsoidal shape, hence v_2 is elliptic flow.

The eccentricity of the momentum-space ellipse due to anisotropic momentum distribution resulting from spatial anisotropy can be related to the quantity v_2^{HF}

$$v_2^{HF} = \frac{\langle p_x^2\rangle - \langle p_y^2\rangle}{\langle p_x^2\rangle + \langle p_y^2\rangle} \tag{5.2}$$

where v_2^{HF} is the the momentum space anisotropy probed by heavy flavors. This momentum space anisotropy arises due to initial spatial anisotropy and subsequent interactions among the constituents of the matter produced in heavy ion collisions. The spatial geometry of the collision zone may be fixed by the Glauber model [156].

For quantitative evaluation of $v_2^{\rm HF}$ the FP equation has been solved for the heavy quarks by using the Greens function technique [81], with the initial p_T distribution taken from NLO MNR formalism [87]. The momentum distribution, $dN/dydp_T d\phi$ of the non-photonic single electron spectra originating from the decays of heavy flavour mesons - *e.g.* $D \to Xe\nu$ at mid-rapidity ($y = 0$) is obtained by following the procedure described in 4.4. The coefficient of elliptic flow, v_2^{HF} then can be obtained as:

$$v_2^{HF}(p_T) = \langle cos(2\phi)\rangle = \frac{\int d\phi \frac{dN}{dydp_T d\phi}|_{y=0} cos(2\phi)}{\int d\phi \frac{dN}{dydp_T d\phi}|_{y=0}} \tag{5.3}$$

The system formed in nuclear collisions at relativistic energies evolves dynamically from the initial QGP to the final hadronic state via an intermediary quark-hadron transition. The space time evolution of this systems has been studied by using the (2+1) dimensional hydrodynamical model [160] with boost invariance along the longitudinal direction [85]. The ϕ dependents of the momentum distribution enter through the (2+1) dimensional hydrodynamical model. For RHIC we have assumed an initial temperature,

$T_i = 400$ MeV and thermalization time of the background QGP, $\tau_i = 0.2$ fm/c. The corresponding quantities for LHC are $T_i = 700$ MeV and $\tau_i = 0.08$ fm/c. It is expected that the central rapidity region of the system formed after nuclear collisions at RHIC and LHC energies is almost net baryon free. Therefore, the equation governing the conservation of net baryon number need not be considered for collisions at these energies. Through the temperature dependence the values of the drag and diffusion coefficients are affected by the collective motion of the background QGP. The collectivity is governed by the relativistic hydrodynamics. We have taken the value of the velocity of sound, $c_s = 1/\sqrt{4}$ which is different from the value for an ideal system $c_s = 1/\sqrt{3}$.

5.3 Results

The total amount of energy dissipated by a heavy quark in the QGP depends on the path length it traverses. Each parton traverse different path length which depends on the geometry of the system and on the point where its is created. The probability that a parton is produced at a point (r, ϕ') in a QGP of ellipsoidal shape depends on the number of binary collisions at that point which can be taken as:

$$P(r,\phi') = \frac{1}{\mathcal{N}}\left(1 - \frac{r^2}{R^2}\frac{(1+\epsilon cos^2\phi')}{(1-\epsilon^2)^2}\right)\Theta(R-r) \tag{5.4}$$

and

$$\mathcal{N} = \frac{1}{\pi R^2\left(1 - \frac{1}{2}\frac{1+\epsilon^2/2}{(1-\epsilon^2)^2}\right)} \tag{5.5}$$

where R is the nuclear radius and ϵ is the (spatial) eccentricity of the ellipse. Note that for central collisions ($\epsilon = 0$) Eq. 5.4 reduces to the expression for $P(r, \phi')$ used in Ref. [134] for spherical geometry. A parton created at (r, ϕ') in the transverse plane propagate a distance $L = \sqrt{R^2 - r^2 sin^2\phi'} - r cos\phi'$ in the medium. We use the following equation for the geometric average of the integral which appear in the solution of the FP equation involving drag coefficient:

$$\Gamma = \frac{\int r dr d\phi' P(r,\phi') \int^{L/v} d\tau \gamma(\tau)}{\int r dr d\phi' P(r,\phi')} \tag{5.6}$$

where v is the velocity of the propagating partons.

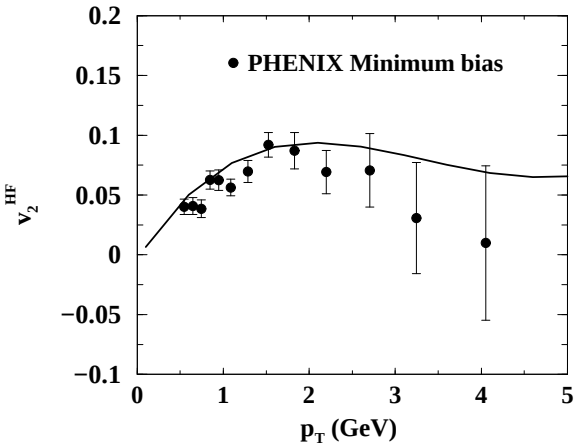

Figure 5.1: Variation of v_2^{HF} with p_T at the highest RHIC energy. Experimental data is taken from [95]. The value of the "effective" impact parameter, $b = 10.2$ fm/c for minimum bias collision of Au nuclei at $\sqrt{s_{NN}} = 200$ GeV.

Similar averaging has been performed for the diffusion co-efficient. For a static system the temperature dependence of the drag and diffusion co-efficients of the heavy quarks enter via the thermal distributions of light quarks and gluons through which it is propagating. However, in the present scenario the variation of temperature with time is governed by the equation of state or the velocity of sound of the thermalized system undergoing hydrodynamic expansion. In such a scenario the quantities like Γ (Eq. 5.6) and hence v_2^{HF} becomes sensitive to the velocity of sound (c_s) in the medium.

The p_T dependence of v_2^{HF} is sensitive to the nature of the initial distributions of heavy quarks, life time of the system, velocity of sound as well as the drag and diffusion coefficients of heavy quarks.

The experimental data [95] for single electron originated from both D and B-decays at RHIC energy ($\sqrt{s_{NN}}$=200 GeV) shows non-zero elliptic flow indicating substantial interactions of the plasma particles with charm and bottom quarks from which electrons are produced through the process: $c(b)$ (hadronization)$\longrightarrow D(B)$(decay)$\longrightarrow e + X$. In Fig. 5.1 we compare the experimental data obtained by the PHENIX [95] collaboration for Au + Au minimum bias collisions at $\sqrt{s_{\rm NN}} = 200$ GeV with theoretical results obtain in the present work. We observe that the data can be reproduced by including both radiative and collisional loss with $c_s = 1/\sqrt{4}$. In this case v_2^{HF} first increases and

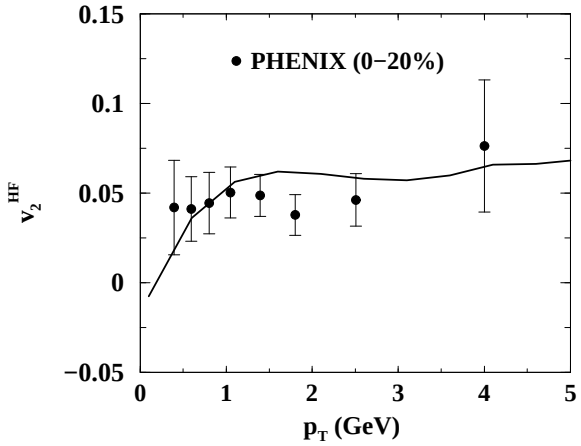

Figure 5.2: Same as Fig. 5.1 for 0-20% centrality. Experimental data contain both the statistical and systematic errors, taken from [96]. The value of the impact parameter, $b = 4.8$ fm/c for collision at $20 - 40\%$ centrality of Au nuclei at $\sqrt{s_{NN}} = 200$ GeV.

reaches a maximum of about 8% then saturates for $p_T > 2$ GeV.

The comparison of results obtained in the present work with the experimental data [96] obtained for two different centralities are depicted in Figs. 5.2 and Fig. 5.3. The agreement is reasonable both for $0 - 20\%$ and $20 - 40\%$ centralities. The non-zero v_2^{HF} indicates that the HQ suffer substantial interaction in the QGP. From the energy dissipation we have evaluated the shear viscosity (η) to entropy (s) density ratio using the relation [161]: $\eta/s \sim 1.25T^3/\hat{q}$, where $\hat{q} = \langle p_T^2 \rangle / L$ and $dE/dx \sim \alpha_s \langle p_T^2 \rangle$ [162], L is the length traversed by the heavy quark and p_T is its transverse momentum. Taking $L \sim 6$ fm, we obtain $\eta/s \sim \frac{2}{4\pi}$, above the AdS/CFT bound [163].

The v_2^{HF} (for 0-10% centrality collision) at LHC energy has been obtained by using the current formalism is displayed in Fig. 5.4. The variation of v_2^{HF} with p_T is similar to that of RHIC, although the magnitude is slightly large. We found that the B meson suffer less flow than D mesons. Some comments on the $R_{\rm AA}$ vis-a-vis v_2^{HF} are in order here. The $R_{\rm AA}$ contains the ratio of p_T distribution of electron resulting from Au+Au to p+p collisions, where the numerator contains the interaction of the heavy quarks with the flowing medium (QGP) and such interactions are absence in the denominator. Whereas for v_2^{HF} both the numerator and the denominator contain the interactions with the medium, resulting in some sort of cancellation. Therefore, the sensitivity of

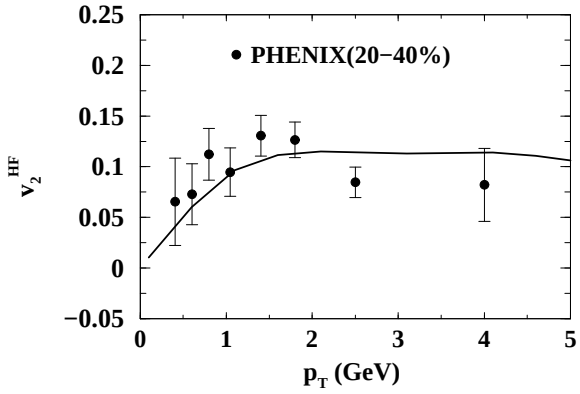

Figure 5.3: Same as Fig. 5.1 for 20-40% centrality. Experimental data contain both the statistical as well as systematic errors, taken from [96]. The value of the impact parameter, $b = 8.2$ fm/c for collision at $20-40\%$ centrality of Au nuclei at $\sqrt{s_{NN}} = 200$ GeV.

R_{AA} and v_2^{HF} on several factors like flow (say) will be different.

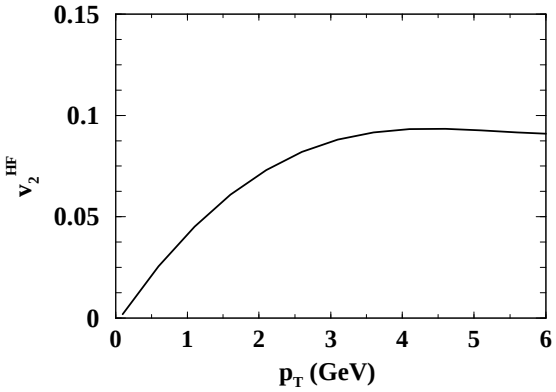

Figure 5.4: The variation of v_2^{HF} with p_T for LHC initial conditions for 0-10% centrality.

Chapter 6

Heavy Meson in Hadronic Phase

6.1 Introduction

Several theoretical attempts [71, 102, 103, 104, 111, 144, 148, 164, 165, 166, 167, 168, 169] have been made to explain $R_{\rm AA}$ and v_2, where the role of hadronic matter has been ignored. However, to make the characterization of QGP reliable the role of the hadronic phase should be taken into consideration and its contribution must be subtracted out from the observables. Although a large amount of work has been done on the diffusion of heavy quarks in QGP, the diffusion of heavy mesons in hadronic matter has received much less attention so far. The present work addresses the relevance of the hadronic sector to some of these issues. Recently the diffusion coefficient of D meson has been evaluated using heavy meson chiral perturbation theory [170] and also by using the empirical elastic scattering amplitudes [171] of D mesons with thermal hadrons. The interactions of D meson with pions, nucleons, kaons and eta have been evaluated using Born amplitudes [172] and unitarized chiral effective $D\pi$ interactions [173].

6.2 Heavy Flavor Transport Coefficients in Hadronic Phase

The drag and diffusion coefficients of the D and B mesons propagating through a hot hadronic matter are evaluated within the ambit of Heavy Meson Chiral Perturbation Theory ($HM\chi PT$) in LO, NLO and NNLO approximations. We consider the elastic interactions of the D and B meson with thermal pions, kaons and eta in the temperature

range $T = 100 - 170$ MeV. First we will focus on B meson transport coefficients in the hadronic medium, then the same formalism will be used to study D meson transport coefficients later.

The drag (γ) and diffusion (B_0 (to avoid confusion with D meson, the diffusion coefficient will be denoted by B_0 here)) coefficients of the heavy mesons are evaluated using elastic interaction with the thermal hadrons. For the (generic) process, $B(p) + h(q) \to B(p') + h(q')$ (h stands for pion, kaon and eta), the drag (γ) and diffusion (B_0) coefficients can be calculated by using the following expression [172, 174]:

$$\begin{aligned}\langle\langle\Gamma(p)\rangle\rangle &= \frac{1}{512\pi^4}\frac{1}{E_p}\int_0^\infty\int_{-1}^1 d(cos\theta_{cm}) \\ &\times \int_0^{2\pi} d\phi_{cm}\frac{q^2dqd(cos\chi)}{E_q}(1+f(q')) \\ &\times \hat{f}(q)\frac{\lambda^{\frac{1}{2}}(s,m_p^2,m_q^2)}{\sqrt{s}}\frac{1}{g}\sum\overline{|M|^2}\Gamma(p\prime)\end{aligned} \tag{6.1}$$

where f's are the phase space factor appropriately chosen for the thermal hadrons and $\overline{|M|^2}$ is the square of the invariant amplitude. With an appropriate substitution of $\Gamma(p\prime)$ one can calculate both the drag and diffusion coefficients using Eq. 6.1 (see section 3.4). The invariant amplitudes have been evaluated using the following prescription.

We start our discussion on the determination of the scattering amplitudes with the Lagrangian of Covariant Chiral Perturbation Theory ($C\chi PT$) involving the heavy B (or D) mesons [175] given by

$$\begin{aligned}\mathcal{L}_{C\chi PT} &= \langle\mathcal{D}_\mu P\mathcal{D}^\mu P^\dagger\rangle - m_B^2\langle PP^\dagger\rangle \\ &-\langle\mathcal{D}_\mu P^{*\nu}\mathcal{D}^\mu P_\nu^{*\dagger}\rangle + m_{B^*}^2\langle P^{*\nu}P_\nu^{*\dagger}\rangle \\ &+ig\langle P_\mu^* u^\mu P^\dagger - Pu^\mu P_\mu^{*\dagger}\rangle + ...\end{aligned} \tag{6.2}$$

where the heavy-light pseudoscalar meson triplet $P = (B^0, B^+, B_s^+)$, heavy-light vector meson triplet $P_\mu^* = (B_\mu^{*0}, B_\mu^{*+}, B_{s\mu}^{*+})$ and $\langle ...\rangle$ denotes trace in flavor space. The covariant derivatives are defined as $\mathcal{D}_\mu P_a = \partial_\mu P_a - P_b\Gamma_\mu^{ba}$ and $\mathcal{D}^\mu P_a^\dagger = \partial^\mu P_a^\dagger + \Gamma_{ab}^\mu P_b^\dagger$ with a, b are the $SU(3)$ flavor indices.

The vector and axial-vector currents are respectively given by $\Gamma_\mu = \frac{1}{2}(u^\dagger\partial_\mu u + u\partial_\mu u^\dagger)$

and $u_\mu = i(u^\dagger \partial_\mu u - u \partial_\mu u^\dagger)$ where $u = \exp(\frac{i\Phi}{2F_0})$. The unitary matrix Φ collects the Goldstone boson fields and is given by

$$\Phi = \sqrt{2} \begin{pmatrix} \frac{\pi^0}{\sqrt{2}} + \frac{\eta}{\sqrt{6}} & \pi^- & K^- \\ \pi^+ & -\frac{\pi^0}{\sqrt{2}} + \frac{\eta}{\sqrt{6}} & K^0 \\ K^+ & K^0 & -\frac{2\eta}{\sqrt{6}} \end{pmatrix}.$$

To lowest order in Φ the vector and axial-vector currents are:

$$\Gamma_\mu = \frac{1}{8F_0^2}[\Phi, \partial_\mu \Phi], \qquad u_\mu = -\frac{1}{F_0}\partial_\mu \Phi \ . \tag{6.3}$$

From the first term (or kinetic part of the P-fields) of $\mathcal{L}_{C\chi PT}$, the matrix elements for contact diagram in terms of Mandelstam variables (s, t, u) are obtained as

$$\begin{aligned} M_{B^+\pi^+} &= -M_{B^+\pi^-} = -\frac{1}{4F_\pi^2}(s-u) \\ M_{B^+\pi^0} &= M_{B^+\eta} = M_{B^+K^+} = M_{B^+K^-} = 0 \\ M_{B^+\overline{K}^0} &= -M_{B^+K^0} = -\frac{1}{4F_K^2}(s-u) \end{aligned} \tag{6.4}$$

These can be represented in the isospin basis as

$$\begin{aligned} M_{B\pi}^{(3/2)} &= -\frac{1}{4F_\pi^2}(s-u) \quad M_{B\pi}^{(1/2)} = \frac{1}{2F_\pi^2}(s-u) \\ M_{B\eta} &= 0 \quad M_{BK}^{(1)} = 0 \quad M_{BK}^{(0)} = -\frac{1}{2F_K^2}(s-u) \\ M_{B\overline{K}}^{(1)} &= -M_{B\overline{K}}^{(0)} = -\frac{1}{4F_K^2}(s-u) \end{aligned} \tag{6.5}$$

where the isospin of the $B\Phi$ system appears in the superscript. Denoting the threshold matrix elements by T, these are obtained from (6.5) and are given by

$$\begin{aligned} T_{B\pi}^{(3/2)} &= -\frac{m_B m_\pi}{F_\pi^2} \quad T_{B\pi}^{(1/2)} = \frac{2m_B m_\pi}{F_\pi^2} \\ T_{B\eta} &= 0 \quad T_{BK}^{(1)} = 0 \quad T_{BK}^{(0)} = -\frac{2m_B m_K}{F_K^2} \\ T_{B\overline{K}}^{(1)} &= -T_{B\overline{K}}^{(0)} = -\frac{m_B m_K}{F_K^2} \end{aligned} \tag{6.6}$$

One can reproduce these T-matrix elements in the isospin basis using the lowest order $HM\chi PT$ Lagrangian for heavy mesons containing a heavy quark Q and a light antiquark of flavor a as given below [176]

$$\begin{aligned} \mathcal{L}_{HM\chi PT} &= -i\ tr_D(\bar{H}_a^Q v^\mu \partial_\mu H_a^Q) \\ &\quad -i\ tr_D(\bar{H}_a^Q v^\mu \Gamma_\mu^{ab} H_b^Q) \\ &\quad +\frac{g}{2}\ tr_D(\bar{H}_a^Q \gamma^\mu \gamma^5 u_\mu^{ab} H_b^Q) + ... \end{aligned} \tag{6.7}$$

where $H_a^Q = \frac{1+\not{v}}{2}(P^*_{a\mu}\gamma^\mu + iP_a\gamma^5)$ and $\bar{H}_a^Q = (P^{*\dagger}_{a\mu}\gamma^\mu + iP_a^\dagger\gamma^5)\frac{1+\not{v}}{2}$ and tr_D denotes trace in Dirac space. In this formalism, since the factor $\sqrt{m_P}$ and $\sqrt{m_{P^*}}$ have been absorbed into the P_a and $P^*_{a\mu}$ fields, the threshold T-matrix element ($\tilde{T}_{th}^{P\Phi}$) now has the dimension of scattering length a_P whereas in $C\chi PT$, we get a dimensionless T-matrix element ($T_{th}^{P\Phi}$). The relation between these two T-matrix elements and the scattering length a_P is given by

$$T_{th}^{P\Phi} = m_P\tilde{T}_{th}^{P\Phi} = 8\pi(m_\Phi + m_P)a_P \tag{6.8}$$

The square of the isospin averaged T-matrix element is given by

$$\sum\overline{|T_{B\Phi}|^2} = \overline{|T_{B\pi}|^2} + \overline{|T_{BK}|^2} + \overline{|T_{B\overline{K}}|^2} \tag{6.9}$$

where $\overline{|T_{B\pi}|^2} = \frac{1}{(2+4)}(2|T_{B\pi}^{(1/2)}|^2 + 4|T_{B\pi}^{(3/2)}|^2)$

and $\overline{|T_{BK/\overline{K}}|^2} = \frac{1}{(1+3)}(|T_{BK/\overline{K}}^{(0)}|^2 + 3|T_{BK/\overline{K}}^{(1)}|^2)$.

6.3 Results

We evaluate the drag coefficient of the B-meson by using the momentum dependent and momentum independent matrix elements given by Eqs. 6.5 and 6.6 respectively. The results are shown by the dot dashed and dashed lines in Fig. 6.1. Inspired by the fact that the results for the two scenarios are not drastically different in the LO we proceed to evaluate the drag coefficient of heavy mesons by replacing $\sum\overline{|M|^2}$ by $\sum\overline{|T|^2}$ in NLO and NNLO. The T-matrix elements are obtained from the scattering lengths.

Liu *et al* [177] have obtained the $B\Phi$ scattering lengths (see also [178]) up to NNLO in $HM\chi PT$ by using the coupling constant from recent unquenched lattice results [179]. Using these NLO and NNLO results we estimate the isospin averaged drag coefficients of B mesons. The results are depicted in Fig. 6.1. The drag coefficient evaluated with NNLO matrix elements increases by 22% compared to the NLO result at $T = 170$ MeV. As shown in Fig. 6.1 and Fig. 6.2 both the drag and diffusion coefficients of the B-meson increase with temperature. This behaviour is similar to the one observed for the partonic phase.

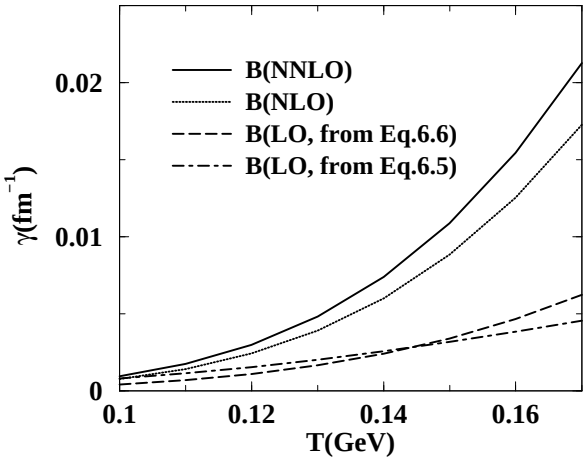

Figure 6.1: The variation of drag coefficients with temperature due to the interaction of B mesons (of momentum 100 MeV) with thermal pions, kaons and eta. The dot-dashed (dashed) line indicates the results obtained by using the matrix elements of Eq. 6.5 (T matrix of Eq. 6.6). Solid (dotted) line indicates the results for NNLO (NLO) contribution [177].

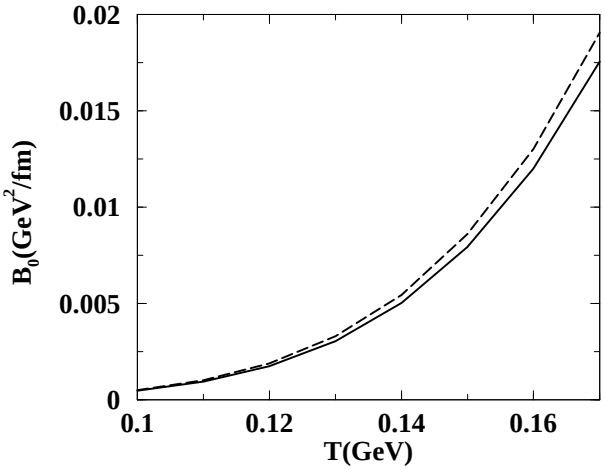

Figure 6.2: Variation of diffusion co-efficient as a function of temperature. The solid line indicates the variation of the diffusion coefficient with temperature obtained from Eq. 6.1. The momentum of the B meson is taken as 100 MeV. The dashed line stands for the diffusion coefficient obtained from the Einstein relation (Eq. 6.10).

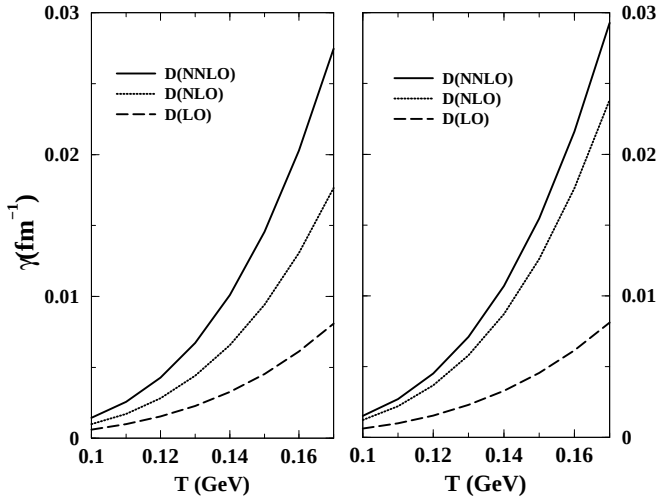

Figure 6.3: The variation of drag coefficients of D mesons with temperature due to interaction with thermal pions, kaons and eta in LO, NLO and NNLO approximations for interactions of D with thermal hadrons taken from Ref. [175] (left panel) and [177] (right panel).

The drag and the diffusion coefficients are related through the Einstein relation as:

$$B_0 = M_B \gamma T. \tag{6.10}$$

where M_B is the mass of the B-meson. The temperature dependence of the diffusion coefficient evaluated by using Eqs. 6.1 and the 6.10 are displayed in Fig. 6.2. The difference between the results obtained from Eq. 6.1 and the Einstein's relation is about $6-7\%$ at $T = 170$ MeV for the B meson momentum, $p = 100$ MeV. This small difference illustrates the validity of the Einstein relation in the low momentum (non-relativistic) domain.

The energy loss of a B meson moving through a hadronic system may be estimated from the relation

$$-\frac{dE}{dx} = \gamma p \ . \tag{6.11}$$

The magnitude of γ obtained in the present calculation reveals that the B mesons dissipate significant amount of energy in the medium. This might have crucial consequences on quantities such as the nuclear suppression factor of single electrons originating from the decays of heavy mesons.

Following similar procedure we also evaluate the D meson drag and diffusion coefficients using the interactions of D mesons with thermal hadrons discussed in Refs. [175] and [177] in LO, NLO and NNLO approximations. The magnitude of drag obtained from the T-matrix of Ref. [175] is similar to that obtained from the interaction given in Ref. [177] in LO. However, for NLO and NNLO, the drag coefficient evaluated using the T-matrix elements obtained from the scattering lengths of Ref. [177] is slightly higher than that obtained from Ref. [175].

The drag of D mesons in hot hadronic matter has recently been studied by using different approaches. While empirical scattering cross sections were used in Ref. [171], the authors of Ref. [173] used unitarized chiral effective $D\pi$ interactions to evaluate the drag. We observe that the magnitude of the drag of D meson obtained in the present work is similar to that obtained in Refs. [171] and [173]. The smaller value in the present case is due to the lower values of the D meson-hadron cross sections.

6.4 Nuclear Suppression in Hadronic medium

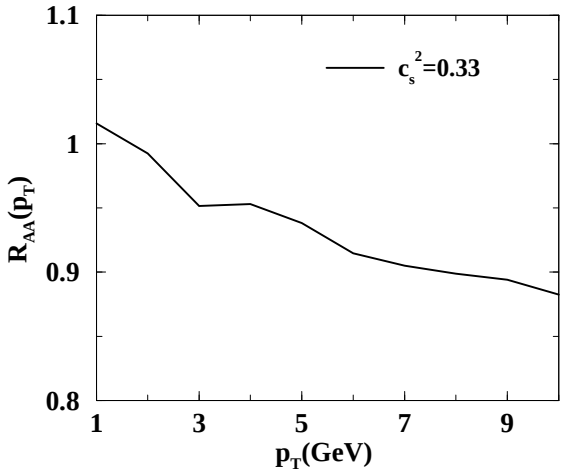

Figure 6.4: Nuclear suppression factor, $R_{\rm AA}$ as function of p_T for D meson.

The abundance of the heavy mesons will be low for the temperature (T) range under consideration ($T = 100 - 170$) MeV; as a result, they do not decide the bulk properties of the matter. Therefore, the propagation of heavy mesons through a thermal

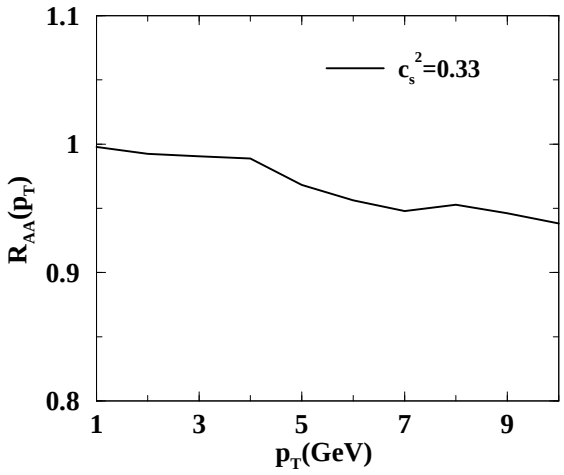

Figure 6.5: Same as Fig. 6.4 for B mesons.

hadronic medium consists of pions, kaons and eta may be treated as the interactions between equilibrium and non-equilibrium degrees of freedom. The FP equation provide an appropriate framework for such processes.

The FP has been solved for the hadronic medium as discused in chapter 3.4. For the initial condition,

$$f(t = 0, p) = f_0(p), \tag{6.12}$$

the $f_0(p)$ corresponding to D and B mesons here are obtained by fragmentation of c and b quarks respectively. The c and b quark distributions are taken from the MNR code [87] for pp collision. Using the drag and diffusion coefficients of the D and B meson as inputs, the FP equation have been solved implementing longitudinal expansion with boost invariance along the z direction [85]. The ratio of the solution of the FP equation at the freeze-out surface to $f_0(p)$ is defined as R_{AA} here.

The variation of R_{AA} for the D and B mesons with p_T are plotted in Fig 6.4 and Fig 6.5 respectively. These results suggest, although the nuclear suppression factor in the hadronic medium is small but it is non-negligible.

Chapter 7

Summary and Outlook

The nuclear collisions at Relativistic Heavy Ion Collider (RHIC) and Large Hadron Collider (LHC) energies are aimed at creating a new state of matter - properties of which are governed by thermal quarks and gluons, such a phase of matter is called Quark-Gluon Plasma(QGP). The study of the properties of QGP is a field of high contemporary interest and the heavy quarks (HQ) namely, charm and bottom quarks play crucial roles in this endeavour. Because HQs (i) are produced in the early stage of the collisions and hence witness the entire evolution scenario of the matter, (ii) do not dictate the bulk properties of the matter (iii) the thermalization time of HQ's are larger than light quarks and gluons. Therefore, the propagation of HQs through a QGP may be treated as the interactions between equilibrium and non-equilibrium degrees of freedom, where the non-equilibrium heavy quark execute Brownian motion in the thermal bath of QGP.

The drag and diffusion coefficients of heavy quarks (charm and bottom) propagating through QGP have been evaluated within the ambit of pQCD. Both the elastic and inelastic or radiative processes have been included in the calculation. We observe that both the transport coefficients increase with temperature. It is noticed that for higher temperature of the QGP and for the higher energy of the propagating HQ the radiative process dominates over the elastic process. The drag and diffusion coefficients for HQ interacting with baryon-rich QGP are also evaluated. It is found that the transport coefficients increase with baryonic chemical potential. Therefore, the present results indicate that the HQ relaxation time will be smaller for a baryon-rich plasma for a

given temperature of the bath.

Here we have solved two sets of differential equations, (i) relativistic hydrodynamic equation (given in Eq. 4.1) for the thermal bath and (ii) Fokker-Planck equation (given in Eq. 3.9) for the heavy quarks propagating in the bath. Therefore, any change in the properties of the bath affect the heavy quarks Brownian motion through the drag and diffusion coefficients. The drag and diffusion coefficients are functions of temperature. The temperature of the bath changes due to the expansion of the bath, which is governed by the relativistic hydrodynamics equations. The initial condition of the hydrodynamic equation has been constrained by the measured hadronic multiplicity at mid-rapidity. The FP equation has been solved with the transport coefficients evaluated in the present work by including both collisional and radiative processes. The initial momentum distributions of HQs are taken from the proton-proton (pp) collisions at RHIC and LHC energies [87]. The solution of the FP equation has been used to evaluate the nuclear suppression factor, $R_{\rm AA}$, for the nonphotonic single-electron spectra resulting from the semileptonic decays of hadrons containing charm and bottom quarks. The theoretical results have been contrasted with experimental data on nonphotonic single-electron spectra measured by STAR and PHENIX collaborations at the highest RHIC energy. The data is well reproduced by including both radiative and collisional losses in the transport coefficients. The same formalism has been used to predict nuclear suppression factors to be measured through the semi-leptonic decays of heavy mesons (D and B) at LHC nuclear collision conditions. We find that the suppression at LHC is large indicating that the heavy quarks undergo substantial interactions in the QGP medium.

The other experimental quantity, the azimuthal anisotropy has also been calculated within the same formalism. We found that the B meson suffer less flow than D mesons. The B-meson contribution reflects itself by the saturation of v_2^{HF} in both LHC and highest RHIC energy. The flow pattern at LHC is similar to that of RHIC, although the magnitude is slightly large. We have simultaneously reproduced the experimental data on the $R_{\rm AA}$ and v_2^{HF} by including radiative as well as collisional loss of heavy quarks due to its interaction with a flowing QGP. Predictions have been made for the

LHC and low energy RHIC run also.

Some comments on the $R_{\rm AA}$ vis-a-vis v_2^{HF} are in order here. The $R_{\rm AA}$ contains the ratio of p_T distribution of electron resulting from Au+Au to p+p collisions, where the numerator contains the interaction of the heavy quarks with the flowing medium (QGP) and such interactions are absence in the denominator. Whereas for v_2^{HF} both the numerator and the denominator contain the interactions with the medium, resulting in some sort of cancellation. Therefore, the sensitivity of R_{AA} and v_2^{HF} on several factors like overall K-factor, flow will be different.

Several theoretical attempts have been made to successfully reproduced the $R_{\rm AA}$, where the role of hadronic matter is ignored. However, to make the characterization of QGP reliable, the role of the hadronic phase should be taken into consideration and its contribution must be subtracted out from the observables. The present work also addresses the relevance of the hadronic sector to some of these issues.

The drag and diffusion coefficients of heavy mesons propagating through a hot hadronic medium consisting of pions, kaons and eta have also been evaluated. The interaction of the probe with the hadronic matter has been treated in the framework of effective field theory. It is observed that the magnitude of both the transport coefficients are non-negligible, indicating substantial amount of interaction of the heavy mesons with the thermal hadronic system. The FP equation has been solved for the expanding hadronic phase. The solution of FP equation has been used to estimate the nuclear suppression factor for the D and B mesons. We find that the nuclear suppression factor in the hadronic medium is small but not negligible.

Further improvement on the work discussed here can be achieved by making the space time evolution picture more rigorous as follow. In the absence of any external force the evolution of the heavy quark phase space distribution is governed by the equation:

$$\left(\frac{\partial}{\partial t} + \mathbf{v_p} \cdot \nabla_{\mathbf{r}}\right) f(\mathbf{p}, \mathbf{r}, t) = C[f(\mathbf{p}, \mathbf{r}, t)] \tag{7.1}$$

where v_p is the velocity of the heavy quark and ∇_r is the spatial gradient operator. As mentioned before the FP equation can be obtained from the above equation by linearizing the collision term [79]. The FP equation so obtained should be solved with

an appropriate initial condition. The inclusion of the non-perturbative effects [89] in the calculation of drag and diffusion coefficients will make the prediction more reliable. In this case the initial distribution may be taken from pp collision [87] as discussed earlier. To take into account the energy loss of the heavy quarks in the thermal bath the hydrodynamic equation needs to be modified as follows:

$$\partial_\mu T^{\mu\nu} = J^\nu \tag{7.2}$$

containing a source term J^ν corresponding to the energy-momentum deposited in the thermal system along the trajectory of the heavy quark, which may be taken as $J^\nu \sim dp^\nu/d\tau$ [180, 181] (p^ν is the four momentum vector). Eq. 7.2 can be used to describe the evolution of the system from an initial QGP to the final hadronic state via an intermediary quark-hadron transition. The initial condition for Eq. 7.2 may be constrained fromed the measured multiplicity. The required EoS may be taken from the Lattice QCD calculation [182]. The solution of the hydrodynamic equation with transverse expansion can be used to obtain the surface of hadronization by setting $T(r,\tau) = T_c$. The solution of Eq. 7.1 for the heavy quark at the hadronization surface should be convoluted with the fragmentation function to obtain the D and B spectra

The D and B spectra so obtained may be used as initial distributions to solve the FP equation in the hadronic phase. The hadronic freeze-out surface may be obtained from the solution of the hydrodynamic Eq. 7.2 by putting the condition $T(r,\tau) = T_f$, where T_f is the value of the freeze-out temperature. Then the solution of the FP equation at the freeze-out surface may be used to obtain the single electron spectra originating from the decays of the D and B mesons.

Appendix

In this appendix we outline the derivation of Eq. 3.45. The typical Feynman diagram for $gg \to gg+g$ is shown in Fig. 7.1. The momentum k_5 of the radiative gluon (Fig. 7.1)

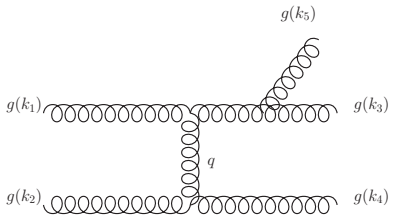

Figure 7.1: A typical Feynman diagram for the process: $gg \to ggg$

is taken to be a soft radiation around zero rapidity in the centre of momentum frame. The $k_\perp$ and $q_\perp$ are the perpendicular component of k_5 and that of the momentum transfer in the centre of momentum frame respectively, m_D is the Debye mass, N_c is the number of colour degrees of freedom.

The invariant amplitude for the process, $gg \to ggg$ can be written as [183]:

$$\begin{aligned} |M_{gg\to ggg}|^2 = \frac{1}{2}g^6\frac{N_c^3}{N_c^2-1}[&(12345)+(12354)\\ &+(12435)+(12453)+(12534)+(12543)\\ &+(13245)+(13254)+(13425)+(13524)\\ &+(14235)+(14325)]\frac{N}{D} \end{aligned} \tag{7.3}$$

where

$$\begin{aligned} N = &(k_1k_2)^4+(k_1k_3)^4+(k_1k_4)^4+(k_1k_5)^4\\ &+(k_2k_3)^4+(k_2k_4)^4+(k_2k_5)^4+(k_3k_4)^4\\ &+(k_3k_5)^4+(k_4k_5)^4, \end{aligned} \tag{7.4}$$

$$D = k_1.k_2 k_1.k_3 k_1.k_4 k_1.k_5 k_2.k_3 k_2.k_4 \\ k_2.k_5 k_3.k_4 k_3.k_5 k_4.k_5 \tag{7.5}$$

and

$$(ijklm) = (k_i.k_j)(k_j.k_k)(k_k.k_l)(k_l.k_m)(k_m.k_i) \tag{7.6}$$

Defining $s = (k_1 + k_2)^2, t = (k_1 - k_3)^2, u = (k_1 - k_4)^2$ and $s' = (k_3 + k_4)^2, t' = (k_2 - k_4)^2, u' = (k_2 - k_3)^2$, we can write $k_1.k_2 = s/2, k_3.k_4 = s'/2, k_1.k_3 = -t/2, k_2.k_4 = -t'/2, k_1.k_4 = -u/2, k_2.k_3 = -u'/2$

Eq. 7.3 contains twelve terms. Using Eqs. 7.4, 7.5 and Eq. 7.6 the first two terms of Eq. 7.3 can be expressed as:

$$\frac{1}{2} g^6 \frac{N_c^3}{N_c^2 - 1} \frac{N}{k_1.k_3 k_1.k_4 k_2.k_4 k_2.k_5 k_3.k_5} \tag{7.7}$$

and

$$\frac{1}{2} g^6 \frac{N_c^3}{N_c^2 - 1} \frac{N}{k_1.k_3 k_1.k_5 k_2.k_4 k_2.k_5 k_3.k_4} \tag{7.8}$$

respectively. All other terms in Eq. 7.3 can be reduced in the above form by following similar procedure.

The quantity N can be written as:

$$N = \frac{1}{16}(s^4 + t^4 + u^4 + s\prime^4 + t\prime^4 + u\prime^4) \\ + \sum_{i=1}^{4} (k_i.k_5)^4 \tag{7.9}$$

In the infrared and small angle scattering limits, we have : $k_5 \to 0, t' \to t, s' \to s, u' \to u$, $s \to -u$.

Using these approximations we get,

$$|M_{gg\to ggg}|^2 = g^6 \frac{N_c^3}{N_c^2 - 1} s^4 [\frac{1}{st^2 k_2.k_5 k_3.k_5} + \\ \frac{1}{st^2 k_1.k_5 k_2.k_5} + \frac{1}{st^2 k_1.k_5 k_4.k_5} + \frac{1}{st^2 k_3.k_5 k_4.k_5}] +$$

$$g^6\frac{N_c^3}{N_c^2-1}s^4[\frac{1}{s^3k_1.k_5k_2.k_5}-\frac{1}{s^2tk_2.k_5k_4.k_5}-\frac{1}{s^2tk_1.k_5k_3.k_5}+\frac{1}{s^3k_2.k_5k_3.k_5}-\frac{1}{s^2tk_1.k_5k_3.k_5}+\frac{1}{s^3k_4.k_5k_3.k_5}+\frac{1}{s^3k_1.k_5k_4.k_5}-\frac{1}{s^2tk_2.k_5k_4.k_5}] \tag{7.10}$$

The above equation may be simplified to obtain:

$$|M_{gg\to ggg}|^2 = 4g^6\frac{N_c^3}{N_c^2-1}\frac{s^3}{t^2}\frac{1}{k_1.k_5k_2.k_5}+ 2g^6\frac{N_c^3}{N_c^2-1}[\frac{2s}{k_1.k_5k_2.k_5}-\frac{s^2}{t(k_2.k_5)^2}-\frac{s^2}{t(k_1.k_5)^2}] \tag{7.11}$$

The first term of the above equation is given by

$$|M_{gg\to ggg}|^2_{1st} = 4g^4\frac{N_c^2}{N_c^2-1}\frac{s^2}{t^2}\frac{g^2N_cs}{k_1.k_5k_2.k_5} = |M_{gg\to gg}|^2\frac{g^2N_cs}{k_1.k_5k_2.k_5} \tag{7.12}$$

Using the following relations [123],

$$k_\perp^2 = 4k_1.k_5k_2.k_5/s, \tag{7.13}$$

$$q_\perp^2 = 4k_1.k_4k_2.k_4/s, \tag{7.14}$$

and

$$(k_\perp - q_\perp)^2 = 4k_1.k_3k_2.k_3/s, \tag{7.15}$$

We get,

$$\frac{4g^2N_cq_\perp^2}{k_\perp^2[(k_\perp-q_\perp)^2+m_D^2]} = \frac{g^2N_cs}{k_1.k_5k_2.k_5} \tag{7.16}$$

and substituting Eq.7.16 in Eq. 7.12 we obtain,

$$|M_{gg\to ggg}|^2_{1st} = \left(\frac{4g^4N_c^2}{N_c^2-1}\frac{s^2}{(q_\perp^2+m_D^2)^2}\right)\left(\frac{4g^2N_cq_\perp^2}{k_\perp^2[(k_\perp-q_\perp)^2+m_D^2]}\right) \tag{7.17}$$

This is the result reported in Ref. [123]. Now we focus on the correction to this result i.e the remaining term in $|M_{gg\to ggg}|^2$, which is given by

$$|M_{gg\to ggg}|^2_{2nd} = 2g^6\frac{N_c^3}{N_c^2-1}[\frac{2s}{k_1.k_5k_2.k_5} - \frac{s^2}{t(k_2.k_5)^2} - \frac{s^2}{t(k_1.k_5)^2}] \tag{7.18}$$

Using Eq. 7.13 we have

$$|M_{gg\to ggg}|^2_{2nd} = 2g^6\frac{N_c^3}{N_c^2-1}[\frac{2s}{k_1.k_5k_2.k_5} - \frac{16(k_1.k_5)^2}{tk_\perp^4} - \frac{16(k_2.k_5)^2}{tk_\perp^4}] \tag{7.19}$$

In the limit $k_5 \to 0$, we have

$$\begin{aligned} |M_{gg\to ggg}|^2_{2nd} &= 2g^6\frac{N_c^3}{N_c^2-1}[\frac{2s}{k_1.k_5k_2.k_5}] \\ &= \frac{g^2N_cs}{k_1.k_5k_2.k_5}\frac{4g^4N_c^2}{N_c^2-1} \\ &= \frac{16g^6N_c^3}{N_c^2-1}\frac{q_\perp^2}{k_\perp^2[(k_\perp-q_\perp)^2+m_D^2]} \end{aligned} \tag{7.20}$$

This is the correction term to the results obtained in [123, 124] for the process $gg \to 2+g$.

Bibliography

[1] D. J. Gross and F. Wilczek, Phys. Rev. Lett **30** 1343 (1973)

[2] D. J. Gross and Frank Wilczek, Phys. Rev. D, **8** 3633 (1973)

[3] H. D. Politzer, Phys. Rev. Lett **30** 1346 (1973)

[4] S. Bethke, J. Phys G **26**, R27 (2000).

[5] M. E. Peskin and D. V. Schroeder, "An Introduction to Quantum Field Theroy" Levant Books, Kolkata, 1995.

[6] T. Muta, "Foundations of Quantum Chromodynamics: An Introduction to Perturbative Methods in Gauge Theories" World Scientific Lecture Notes in Physics - Vol. **57**, 1994

[7] C. "Quigg, Hauge Theories of the Strong, Weak and Electromagnetic", Addison-Wesley Publishing Company, 1994

[8] J. C. Collins and M. J. Perry, Phys. Rev. Lett **34**,1354 (1975).

[9] F. Karsch, Lect. Notes Phys.**583** 209 (2002) [arXiv:hep-lat/0106019]; Nucl. Phys. A **698**, 199 (2002)

[10] E. Shuryak, Rev. Mod. Phys. **61**, 71 (1980)

[11] F. Karsch, E. Laermann and A. Peikert, Phys. Lett. B **478**, 447 (2000)

[12] M. A. Stephanov, PoS LAT2006 **024** (2006).

[13] P. Braun-Munzinger, I. Heppe and J. Stachel, Phys. Lett. B **465**, 15 (1999)

[14] L. D. Mclerran and B. Svetitsky, Phys. Lett. B **98**, 195 (1981)

[15] L. D. Mclerran and B. Svetitsky, Phys. ReV. D **24**, 450 (1981)

[16] J. Kuti, J. Poloenyi and K. Szlachaenyi, Phys. Lett. B **98**, 199 (1981)

[17] V. Koch, Int.J.Mod.Phys. E **6**, 203 (1997).

[18] B. Muller, "The Physics of Quark Gluon Plasma," Springer-Verlag, Heidelberg, 1985.

[19] R. C. Hwa (Ed.), "Quark Gluon Plasma," Vols. **1** and **2**, World Scientific, Singapore, 1990, 1995.

[20] C. Y. Wong, "Introduction to High Energy Heavy Ion Collisions," World Scientific, Singapore,1994.

[21] T. Hirano, Naomi van der Kolk and A. Bilandzic, Lect.Notes Phys. **785** 139 (2010).

[22] L. McLerran and T. Toimela, Phys. Rev. D **31**, 545 (1985).

[23] C. Gale and J.I. Kapusta, Nucl. Phys. B **357**, 65 (1991).

[24] R. Chatterjee, L. Bhattacharya and D. K. Srivastava, arXiv:0901.3610v1 [nucl-th].

[25] L. E. Gordon and W. Vogelsang, Phys. Rev. D **50**, 1901 (1994).

[26] A. Adare *et al.* (PHENIX collaboration), Phys. Rev. Lett. **104**, 132301 (2010).

[27] M.M. Aggarwal *et al.* (WA98 Collaboration), Phys. Rev. Lett. **85**, 3595 (2000).

[28] J. Kapusta, P. Lichard, and D. Seibert, Phys. Rev. D **44**, 2774 (1991).

[29] R. Bair, H. Nakkagawa, A. Niegawa, and K. Redlich, Z. Phys.C **53**, 433 (1992).

[30] E. Braaten and R. D. Pisarski, Nucl. Phys. B **337**, 569 (1990);**339**, 310 (1990).

[31] P. Aurenche, F. Gelis, H. Zaraket, and R. Kobes, Phys. Rev. D **58**, 085003 (1998).

[32] S. Sarkar, J. Alam, P. Roy, A. K. Dutt-Mazumder, B. Dutta-Roy, and B. Sinha, Nucl. Phys. A **634**, 206 (1998).

[33] P. Roy, S. Sarkar, J. Alam, and B. Sinha, Nucl. Phys. A **653**, 277 (1999).

[34] J. Alam, P. Roy, and S. Sarkar, Phys. Rev. C **71**, 059802 (2005).

[35] S. Turbide, R. Rapp, and C. Gale, Phys. Rev. C 69, 014903 (2004).

[36] K. L. Haglin, J. Phys. G **30**, L27 (2004).

[37] S. Sarkar, arXiv:nucl-th/0007011.

[38] S. D. Drell and T.M. Yan, Phys. Rev. Lett. **25**, 316 (1970); Ann. Phys. (N.Y.) **66**, 578 (1971).

[39] S. Gavin, P. L. McGaughey, P. V. Ruuskanen and R. Vogt, Phys. Rev. C **54**, 2606 (1996).

[40] B. Kampfer and O. P. Pavlenko, Phys. Lett. B **391**, 185 (1997).

[41] H. A. Weldon, Phys Rev D **42**, 2344 (1990).

[42] J. Alam, S. Raha and B. Sinha, Phys. Rep. **273**, 243 (1996).

[43] J. Alam, S. Sarkar, P. Roy, T. Hatsuda and B. Sinha, Ann. Phys. **286**, 159 (2000).

[44] R. Rapp and J. Wambach, Adv. Nucl. Phys. **25**, 1 (2000)

[45] K. Kajantie, J. Kapusta, L. McLerran, and A. Mekjian, Phys. Rev. D **34**, 2746 (1986).

[46] T. Altherr and P. V. Ruuskanen, Nucl. Phys. B **380** 377 (1992).

[47] M. H. Thoma and C. T. Traxler, Phys. ReV. D **56**, 198 (1997)

[48] E. V. Shuryak, Rev. Mod. Phys. **65** 1 (1993).

[49] J. Rafelski and B. Muller, Phys. Rev. Lett. **48**, 1066 (1982); (E) **56** 2334 (1986).

[50] P. Koch, B. Muller and J. Rafelski, Phys. Rep. **142**, 167 (1986)

[51] J. Rafelskia, Eur. Phys. J ST **155**, 139, (2008)

[52] M. Gazdzicki, J. Phys. G **30**, S701 (2004).

[53] J. Cleymans, H. Oeschler, K. Redlich and S. Wheaton, Eur.Phys.J.A **29**, 119 (2006)

[54] E. Eichten, K. Gottfried, T. Kinoshita, K. D. Lane and T. M. Yan, Phys. Rev. D **17**, 3090 (1978)

[55] E. Eichten, K. Gottfried, T. Kinoshita, K. D. Lane and T. M. Yan, Phys. Rev. D **21**, 203 (1980)

[56] T. Matsui and H. Satz, Phys. Lett. B **178** , 416 (1986)

[57] T. Hashimoto, O. Miyamura, K. Hirose, and T. Kanki Phys. Rev. Lett. **57** 2123 (1986).

[58] M. Gyulassy, I. Vitev, X. N. Wang, and B.W. Zhang, in QuarkGluon Plasma 3, edited by R. C. Hwa and X. N.Wang (World Scientific, Singapore, 2004) [arXiv:nucl-th/ 0302077].

[59] J.D. Bjorken, FERMILAB-PUB-82-59-THY (1982).

[60] J. Adams *et al.* (STAR Collaboration) Nucl. Phys. A **757**, 102 (2005).

[61] K. Adcox *et al.* (PHENIX Collaboration), Nucl. Phys. A **757**, 184 (2005).

[62] J. Y. Ollitrault, Phys. Rev. D **46**, 229 (1992).

[63] S. Voloshin and Y. Zhang, Z.Phys.C **70**, 665 (1996).

[64] P. Huovinen, P.V. Ruuskanen, Ann. Rev. Nucl. Part. Sci. **56**, 163 (2006)

[65] P. Huovinen and P. V. Ruuskanen, Ann. Rev. Nucl. Part. Sci. **56**, 163 (2006).

[66] D. A. Teaney, arXiv:0905.2433 [nucl-th].

[67] S. S. Adler *et al.* (PHENIX Collaboration), Phys. Rev. Lett. **91**, 182301 (2003).

[68] K. H. Ackemann *et al.* (STAR Collaboration), Phys. Rev. Lett. **86**, 402 (2003).

[69] U. Heinz and P. F. Kolb, Nucl. Phys. A **702**, 269 (2002).

[70] P. F. Kolb and U.W. Heinz, in QuarkGluon Plasma 3, edited by R. C. Hwa and X. N.Wang (World Scientific, Singapore, 2004) [arXiv:nucl-th/0305084].

[71] G. D. Moore and D. Teaney, Phys. Rev. C **71**, 064904 (2005)

[72] R. Baier, A. H. Mueller, D. Schiff and D. T. Son, Phys. Lett. B **539**, 46 (2002).

[73] S. K Das, J. Alam and P. Mohanty, Indian J Phys. **85**, 1149 (2011)

[74] J. Alam, S. Raha and B. Sinha, Phys. Rev. Lett. **73**, 1895 (1994).

[75] E. Shuryak, Phys. Rev. Lett. **68**, 3270 (1992).

[76] E. M. Lifshitz and L. P. Pitaevskii, Physical Kinetics, Butterworth-Hienemann, Oxford 1981.

[77] R. Balescu, Equilibrium and Non-Equilibrium Statistical Mechanics (Wiley, New York, 1975).

[78] S. Chakraborty and D. Syam, Lett. Nuovo Cim. **41**, 381 (1984).

[79] B. Svetitsky, Phys. Rev. D **37**, 2484(1988)

[80] M. G. Mustafa, D. Pal and D. K. Srivastava, Phys. Rev. C **57**, 889 (1998)

[81] H. van Hees, R. Rapp, Phys. Rev. C,**71**, 034907 (2005)

[82] J. Bjoraker and R. Venugopalan, Phys. Rev. C **63**, 024609 (2001).

[83] P. Roy, J. Alam, S. Sarkar, B. Sinha and S. Raha, Nucl. Phys. A **624**, 687 (1997).

[84] P. Roy, A. K. Dutt-Mazumder and J. Alam, Phys. Rev. C **73**, 044911 (2006).

[85] J. D. Bjorken, Phys. Rev. D **27**, 140 (1983).

[86] G. Baym, Phys. Lett. B **138**, 18 (1984).

[87] M. L. Mangano, P. Nason and G. Ridolfi, Nucl. Phys. B **538**, 282 (2002).

[88] M. Cacciari, S. Frixione, M.L. Mangano, P. Nason and G. Ridolfi, J. High Ener. Phys. **0407**, 033 (2004); M. Cacciari and P. Nason, Phys. Rev. Lett. **89**, 122003 (2002); M. Cacciari and P. Nason, J. High Ener. Phys. **0309**, 006 (2003); M. Cacciari, P. Nason and R. Vogt, Phys. Rev. Lett. **95**, 122001 (2005).

[89] H. van Hees, M. Mannarelli, V. Greco and R. Rapp, Phys. Rev. Lett. **100**, 192301 (2008).

[90] T. Sakaguchi (PHENIX collaboration), arXiv:0908.3655 [hep-ex].

[91] B. I. Abelev (Star Collaboration), arXiv:0909.4131 [nucl-ex].

[92] J. M. Heuser (CBM collaboration), J. Phys. G: Nucl. Phys. **35**, 044049 (2008).

[93] B. I. Abeleb *et al.* (STAR Collaboration), Phys. Rev. Lett. **98**, 192301 (2007).

[94] S. S. Adler *et al.* (PHENIX Collaboration), Phys. Rev. Lett. **96**, 032301 (2006).

[95] A. Adare *et al.* (PHENIX Collaboration), Phys. Rev. Lett. **98**, 172301 (2007).

[96] A. Adare *et al.* (PHENIX Collaboration), arXiv 1005.1627[nucl-ex].

[97] M. H. Thoma and M. Gyulassy, Nucl. Phys. B **351**, 491 (1991).

[98] A. Peshier, Phys. Rev. Lett. **97**, 212301 (2006).

[99] A. K. Dutt-Mazumder, J. Alam, P. Roy and B. Sinha, Phys. Rev. D **71** 094016 (2005).

[100] M. G. Mustafa and M. H. Thoma, Acta Phys. Hung. A **22**, 93 (2005).

[101] E. Braaten and M. H. Thoma, Phys. Rev. D **44**, 2625 (1991).

[102] C. M. Ko and W. Liu, Nucl. Phys. A **783**, 23c (2007).

[103] A. Adil and I. Vitev, Phys. Lett. B **649**, 139 (2007).

[104] P. B. Gossiaux and J. Aichelin, Phys. Rev. C **78**, 014904 (2008).

[105] B.L. Combridge, Nucl.Phys.B **151**, 429 (1979).

[106] M. Gyulassy, P. Levai and I. Vitev, Nucl. Phys. B **571**, 197 (2000); M. Gyulassy, P. Levai and I. Vitev, Phys. Rev. Lett, **85**, 5535 (2000)

[107] H. Zhang, J. F. Owens, E. Wang and X. N. Wang, Phys. Rev. Lett. **98**, 212301 (2007).

[108] R. Baier, Y. L. Dokshitzer, S. Peigne and D. Schiff, Phys. Lett. B **345**, 277 (1995); R. Baier, Y. L. Dokshitzer, A. H. Mueller and D. Schiff, Nucl. Phys. B **531**, 403 (1998).

[109] C. A. Salgado and U. A. Wiedemann, Phys. Rev. Lett. **89**, 092303 (2002).

[110] P. Jacobs and X. N. Wang, Prog. Part. Nucl. Phys. **54**, 443 (2005); R. Baier, D. Schiff, B. G. Zakharov, Ann. Rev. Nucl. Part. Sci. **50**, 37 (2000).

[111] S. Wicks, W. Horowitz, M. Djordjevic and M. Gyulassy, Nucl. Phys. A **784**, 426 (2007).

[112] Y. L. Dokshitzer and D. E. Kharzeev, Phys. Lett. B, **519**, 199 (2001).

[113] R. K. Ellis, W. J. Stirling and B. R. Webber, QCD and Collider Physics, Cambridge University Press, Cambridge, 1996.

[114] B. G Zakharov, JETP Lett. **86**, 444(2007); P. Aurenche and B. G. Zakharov, JETP Lett. **90**, 237 (2009).

[115] N. Armesto, C. A. Salgado and U. A. Wiedemann, Phys. Rev. D **69**, 114003 (2004).

[116] B. W. Zhang, E. Wang and X.-N. Wang, Phys. Rev. Lett. **93**, 072301 (2004).

[117] N. Armesto, A. Dainese, C. A. Salgado and U. A. Wiedemann, Phys. Rev. D **71**, 054027 (2005).

[118] Roy A. Lacey *et al.*, Phys. Rev. Lett.**103**,142302(2009).

[119] M. Gyulassy and X.-N. Wang, Nucl. Phys. B **420**, 583 (1994).

[120] S. Klein, Rev of Modern Phys, **71**, 1501(1999).

[121] M. Djordjevic and M. Gyulassy, Nucl. Phys. A **733**, 265 (2004).

[122] S. K. Das and J. Alam, Phys. Rev. D **82**,051502(R),2010.

[123] S. M. H. Wong, Nucl. Phys. A **607**,442(1996).

[124] J.F. Gunion, G.Bertsch, Phys. Rev. D, **25**,746(1982).

[125] R. Abir, C. Greiner, M. Martinez, and M. G. Mustafa, Phys.Rev.D **83**,011501(2011).

[126] T. Bhattacharyya, S. Majumdar, S. K. Das and J. Alam, Phys.Rev.D **85**,034033(2012).

[127] J.W. Chen, J. Deng, H. Dong, Q. Wang, Phys.Rev.D, **83**, 034031 (2011).

[128] O. Kaczmarek and F. Zantow, Phys. Rev. D, **71**, 114510(2005).

[129] S. K. Das and J. Alam Phys. Rev. D, **83**,114011 (2011).

[130] I. Arsene *et al.* (BRAHMS Collaboration), Nucl. Phys. A **757**, 1 (2005); B. B. Back *et al.* (PHOBOS Collaboration), Nucl. Phys. A **757**, 28 (2005); J. Adams *et al.* (STAR Collaboration), Nucl. Phys. A **757**, 102 (2005); K. Adcox *et al.* (PHENIX Collaboration), Nucl. Phys. A **757**, 184,(2005).

[131] K. Aamodt *et al.* (for ALICE collaboration) arXiv:1011.3914.

[132] M. G. Mustafa, D. Pal, D. K. Srivastava and M. H. Thoma, Phys. Lett. B, **428**,234(1998).

[133] X. W. Chang et al, Chin. Phys. Lett. **22**, 72 (2005).

[134] S. Turbide, C. Gale, S. Jeon and G. D. Moore, Phys. Rev. C **72**, 014906 (2005).

[135] N. Armesto, N. Borghini, S. Jeon, U.A. Wiedemann (ed), J. Phys. G: Nucl. Part. Phys. **35**, 054001 (2008).

[136] M. G. Bowler, Z. Phys. C **11**, 169 (1981).

[137] V. G. Kartvelishvili, A. K. Likhoded and V. A. Petrov, Phys. Lett. B **78**, 615 (1978).

[138] C. Peterson *et al.*, Phys. Rev. D **27**, 105 (1983).

[139] B. I. Abelev *et al.*, arXiv:0805.0364[nucl-ex].

[140] P. V. Ruuskanern, Acta Phys. Pol. B **18**, 551 (1986).

[141] E. Schnedermann, J. Sollfrank and U. Heinz, Phys. Rev. C **48**, 2462 (1993).

[142] M. Gronau, C. H. Llewellyn Smith, T. F. Walsh, S. Wolfram and T. C. Yang, Nucl. Phys. B **123**, 47 (1977).

[143] A. Ali, Z. Phys. C **1**, 25 (1979).

[144] S. K Das, J. Alam and P. Mohanty, Phys. Rev. C **80**, 054916 (2009).

[145] X. N. Wang, M. Gyulassy, and M. Plumer, Phys. Rev. D **51**, 3436 (1995).

[146] Z. W. Lin, R. Vogt, and X. N. Wang, Phys. Rev. C **57**, 899 (1998).

[147] M Djordjevic, Phys. Rev. C **74**, 064907 (2006).

[148] S. K Das, J. Alam and P. Mohanty, Phys. Rev. C **82**, 014908 (2010).

[149] M. G. Mustafa, Phys. Rev. C **72**, 014905 (2005).

[150] M. Djordjevic, M. Gyulassy and S. Wicks, Phys. Rev. Lett. **94**, 112301 (2005).

[151] J. Uphoff, O. Fochler, Z. Xu, and C. Greiner, Phys. Rev. C **84**, 024908 (2011).

[152] N. Armesto, M. Cacciari, A. Dainese, C. A. Salgado and U. A. Wiedemann, J. Phys. G **32**, S421 (2006); N. Armesto, M. Cacciari, A. Dainese, C. A. Salgado and U. A. Wiedemann, J. Phys. G **35**, 054001 (2008); W. A. Horowitz, J. Phys. G **35**, 054001 (2008); I. Vitev, J. Phys. G **35**, 054001 (2008).

[153] O. Ristea (for the BRAHMS collaboration) Romanian Reports in Physics, **56**, 659(2004).

[154] A. Andronic, P. Braun-Munzinger and J. Stachel, Nucl. Phys. A **772**, 167 (2006).

[155] D. Kharzeev and M.Nardi, Phys. Lett. B, **507**, 121 (2001).

[156] R. J. Glauber, in lecture in Theoretical Physics, edited by W. E. Brittin and L. G. Dunham (Interscience, N.Y., 1959), Vol **1**, p. 315.

[157] B. B. Back *et al.* (PHOBOS Collaboration), Phys. Rev. C **70**, 021902 (2004).

[158] R. D. Field, Application of Perturbative QCD, Addison-Wesley Pub. Company, N.Y. 1989.

[159] D. Molnar and M. Gyulassy, Nucl. Phys. A **697**, 495 (2002).

[160] P. F. Kolb, J. Sollfrank and U. Heinz, Phys. Rev. C **62**, 054909 (2000); P. F. Kolb and R. Rapp, Phys. Rev. C **67**, 044903 (2003); J. Sollfrank, P. Koch and U. Heinz, Phys. Lett. B **252**, 256 (1990); J. Sollfrank, P. Koch and U. Heinz, Z. Phys. C **52**, 593 (1991).

[161] A. Majumder, B. Müller and X. N. Wang, Phys. Rev. Lett. **99**, 192301 (2007).

[162] R. Baier, arXiv hep-ph/0209038.

[163] P. Kovtun, D. T. Son and A. O. Starinets, Phys. Rev. Lett. **94**, 111601 (2005).

[164] H. van Hees, V. Greco and R. Rapp, Phys. Rev. C **73**, 034913 (2006).

[165] Y. Akamatsu, T. Hatsuda and T. Hirano, Phys. Rev. C **79**, 054907 (2009).

[166] S. K Das, J. Alam, P. Mohanty and B. Sinha Phys. Rev. C **81**, 044912 (2010)

[167] S. K Das and J. Alam, arXiv:1008.2643 [nucl-th], 1101.3385 [nucl-th]

[168] W. M. Alberico *et al.*, Eur.Phys.J.C **71** 1666 (2011)

[169] S Majumdar, T Bhattacharyya, J Alam and S K Das, arXiv:1106.2615 [nucl-th].

[170] M. Laine,JHEP **04** 124, 2011, arXiv:1103.0372 [hep-ph].

[171] M. He, R. J. Fries and R. Rapp, Phys. Let. **B701**, 445 (2002)

[172] S. Ghosh, S. K. Das, S. Sarkar and J. Alam, Phys. Rev. D(R) **84**,011503(R) (2011).

[173] L. Abreu, D. Cabrera, F. J. Llanes-Estrada3 and J. M. Torres-Rincon, arXiv:1104.3815 [hep-ph]

[174] S. K. Das, S. Ghosh, S. Sarkar and J. Alam, arXiv:1109.3359

[175] L.S. Geng, N. Kaiser, J.Martin-Camalich and W.Weise, Phys. Rev. **D82**, 054022 (2010).

[176] A. V. Manohar and M. B. Wise, Heavy quark physics, Camb. Monogr. Part. Phys. Nucl. Phys. Cosmol. 10, 1 (2000).

[177] W.Liu and C.M.Ko, Phys. Let. **B533**, 259 (2002).

[178] F.K. Guo, C. Hanhart, U. G. Meissner, Eur. Phys. J. A **40** 171 (2009)

[179] H. Ohiki, H. Matsufuru, and T. Onogi, Phys. Rev. D 77, 094509 (2008)

[180] A. K. Chaudhuri and U. Heinz, Phys. Rev. Lett. **97**, 062301 (2006)

[181] B. Betz, M. Gyulassy, D. H. Rischke, H. Stoecker and G. Torrieri, J. Phys. G **35**, 104106 (2008).

[182] S. Borsanyi et al. JHEP **11**, 077 (2010).

[183] F. A. Berends *et al.*, Phys. Lett. B **103**, 124 (1981).